UNIVERSITY OF CALIFORNIA, SAN DIEGO

Cortical Feedback Control of Olfactory Bulb Circuits

A dissertation submitted in partial satisfaction of the
requirements for the degree Doctor of Philosophy

in

Neurosciences

by

Alison M. Boyd

Committee in charge:

Professor Jeffry S. Isaacson, Chair
Professor Edward M. Callaway
Professor Takaki Komiyama
Professor William Kristan
Professor Massimo Scanziani

2015

The Dissertation of Alison M Boyd is approved, and it is acceptable in quality and form for publication on microfilm and electronically:

_____

_____

_____

_____

_____

Chair

University of California, San Diego

2015

Table of Contents

Signature Page iii

Table of Contents iv

List of Figures vi

Acknowledgments vii

Vita viii

Abstract of the Dissertation ix

Introduction 1

Odor representation in the olfactory bulb: spatial mapping of excitatory input 1
Inhibitory circuits in the olfactory bulb 3
Function of the piriform cortex 6
Circuits in the piriform cortex 6
Cortical feedback in sensory systems 8
Corticothalamic feedback 9
Cortico-bulbar feedback 11

Experimental Procedures 14

Experimental procedures pertaining to Chapter 1 14
Viral injections of Ntsr1-cre mice 14
Slice recording 14
In vivo recording 16
Experimental procedures pertaining to Chapter 2 19
Animals 19
Odor stimulation and 2-photon imaging 19
Data Analysis 21
Intrinsic Imaging 23

Chapter 1. Cortical feedback control of olfactory bulb circuits 24

Abstract 24
Introduction 25
Results 27
Discussion 42
Acknowledgments 63

Chapter 2. Broadcasting of cortical activity to the olfactory bulb..... 64

Summary 64
Introduction 65
Results..... 67
Discussion..... 73
Acknowledgments 92

Conclusion 93

Cortical feedback drives inhibition of M/T cells 94
Cortical feedback generates excitation in granule cells 95
Cortical feedback drives inhibition of granule cells via excitation of dSACs 97
Glomerular layer targets of cortical feedback 98
Characterization of feedback projections in awake animals 100
Cortical feedback projections show no functional topography 102

References 104

List of Figures

Chapter 1.

Figure 1.1 Conditional expression of channelrhodpsin-2..... 50
Figure 1.2 Cortical feedback drives disynaptic inhibition of M/T cells..... 51
Figure 1.3 Cortical feedback directly excites granule cells..... 52
Figure 1.4 Cortical feedback drives disynaptic feedforward inhibition..... 53
Figure 1.5 Deep short axon cells (dSACs) mediate disynaptic..... 54
Figure 1.6 Cortical feedback projections activate circuits in the glomerular layer..... 55
Figure 1.7 Photoactivation of pyramidal neurons expressing ChR2 *in vivo* drives a sustained increase in gamma-synchronized..... 56
Figure 1.8 Activation of piriform cortex *in vivo* amplifies odor-evoked inhibition in the olfactory bulb..... 58
Figure S1.1 Activation of cortical fibers elicits small excitatory currents in mitral cells..... 60
Figure S1.2 Cortical activation has variable effects on spontaneous firing rates of M/T single units..... 61

Chapter 2.

Figure 2.1 Cortical feedback inputs have diverse response properties..... 77
Figure 2.2 Cortical feedback activity is enhanced during wakefulness..... 79
Figure 2.3 Cortical feedback inputs representing different odors are diffusely distributed..... 81
Figure 2.4 Glomerular layer targeting of feedback inputs is unrelated to glomerular odor specificity..... 83
Figure S2.1 GCaMP expression in PCx, determining the impact of residual uncorrected movement on bouton GCaMP signals, and estimation of the numbers of axons..... 85
Figure S2.2 A larger panel of odors yields similar results, and the effects of anesthesia produced by ketamine and urethane are equivalent..... 87
Figure S2.3 No relationship between tuning similarity and distance between boutons..... 89
Figure S2.4 Tiling across six identified glomerular imaging fields with odors representing distinct functional groups does not reveal co-tuning of feedback projections..... 90
Figure S2.5 Graphical Abstract of the paper..... 91

Acknowledgments

My deepest gratitude goes to:

Jeff Isaacson, for his consistent and caring support both scientifically and beyond, for being such an exceptional, patient mentor and for allowing me the freedom to explore and learn new things on my own while remaining a constant and unfailing resource and teacher.

Massimo Scanziani, to whom this work owes a great intellectual and scientific debt, for being so engaged and helpful throughout.

Cindy Poo, Caleb Stokes and Fitz Sturgill, for their patient teaching, constant encouragement, and for making lab such a fun and interesting environment.

Hiroyuki Kato and Andy Peters, and Takaki Komiyama, for their generosity with code as well as intellectual and technical assistance.

All the members of the Isaacson and Scanziani labs, for outstanding discussion, advice, food, and fun.

Chapter 1 is a reprint of Boyd AM, Sturgill JF, Poo C, Isaacson JS. Cortical feedback control of olfactory bulb circuits. Neuron. 2012 Dec 20;76(6):1161-74. The dissertation author was a primary author of this material. Chapter 2 is a reprint of Boyd AM, Kato HK, Komiyama T, Isaacson JS. Broadcasting of cortical activity to the olfactory bulb. Cell Reports 2015 *In Press.* The dissertation author was the first author of this paper.

Vita

2015 Ph.D. in Neurosciences, **University of California, San Diego** La Jolla, CA

2009 B.S. in Neuroscience, **Brown University**, Providence, RI, USA

Research

PhD thesis: Dr. Jeffry S. Isaacson. University of California, San Diego, La Jolla, CA
Project: Investigating the postsynaptic targets, local circuit effects, and in vivo properties of cortical feedback projections in the mammalian olfactory system.

Advisor: Dr. Mayank Mehta. Brown University, Providence RI
Project: The role of gamma oscillations in the medial prefrontal cortex of freeing behaving rats.

Publications

Boyd AM, Sturgill JF, Poo C, Isaacson JS. Cortical feedback control of olfactory bulb circuits. Neuron. 2012 Dec 20;76(6):1161-74.

Boyd AM, Kato HK, Komiyama T, Isaacson JS. Broadcasting of cortical activity to the olfactory bulb. Cell Reports 2015 *In Press.*

ABSTRACT OF THE DISSERTATION

Cortical Feedback Control of Olfactory Bulb Circuits

by

Alison M. Boyd

Doctor of Philosophy in Neurosciences

University of California, San Diego, 2015

Professor Jeffry S. Isaacson, Chair

Cortical feedback is a universal feature of all sensory systems, and represents an important general strategy for optimizing sensory encoding. The primary olfactory, or piriform, cortex (PCx) sends dense feedback projections to the olfactory bulb (OB) which can modulate incoming sensory information. Previous work has illuminated many details regarding the ascending pathway by which mammalian olfactory circuits encode odors; however information regarding the anatomy and function of the complementary descending feedback pathways remains rudimentary.

Here we use optogenetic activation of cortical feedback projection (CFP) axons in order to establish their postsynaptic targets in mouse acute OB slices. We find that CFPs target a diverse array of GABAergic interneurons in the OB, and ultimately drive

disynaptic inhibition of mitral and tufted (M/T) cells via monosynaptic excitation of inhibitory granule (GC) and periglomerular (PG) cells. In vivo activation of PCx suppresses odor evoked M/T cell activity, and enhances odor evoked inhibition. Together, these results suggest that PCx can gate OB output, and thus control the gain of its own input.

We subsequently sought to characterize CFPs via 2-photon calcium imaging of feedback axons in the OB of awake mice. We find that odor-evoked activity in CFPs is diverse, with some axons displaying high odor selectivity while others are broadly tuned. We further observe that anesthesia reduces the frequency, amplitude, and duration of odor evoked cortical feedback excitation. In the OB, glomeruli form a spatially stereotyped map of odor molecular features. In contrast, in PCx odors activate dispersed ensembles of pyramidal cells lacking spatial topography, raising the question of whether CFPs have functional organization matching that of their postsynaptic targets in OB or retain the dispersed organization of PCx. We addressed this question via intrinsic optical imaging to map the odor evoked activation of OB glomeruli and calcium imaging of CFPs underlying identified glomeruli. Our results suggest that cortical inputs tuned to different odors are spatially interspersed and target individual glomerular channels diffusely and indiscriminately. This work establishes the circuitry of cortical feedback projections in the mammalian olfactory system, and demonstrates a functional role for PCx feedback in driving inhibition of OB output.

Introduction

Our sense of smell helps protect us from spoiled foods, environmental hazards such as gas leaks or smoke, and has a profound impact on the reward value and enjoyment of food. Olfactory cues can powerfully evoke memories, be strongly linked to emotions, and provide a rich background to our daily lives (Jones and Rog, 1998). In addition, most mammalian species depend on olfaction to localize food and potential mates while avoiding predation. How is the inhalation of airborne compounds with varied physical and chemical characteristics transformed by the brain into a unified perception of smell? Although our understanding of the early stages of sensory processing in the olfactory system has been significantly advanced in recent years, our knowledge of how higher-order areas influence early sensory processing remains rudimentary. The overarching aim of this graduate work has been to understand how cortical feedback projections from the primary olfactory (piriform) cortex (PCx) influence olfactory bulb (OB) circuits, and thus the initial representation of odor in mammals.

Odor representation in the olfactory bulb: Spatial mapping of excitatory input

Upon inhalation, odorants are first encoded via activation of a diverse family of approximately 1000 G-coupled odorant receptors expressed on the dendrites of olfactory sensory neurons (OSNs) located in the nasal epithelium (Buck and Axel, 1991). OSNs are thought to express only one or a few specific types of odorant

receptors, and despite being spatially intermixed at the level of the olfactory epithelium, the axons of OSNs expressing the same odorant receptor converge selectively within the dorsal layer of the olfactory bulb into one or two specialized regions of neuropil called glomeruli (Ressler *et al*, 1994; Vasser *et al*, 1994; Mombaerts *et al*, 1996). The odor preference and activation profile of an individual glomerulus is thus dictated by the molecular features which best bind with the odorant receptor expressed by its OSN population.

Odors evoke complex spatiotemporal patterns of glomerular activation and the combination and activity level of glomeruli are thought to form the first representation of odor in the brain (Friedrich and Korsching, 1997; Rubin 1999; Wachowiak and Cohen, 2001). Glomerular activation forms a highly ordered spatial activity map within the olfactory bulb which is largely conserved across animals, as genetically determined OSN populations terminate in spatially conserved locations across the glomerular sheet (Schaefer *et al*, 2001). While there is some evidence of very coarse chemotopic organization within the glomerular layer, monomolecular odorants often activate spatially dispersed sets of glomeruli, and chemically distant odors can activate immediately adjacent glomeruli (Uchida *et al*, 2000; Belluscio and Katz 2001; Meister and Bonhoeffer, 2001). Indeed, the activation profile of a given glomerulus is not useful in predicting the odor preferences of its near neighbors (Soucy *et al*, 2009; Linster and Cleland, 2010), indicating a lack of fine scale chemotopy.

Within each glomerulus, OSNs synapse on the primary apical dendrites of mitral and tufted (M/T) cells, the principal neurons of the OB. The majority of M/T

cells project a single apical dendrite into one glomerulus (Buonviso *et al*, 1991; Shepherd *et al*, 2004). Individual glomeruli and their associated M/T neurons are thus thought to form a functional channel, representing information about a particular molecular feature of a given odorant (Buck, 1996; Wachowiak and Shipley, 2006).

Inhibitory circuits in the olfactory bulb

The OB is a highly laminar structure, and M/T neuron activity is affected by local interactions with several distinct populations of GABAergic interneurons in different layers of the bulb. In the glomerular layer, individual glomeruli are surrounded by a shell of juxtaglomerular neurons, the majority of which are small GABAergic periglomerular (PG) cells which receive inputs from either OSNs or the dendrites of M/T neurons themselves (Shepherd *et al*, 2004). PGs provide both feed-forward and feedback inhibition onto the apical dendritic tufts of M/T cells (Wachowiak and Shipley, 2006). Although PG cells are usually confined to a single or a few closely adjacent glomeruli, another juxtaglomerular cell type, the short axon cell (SA), may contact several glomeruli across distances of several hundred microns (Pinching and Powell, 1971b, Aungst *et al*, 2003) and thus form an interglomerular circuit. Although classically believed to be GABAergic, recent evidence suggests some SAs also release dopamine and their activation may trisynaptically excite PG cells (Pinching and Powell, 1971b, Aungst *et al*, 2003; Kiyokage *et al*, 2010). SA activity thus may serve to inhibit M/T neurons at distant glomeruli directly or via the activation of PG cells. However, inhibition in the glomerular layer is predominantly local and

glomerulus specific. One function of OSN->PG->M/T cell feed-forward inhibition is thought to be contrast enhancement, such that only when an OSN population is strongly activated by binding with its highest affinity ligands will the excitation onto M/T cells be sufficient to produce spiking. When OSNs are more weakly activated, net inhibition onto M/T cells results (Luo and Katz, 2001; Linster and Cleland, 2010).

Below the glomerular layer lies the external plexiform layer (EPL), a region sparsely populated by parvalbumin expressing GABAergic interneurons which make reciprocal connections onto M/T cell dendrites and provide broadly tuned inhibition. These neurons are thought to modulate the gain of M/T cell output without substantially impacting M/T cell tuning or odor preference (Shepherd, 2004; Kato *et al*, 2013, Miyamichi *et al*, 2013).

The somas of M/T cells form a thin principal neuron cell layer below the EPL, underneath which the deepest layer of OB is densely packed with axon-less GABAergic granule cells (GCs) which are the most numerous cell type in OB and outnumber M/T cells by 50-100 fold (Shepherd *et al*, 2004). GCs are narrowly tuned and provide self and lateral inhibition to M/T neurons via reciprocal dendrodendritic synapses onto M/T lateral dendrites located in the EPL (Yokoi *et al*, 1995; Isaacson and Strowbridge 1998; Schoppa *et al*, 1998; Schoppa and Urban,2003; Arevian *et al*, 2008). As M/T lateral dendrites can span millimeter long distances within the EPL, individual granule cells may be excited by, and provide inhibition to, M/T cells contacting different and distant glomerular channels.

The impact of a uniform quantity of lateral inhibition onto a given M/T cell is dependent on its firing rate, providing a mechanism for the enhancement of lateral inhibition between M/T cells with correlated activity and similar tuning properties, regardless of distance (Arevian *et al*, 2008). In addition, back-propagating action potentials which spread throughout M/T cell lateral dendrites have been proposed to further amplify lateral inhibition between co-activated M/T cells which are not immediately adjacent (Migliore and Shepherd, 2008). Granule cell mediated inhibition has been previously shown to have extremely versatile effects on M/T cells, including increasing their odor selectivity (Tan *et al*, 2010), bi-directionally modulating M/T spiking (Balu and Strowbridge, 2007) and enhancing the speed and accuracy of odor discrimination (Abraham *et al*, 2010). GCs do not make synapses onto other GCs, however another type of granule cell layer interneuron, the deep short axon cell (dSAC), has been shown to provide inhibition to GCs; presumably dis-inhibiting M/T cells, onto which they make no direct contacts (Pressler and Strowbridge, 2006, Eyre *et al*, 2009). The source of excitatory input to dSACs has not been previously established.

Thus odor information contained within the spiking activity of M/T cells is not merely a relay of spatially mapped excitatory inputs from OSNs, but also reflects extensive local processing. Odor information exits the OB via the lateral olfactory tract, a dense bundle of M/T cell axons which project to a both cortical and subcortical regions. The largest cortical direct recipient of OB input is the PCx, a three layer paleocortex (Neville and Haberly 2004).

Function of the Piriform Cortex

The identification of an odor which has an innate or learned behavioral significance to an animal against a constantly varying olfactory background is no simple task, as individual natural odor such as urine contains many hundreds of molecules. A primary function of PCx is thought to be tying together information pertaining to numerous individual molecular odorant features into a unified whole, creating an odor percept (Haberly, 2001; Kadohisa and Wilson, 2006; Barnes *et al*, 2008).

In mice, PCx has been shown to be essential for certain types of olfactory learning and memory (Wilson and Stevenson, 2003; Wilson *et al* 2006), and artificial activation of random small subpopulations of PCx neurons paired with shock or reward generates robust associational learning (Choi *et al*, 2011). Lesions of PCx are associated with impaired olfactory discrimination, identification, and memory (Staubli *et al*, 1987; Zhang *et al*, 1998; Gottfried 2010).

Circuits in the piriform cortex

Structurally, PCx is similar to associational areas of cortex (Johnson *et al*, 2000). PCx is comprised of a sparse superficial layer containing predominantly GABAergic interneurons, a middle layer dense with pyramidal neurons, and a poorly delineated deep layer which contains somewhat sparser pyramidal neuron somata (Young and Sun, 2009; Bekkers and Suzuki, 2013). M/T cell axons terminate in L1, where they make synapses on the apical dendrites of L2/3 pyramidal cells as well as

local interneurons (Haberly, 1985; Stokes and Isaacson, 2010). Tracing experiments show that M/T cells have highly overlapping, diffuse, non-topographically organized axonal distribution throughout the PCx (Buonviso *et al*, 1991; Ojima *et al*, 1984; Illig and Haberly, 2003; Wilson and Sullivan 2011). Calcium imaging experiments in cortico-bulbar slices have shown that stimulating multiple glomeruli can generate cooperative recruitment of pyramidal neurons, which integrate converging subthreshold inputs from multiple glomerular channels (Apicella *et al*, 2010). Trans-synaptic tracing further confirms that each region of PCx samples from widely distributed glomeruli, and that individual L2/3 pyramidal cells receive inputs from multiple M/T cells innervating different glomeruli (Miyamichi *et al*, 2011).

In addition to M/T cell input, L2/3 pyramidal neurons make extensive glutamatergic recurrent connections (Haberly and Price, 1978; Poo and Isaacson, 2011; Franks *et al*, 2011) and receive both feedforward and feedback inhibition via local GABAergic interneurons (Haberly *et al*, 1987; Poo and Isaacson, 2009; Stokes and Isaacson, 2010; Suzuki and Bekkers, 2010; Suzuki and Bekkers, 2012). Interestingly, unlike in sensory neocortex, pyramidal cells in PCx are equally likely to make recurrent connections with other pyramidal cells regardless of proximity, forming long range connections spanning millimeters of cortical tissue (Franks *et al*, 2011).

Individual PCx pyramidal cells show narrowly tuned output, responding with spiking to only a few odors of many tested (Poo and Isaacson, 2009; Stettler and Axel 2009; Zhan and Luo, 2010). Whole cell recordings of L2/3 pyramidal cells reveal that this odor selectivity is generated in part by broadly tuned odor-evoked inhibition onto

pyramidal cells (Poo and Isaacson, 2009) coupled with more narrowly tuned excitation. Differences in the relative amount of bulbar and intracortical input can also impact the functional tuning properties of L2/3 neurons, for example in narrowly tuned PCx cells, OB inputs dominate excitatory responses whereas in more broadly tuned neurons, intracortical connections make larger contributions (Poo and Isaacson, 2011). Together, converging M/T cell input, dense associational connections between pyramidal cells, and broadly tuned odor evoked inhibition generate odor representations encoded by diffuse overlapping ensembles of pyramidal cells which lack obvious spatial order (Illig and Haberly 2003; Rennaker *et al*, 2007; Stettler and Axel, 2009; Poo and Isaacson, 2009).

Cortical feedback in sensory systems

Sensory processing is often simplistically viewed as a series of hierarchical steps in which information flows from the periphery to the cortex, with each processing stage en route having larger/more complex receptive fields and extracting increasing complex stimulus features along the way. However, sensory input is not only modified by local connections at each subsequent stage of sensory processing, but is also subject to modulation by long range descending connections. Many of these descending connections arise from the cortex, and can provide broader contextual information to early representations of incoming sensory stimuli. This general layout – whereby 'higher' order brain are able to directly influence early sensory circuits may permit the brain to optimize processing power, reducing resources allotted to expected and

unimportant sensory stimuli while maximizing encoding of attended or relevant stimuli (Sillito *et al*, 2006).

Corticothalamic feedback

In most sensory systems, incoming sensory information from the periphery is routed first through the thalamus, before passing to primary sensory cortex. Traditionally, thalamus has been thought of as a gatekeeper, regulating the flow of information from the periphery to the cortex. Corticothalamic feedback projections are thus uniquely poised to modulate the course and content of this information transfer. Prior studies have demonstrated that corticothalamic feedback can change temporal coherence between thalamus and cortex (Sillito *et al*., 1994; Contreras *et al*., 1996), and thus the efficacy of information transfer, as well as modifying the receptive field properties of thalamic relay neurons (Murphy and Sillito, 1987, 1989; Sillito *et al*, 1994; Murphy *et al*., 1999; Sillito and Jones, 2002; Andolina *et al*, 2007). In addition, corticothalamic feedback has been shown to have a role in general activity regulatory functions such as gain control (Ghosh *et al*, 1994; Briggs and Usrey, 2008; Olsen *et al*, 2012).

Corticothalamic projections provide excitatory drive both directly to thalamic relay neurons and to GABAergic inhibitory cells, which drive disynaptic inhibition of relay neurons. In the visual system, corticothalamic feedback projection terminals from layer 6 of primary visual cortex to the dorsal lateral geniculate nucleus (visual thalamus) have been estimated to provide ~30% of synaptic input to thalamic neurons

compared to only 10% arising from retinal afferents, a prevalence that strongly suggests an important functional role in early visual processing. (Sillito and Jones, 2002). The impact and specificity of corticothalamic projections will be greatly affected by their connectivity, raising the question of whether cortical cells preferentially target thalamic neurons with similar functional tuning. In the visual, auditory and somatosensory systems, both the thalamus and the primary sensory cortex have topographic order that follows primary stimulus parameters: retinotopy, tonotopy, and somatotopy, respectively.

Anatomical evidence has shown reciprocity between the visual thalamus, or dorsal lateral geneculate nucleus (dLGN), and primary visual cortex, such that regions encoding the same areas of visual space are preferentially and reciprocally connected (Murphy and Sillito, 1996; Murphy *et al*, 1999). For example, reconstructions of cortical feedback axons from cat area 17 to the dLGN have shown that although corticothalamic projections ramify and form sparse connections over large regions of the dLGN, the majority of terminals occur in a core, high density region retinotopically matching the receptive field area of the cortical cells themselves (Murphy and Sillito 1996). Similar anatomical reciprocity between the thalamus and cortex has been seen in the rat auditory system, where both the auditory thalamus and corticothalamic projections show coarse tonotopic organization (Hazama *et al*, 2004).

Functional evidence of specificity and co-tuning between cortical feedback projection neurons and their thalamic postsynaptic targets has also been observed. Studies in the auditory system have shown that stimulating a region of primary auditory

cortex (A1) enhances the activity of medial geniculate body (auditory) thalamic neurons tuned to the same frequency preferred by that region of cortex, while suppressing activity of thalamic neurons tuned different frequencies (Yan and Suga, 1996; Zhang *et al*, 1997; He, 1997). This 'egocentric selection' has also been observed in the mouse vibrissae system, where stimulating a cortical column pertaining to a given whisker ('barrel') causes enhancements of thalamic neurons encoding that same whisker ('barreloid'), while suppressing the activity of thalamic neurons encoding neighboring whiskers (Temereanca and Simons, 2004). 'Egocentric selection' is often cited as additional evidence for functional topographic matching of cortical feedback projections and their thalamic targets.

Cortico-bulbar feedback

Unlike other sensory systems, olfactory information bypasses the thalamus and passes directly from the nasal epithelium to the olfactory bulb and subsequently to the primary olfactory cortex. However, just as the thalamus is the recipient of dense modulatory feedback projection from primary sensory neocortex, the olfactory bulb receives a massive feedback projection from the Piriform cortex and anterior olfactory nucleus (de Olmos *et al*., 1978; Haberly and Price, 1978; Luskin and Price, 1983; Shipley and Adamek, 1984). Individual axon tracing has shown that projections from the anterior piriform cortex predominantly terminate within the ipsilateral granule cell layer, with some extending radially up into the glomerular layer where they further ramify (Matsutani 2010). In intact animals and the combined cortico-bulbar slice, some

of these projections have been shown to form monosynaptic excitatory contacts with granule cells, and are thought to 'gate' granule cell spiking and thus inhibition onto M/T neurons (Balu *et al,* 2007, Halabisky and Strowbridge 2003, Nakashima *et al*, 1978). These synapses, which occur on the proximal dendrites of GCs, have also been shown to be extremely plastic, and may be an important substrate of olfactory learning (Gao and Strowbridge 2009; Nissant *et al,* 2009; Cauthron and Stripling 2014). In addition, studies in both rabbits and rats have suggested an important role for the cortical feedback loop in regulating the coherency of bulbar activity, as well as oscillatory activity in certain frequency ranges (Gray and Skinner, 1988; Neville and Haberly, 2003; Martin *et* al, 2004; Martin *et al*, 2006), which can greatly impact the efficacy of information transfer**.** Despite the anatomical density and potential functional importance of cortical feedback projections to the olfactory bulb, our knowledge about their role in modulating early sensory representations in the bulb remains rudimentary and fragmented.

The paucity of currently available information on olfactory cortical feedback projections stems in part from the experimental difficulty in selectively and acutely manipulating this pathway using conventional methods. As the axons of pyramidal cells from piriform cortex projecting back to the bulb are spatially intermixed with the axons of M/T cells exiting the bulb, as well as the somas of interneurons in the granule cell layer, it is difficult to selectively stimulate cortical fibers using conventional extracellular stimulation. In a combined cortico-bulbar slice, which allows for highly specific stimulation, many connections cannot be preserved during slicing (Balu *et al*,

2007). These limitations have prevented a detailed study of cortico-bulbar feedback circuitry, or selective activity manipulation to investigate the effect of PCx feedback on M/T cell odor representations. In addition, due to the anatomical constraints of imaging PCx (which requires removal of the jaw or eye to access) no direct observations of the specific activity of labeled PCx feedback projections have been previously attempted, and the majority of studies of general PCx function have been performed in anesthetized animals.

Thanks to technical advances such as new more sensitive genetically encoded calcium indicators and channelrhodopsin variants which are powerful enough to generate spiking upon axonal stimulation, we can now overcome these limitations, and begin to examine cortical feedback in the olfactory system more selectively and directly. The goal of this thesis work has been to address three fundamental questions about olfactory cortical feedback to the OB: what are the postsynaptic targets of cortical feedback projections, what information is the PCx conveying to the bulb, and do cortical feedback projections adopt the spatial mapping of their bulbar targets or retain the diffuse non-topographic organization of PCx?

Experimental Procedures

Experimental procedures pertaining to Chapter 1:

Viral Injections of Ntsr1-cre mice

Experiments followed approved national and institutional guidelines for animal use. Ntsr1-cre animals (Tg(Ntsr1-cre)209Gsat) were obtained from the Gensat Project. The full expression pattern of Cre-recombinase in this line can be viewed at www.gensat.org. Cre^{+} neurons in olfactory cortex have previously been characterized as layer 2/3 pyramidal neurons (Stokes and Isaacson, 2010).

High-titer ($1.2*10^{12}$) stock of AAV (2/8) containing pAAV-EF1a-double floxed-hChR2(H134R)-mCherry-WPRE-HGHpA (Addgene 20287) was produced by the UCSD Vector Core. Neonatal Ntsr1-cre mice (postnatal day 0-2) were anesthetized and virus injection sites targeting the anterior PCx were determined based on landmarks including the superficial temporal vein and the posterior border of the eye. Injections (23 nl) were made using beveled pipettes (Nanoject II, Drummond) at 4 injection sites at depths of 0.18-0.25 mm. Although the majority of mice received injections into only one PCx, virus was injected bilaterally into some animals to express ChR2 in cortical projections to both OBs and data from these two groups of animals were pooled.

Slice Recording

Mice (postnatal day 10-30) were anesthetized with isoflurane and decapitated. OBs were removed and placed into ice cold artificial cerebrospinal fluid (aCSF)

containing (in mM) 83 NaCl, 2.5 KCl_2, 0.5 $CaCl_2$, 3.3 $MgSO_4$, 1 NaH_2PO_4, 26.2 $NaHCO_3$, 22 glucose, and 72 sucrose, equilibrated with 95% O_2 and 5% CO_2. Coronal or horizontal slices (300-400 μm) were cut using a vibrating slicer and incubated at 35° C for 30 minutes. Slices were transferred to a recording chamber and superfused with aCSF containing (in mM): 119 NaCl, 2.5 KCl, 2.5 $CaCl_2$, 1.3 $MgSO_4$, 1 NaH_2PO_4, 26.2 $NaHCO_3$ and 22 glucose, equilibrated with 95% O_2 and 5% CO_2. All experiments were conducted at 28–30° C.

Patch-clamp recordings were performed using an upright microscope and DIC optics. Neuron types were identified by their morphology, intrinsic properties, and laminar location. For glomerular layer recordings, juxtaglomerular cells were filled with fluorescent dye (Alexa 488, 40 μM) and classified based on morphological and electrophysiological criteria (Hayar *et al*., 2004; Murphy *et al*., 2005). ET cells were identified as having large (~20 μm) somata, a single dendrite and tuft ramifying within one glomerulus, an axon extending into the EPL and a relatively low input resistance (197 ± 36 MΩ, n=10). PG cells were distinguished by their small somata (~10 μm diameter) and high input resistance (~1 GΩ). sSACs were distinguished by their unique dendritic arbors that are exclusively periglomerular, span multiple glomeruli, lack tufts, and are poorly branched. Recordings were made using a Multiclamp 700A amplifier (Molecular Devices) digitized at 10-20 kHz and acquired using AxographX software. For most recordings, pipettes (3-6 MΩ) contained (in mM: 130 D-gluconic acid, 130 CsOH, 5 NaCl, 10 HEPES, 10 EGTA, 12 phosphocreatine, 0.2 spermine, 3 Mg-ATP, and 0.2 Na-GTP [pH 7.3]). For some voltage clamp recordings and all

current clamp recordings, a K^+-based internal solution was used (in mM: 150 Kgluconate, 1.5 $MgCl_2$, 5 HEPES buffer, 0.1 EGTA 10 phosphocreatine, and 2.0 Mg-ATP [pH 7.4]). Series resistance was routinely <20 MΩ and continuously monitored. In some experiments biocytin (0.2%) or fluorescent dye (Alexa 488) was added to the pipette to allow for reconstruction of cell morphology (Neurolucida). Voltages were corrected for a junction potential of 15 mV.

A collimated LED light source (455 nm, 210 mW, ThorLabs) or output from a xenon lamp (470 nm, TILL) was directed through the 40X microscope objective for photoactivation of ChR2. Full-field illumination was used unless stated otherwise. In mitral cell recordings, the objective was centered at the midpoint of the GC layer directly below the recorded cell. For all other experiments of neurons in the GC or glomerular layer, illumination was centered over the recorded cells. With full-field illumination, translation of the objective <200 μm did not alter the amplitude of light-evoked responses.

In vivo recording

We made recordings from Ntsr1-cre mice (postnatal day 28 –60) previously injected in PCx with AAV-ChR2-mCherry (n=25). In some experiments (n=3), we expressed ChR2 conditionally by crossing Ntsr1-cre mice with a transgenic ChR2 reporter line (Ai32) (Madisen *et al*., 2012). We did not see any obvious differences using these two expression systems and results were pooled. Mice were anesthetized with urethane (1.5 g/kg) and chlorprothixene (2 mg/kg). Animals were headfixed using

a custom stereotax and skin overlaying the massiter muscle and a portion of the zygomatic arch was removed. The coronoid and condyloid processes were retracted and the skull overlaying anterior PCx was thinned with a surgical drill. In some experiments, a small craniotomy was made for insertion of the recording probe. In all experiments, a second craniotomy was performed over the OB after carefully thinning the skull in this region. Body temperature was maintained at 35-37° C.

Odors were delivered via a computer-controlled olfactometer with a 1 L/min constant flow. Odors were diluted in mineral oil, and further diluted with charcoal-filtered air to achieve 50 ppm, unless otherwise stated. Odors consisted of 3-component mixtures: 1) cis-3-hexen-1-ol, methyl acetate, octanal; 2) acetophenone, eugenol, hexanol; 3) isoamyl acetate, hexanal, 2-heptanone; 4) cineole, phenylethyl alcohol, amyl acetate; 5) heptaldehyde, cyclohexanone, cumene; 6) propyl propionate, citral, (r)-limonene; 7) isoamyl butyrate, carvone, ethyl tiglate.

Unit and LFP activity was recorded with 16 channel silicon probes (Neuronexus) and a 16 channel amplifier (AM systems) at 20 kHz. Data were digitized (National Instruments) and acquired with a custom software package written in Matlab (Olsen *et al*., 2012). For cortical recordings, penetration depths of the tip of the probe were between 500-700 μm. For the bulb, dorsal penetration depths were approximately 500 μm and both dorsal and ventral recordings from M/T cells were guided by photoinduced field potentials (see below). Respiration was monitored using a piezoelectric strap mounted across the chest of the animal.

LED stimulation of PCx was accomplished using a fiber-coupled LED (470nm, 20 mW, 1 mm fiber, 0.48 N.A., Doric Lenses). In a subset of experiments, activation of cortex was monitored directly by extracellular recording. Otherwise, a train of 3 LED flashes (3 ms duration, 50 ms ISI) to the cortex and extracellular recording in the bulb with the linear probe were used to assess effective stimulation of cortex and guide the probe to the mitral cell layer. Each flash caused a field EPSP that varied in intensity across depth and reversed approximately at the mitral cell layer (Neville and Haberly, 2003) where a band of unit activity from presumptive M/T cells was observed in multichannel recordings. A ramped (9 mW/s), trapezoidal light stimulus was chosen to effectively drive sustained activity in PCx and mitigate sharp transitions in LFP activity produced by an immediate transition to full LED intensity.

Data analysis was performed using Matlab. Spike sorting was accomplished using a K-means clustering algorithm and spike-sorting package (UltraMegaSort2000, Hill and Kleinfeld). Single units with >20% estimated spike contamination or >20% missing spikes were excluded. Spectral analysis was accomplished using the Chronux package. Spectrograms and power spectra were calculated from the derivative of the corresponding time series to remove the $1/f^2$ trend in spectral power. For spectral analysis of cortical signals, we used a superficial recording site on the probe situated in layer 1. For OB LFP measurements, the deepest channel in the GC layer was chosen for spectral analysis. LFP traces were bandpass filtered at 10-80 Hz.

Experimental Procedures pertaining to Chapter 2:

Animals

Experiments followed approved national and institutional guidelines for animal use. We used either C57BL/6 wild type or Ntsr1-cre mice (Tg(Ntsr1-cre)209Gsat) that express Cre recombinase selectively in olfactory cortex pyramidal cells (Boyd *et al*., 2012). For the majority of experiments, we injected AAV 2/9-syn-GCaMP6s into the PCx of adult (≥40 days old) C57BL/6 mice at three locations (100 nl/site). We used similar injections of AAV2/9-FLEX-syn-GCaMP5G for conditional expression in a subset of Ntsr1-cre mice. AAV 2/9-syn-tdTomato was co-injected (50 nl/site) in a subset of mice to determine the effects of residual motion. Results were similar using GCaMP6s and GCaMP5G, thus all data were pooled. Coordinates of the injections sites, measured from the intersection of the midline and bregma were (in mm: anterior, lateral, depth): (2.8, 1.8, 4.2), (2.4 2.1, 4.2), (1.9, 2.8, 4.6). All viruses were high titer stocks from U. Penn. Vector Core.

Window implantations were performed as described previously (Kato *et al*., 2012). Briefly, mice were anesthetized with isoflurane (2%), the skull exposed and a custom stainless steel head-plate implanted. A craniotomy (~1-2 mm diameter) was made over the right olfactory bulb and a glass window (350 μm thick) secured over the craniotomy. Animals recovered for >2 weeks before imaging was performed.

Odor Stimulation and 2-Photon Imaging

Odors were first diluted in mineral oil to a concentration of 200 ppm. A computer-controlled olfactometer mixed saturated odor vapor with filtered air 1:1 for a final concentration of 100 ppm (1L/min flow rate). Odors (Sigma) used: ethyl tiglate, heptanal, butyric acid, heptan-4-on, cineole, citral, isoamyl acetate, cyclohexanone, octanal, R-limonene, hexanol, cumene, isoamyl butyrate, propyl propionate, cis-3-hexen-1-ol, amyl acetate, 2-heptanone, anisole, 2-4 dimethylthiazide, and acetophenone. Each odor was applied (4 s duration, 1 min inter-trial interval) for 5-10 trials per experiment. Every series of odor trials included a mock trial of filtered air application to estimate the noise level, which we used for receiver-operator characteristic (ROC) analysis to establish response threshold.

All imaging sessions started at least 15 minutes after mice had been head-fixed. During imaging sessions, mice showed little signs of distress, such as excessive struggling. GCaMP and tdTomato were excited at 920 nm (Ti-Sa laser, Newport) and images (512 x 512 pixels) were acquired with a commercial microscope (Thorlabs) using a 16x objective (Nikon) at ~15 Hz. Images were acquired from the glomerular layer (50-150 μm below the surface) or the granule cell layer (300-400 μm below the surface). In a subset of experiments, mice were anesthetized with subcutaneous injections of ketamine/xylazine (100 mg/kg and 8 mg/kg, respectively) or urethane (1.5 g/kg) and maintained on a feedback regulated heat pad at 37°C. Adequate anesthesia was monitored via lack of response to toe pinch and respiration rate. Respiration was monitored via a thermocouple in front of the left naris. Tail vein injections of Texas red

dextran (70,000 MW, Invitrogen, 75-100 µl of a 5% v/v solution in saline) were used to visualize vasculature landmarks.

Data Analysis

Lateral motion was corrected by cross correlation-based image alignment (Turboreg (Thévenaz *et al*., 1998), ImageJ plugin). We estimate the lateral motion, using frame-by-frame motion correction, to be <2.9 µm in 90% of frames (3.9±1.9 µm in the remainder). Regions of interest (ROIs) corresponding to individual axonal boutons were manually drawn based on the image obtained by averaging all frames collected during a 60 s trial for each odor. Pixels in each ROI were averaged for fluorescence measurements. The time-varying baseline fluorescence trace was estimated by smoothing inactive portions of the trace as described previously (Peters *et al*., 2014). For each odor response, the trace was smoothed (15 frame sliding window average) and normalized by the baseline.

Using a response detection period of 10 s beginning with the onset of odor application, ROIs were classified as having an excitatory response to an odor if dF/F increased by 2.6X standard deviation (SD) of the baseline for 10 continuous frames, both in the average trace and in ≥ 50% of individual trials. The 2.6 SD threshold was chosen to yield a false positive (FP) rate (estimated from air trials) of 9.5%. In addition, all responses had to be ≥20% dF/F, to avoid FPs caused by residual motion (Fig. S2.1). Two separate, independent criteria were used for detecting inhibition. The first was a ≥60% reduction in the standard deviation relative to baseline. The second

was a ≥20% decrease in dF/F lasting ≥2 seconds (FP rate= 9.1%). Average response time course was derived by aligning responses to their 50% rise time and decay time was calculated from the time to 0.37 of peak amplitude. For analysis of response amplitude, the maximum dF/F value of the average trace (5-10 trials) during the response detection window was used. In experiments comparing the responses of the same boutons in the awake and anesthetized state, the dF/F value was included for each bouton-odor pair under both conditions, regardless of whether it was classified as a response in one or both conditions.

For analysis of boutons based on matched or mismatched response properties, we used correlation analysis to select one bouton from axons contributing multiple boutons. This is due to the fact that spacing between boutons along the same fiber can be very small (<5 μm), yielding a disproportionately small distance between boutons with matching response properties. We performed simulations to investigate whether the observed distribution of ranked odor response probabilities (using seven odors per imaging field, n=22 fields) could be explained by subsampling from a distribution in which each odor had an equal probability of eliciting a response. Simulations were performed by subsampling from a random distribution of 10000 values (integers 1 through 7). We determined the distributions expected using the smallest (n=23) and largest (n=406) number of odor-response pairs observed in our 22 imaging fields. We also confirmed that our experimentally measured value for the most preferred odor response probability could be explained by random subsampling. We did this by subsampling using the actual sample size of the 22 fields, determining the average

probability for the preferred odor, and repeating this process 10000 times. This generated a response probability distribution derived by random chance under conditions identical to the sampling parameters of our data.

Intrinsic Imaging

Intrinsic images were acquired using a tandem lens macroscope and 12 bit, CCD camera (CCD-1300QF, VDS Vosskühler) in ketamine-anesthetized animals. Images of the vasculature on the surface of the brain were acquired using green LED illumination (540 nm) and intrinsic signals were recorded (27 Hz) using red illumination (615 nm LED). Each trial consisted of 1 s baseline period followed by 2 s odor exposure and 15-20 trials for each odor were collected for analysis. Images (1280 X 1024) of reflectance (R) from the baseline period were summed and subtracted from the average image during the odor period. These images (dR/R) were Gaussian blurred (100 pixel radius) to produce images for subtraction of diffuse odor-evoked reflectance and subsequently median filtered (20 pixel radius).

Chapter 1. Cortical feedback control of olfactory bulb circuits

Abstract

Olfactory cortex pyramidal cells integrate sensory input from olfactory bulb mitral and tufted (M/T) cells and project axons back to the bulb. However, the impact of cortical feedback projections on olfactory bulb circuits is unclear. Here we selectively express channelrhodopsin-2 in olfactory cortex pyramidal cells and show that cortical feedback projections excite diverse populations of bulb interneurons. Activation of cortical fibers directly excites GABAergic granule cells, which in turn inhibit M/T cells. However, we show that cortical inputs preferentially target short axon cells that drive feedforward inhibition of granule cells. *In vivo*, activation of olfactory cortex that only weakly affects spontaneous M/T cell firing strongly gates odor-evoked M/T cell responses: cortical activity suppresses odor-evoked excitation and enhances odor-evoked inhibition. Together, these results indicate that although cortical projections have diverse actions on olfactory bulb microcircuits, the net effect of cortical feedback on M/T cells is an amplification of odor-evoked inhibition.

Introduction

Cortical regions underlying vision, audition, and somatosensation receive sensory information from the thalamus and also make corticothalamic feedback projections that influence thalamic sensory processing (Briggs and Usrey, 2008; Cudeiro and Sillito, 2006). Thus, the cortex has the fundamental capacity to modulate the nature of its own input. In contrast to other sensory modalities, the olfactory system is unusual in that sensory information is initially processed in the olfactory bulb (OB) and conveyed directly (without a thalamic relay) to the olfactory cortex. Like the corticothalamic pathway, anatomical studies show that the axons of olfactory cortex pyramidal cells send abundant, long-range "centrifugal" projections back to the OB (de Olmos *et al*., 1978; Haberly and Price, 1978; Luskin and Price, 1983; Shipley and Adamek, 1984). However, functional properties of cortical feedback projections such as their neuronal targets, effects on local circuits, and impact on OB odor processing *in vivo* are poorly understood.

In the OB, principal mitral and tufted (M/T) cells belonging to unique glomeruli are activated by particular molecular features of individual odorants (Rubin and Katz, 1999; Soucy *et al*., 2009; Uchida *et al*., 2000). M/T cell output is strongly regulated by local GABAergic interneurons (Shepherd *et al*., 2004). Indeed, odors can elicit purely inhibitory M/T cell responses reflecting a major role for circuits mediating lateral inhibition in the OB (Cang and Isaacson, 2003; Davison and Katz, 2007; Yokoi *et al*., 1995). Reciprocal dendrodendritic synapses between M/T cell lateral dendrites and the distal dendritic spines of GABAergic granule cells (GCs) are the major source of

recurrent and lateral inhibition of M/T cells and dendrodendritic inhibition triggered by M/T cell glutamate release is strongly dependent on the activation of GC NMDA receptors (NMDARs) (Chen *et al*., 2000; Isaacson and Strowbridge, 1998; Schoppa *et al*., 1998).

Sensory information from the OB is relayed via M/T cell axons within the lateral olfactory tract (LOT) directly to pyramidal cells in piriform cortex (PCx), a three-layered cortical region where bulbar inputs are integrated to form odor percepts (Haberly, 2001). Axon collaterals of PCx pyramidal cells provide excitatory projections back to the OB that are densest in the GC layer (Shipley and Adamek, 1984), suggesting that M/T cell inhibition is regulated by a long-range cortical feedback loop (Nakashima *et al*., 1978). In bulb-cortex slices, extracellular stimulation of PCx produced excitatory postsynaptic currents (EPSCs) in GCs and cortical input that drives GC action potentials (APs) is proposed to enhance M/T cell dendrodendritic self- and lateral inhibition (Balu *et al*., 2007; Halabisky and Strowbridge, 2003). This bulbo-cortical loop is also thought to contribute to oscillatory dynamics in the OB and cortex (Neville and Haberly, 2003) and proximal (presumptive cortical) inputs on GCs express long-term potentiation (LTP), suggesting they may play a role in olfactory learning (Gao and Strowbridge, 2009; Nissant *et al*., 2009). Furthermore, recordings in awake, behaving rodents show that M/T cell activity can be modulated by contextual information suggesting that higher cortical regions can influence odor processing in the OB (Kay and Laurent, 1999).

Despite the potential importance of cortical feedback in the regulation of OB

circuits, the functional properties of these long-range projections are unclear. In large part, this reflects the challenge of selectively manipulating this feedback pathway using conventional extracellular electrical stimulation since cortical fibers are intermingled with the axons and dendrites of bulbar neurons. In this study, we express channelrhodopsin-2 (ChR2) selectively in olfactory cortex pyramidal cells and examine the impact of cortical feedback on circuits in OB slices and its actions on odor-evoked activity *in vivo*.

Results

We took advantage of a transgenic mouse line (Ntsr1-creGN209 from the GENSAT project) that expresses Cre recombinase in olfactory cortex pyramidal cells, but not in pyramidal cells of other cortical regions or in inhibitory interneurons (Experimental Procedures, (Stokes and Isaacson, 2010)). We injected the anterior PCx of neonatal mice with an adeno-associated virus (AAV-double floxed-ChR2-mCherry) to drive Cre-dependent co-expression of the light-activated channel channelrhodopsin-2 (ChR2) (Atasoy *et al*., 2008; Petreanu *et al*., 2009) and the fluorescent protein mCherry. We chose this conditional strategy since injections of unconditional AAV-ChR2 could reach the lateral ventricle, leading to ChR2 expression in OB interneurons of wild-type mice (not shown). With this conditional approach, unilateral injections labeled layer 2/3 pyramidal cells in PCx and fibers that projected rostrally (Fig. 1.1A_{1-2}). Consistent with anatomical studies of the axonal projections of PCx pyramidal cells (Matsutani, 2010; Shipley and Adamek, 1984), expression of ChR2-mCherry was

present in the ipsi- but not contralateral OB with the densest labeling in the GC layer and lesser expression in the glomerular layer (Fig. 1.1A_{3-4}). 2-photon imaging of the GC layer confirmed that ChR2 was present only in fibers and axonal varicosities (Fig. 1.1B) rather than cell bodies of OB neurons. Consistent with tracing studies of the axonal trajectories of PCx pyramidal cells (Matsutani, 2010), we observed only scattered expression of ChR2-expressing fibers in the EPL, yet fibers and varicosities were found to surround but not extend into glomeruli (Fig. 1.1C). Pyramidal cells of the anterior olfactory nucleus (AON, the most rostral region of olfactory cortex) project to both ipsi- and contralateral OBs, however, only rarely (5/39 injections) did we observe labeled fibers in the anterior pole of the anterior commissure or contralateral OB. Together, these results indicate that we can exclusively express ChR2 in long-range axonal projections within the OB that predominantly arise from PCx.

Cortical feedback drives disynaptic inhibition of mitral cells

We first examined the influence of cortical feedback projections on mitral cells by activating ChR2-expressing cortical fibers in OB slices using brief (1-4 ms) flashes of blue light. In mitral cells voltage-clamped at the reversal potential for EPSCs (V_m= 0 mV), light flashes elicited inhibitory postsynaptic currents (IPSCs, Fig. 1.2A) that were abolished by the $GABA_A$ antagonist gabazine (10 μM, n=5, Fig 1.2A_2). Light-evoked mitral cell IPSCs were unaffected by application of the NMDAR antagonist APV alone (100 μM, 97±9% of control, n=4) but completely blocked in the presence of the AMPA receptor (AMPAR) antagonist NBQX (20 μM, 1.2±0.7% of control, n=11, Fig. 1.2A_3).

Thus, activation of cortical fibers elicits indirect inhibition of mitral cells that is mediated by AMPAR-driven excitation.

We next recorded from mitral cells in current clamp to determine the effects of cortical inputs on cell excitability. We depolarized cells (V_m=-51.3±2.6 mV, n=9) so that they were suprathreshold for firing APs and interleaved control trials with those containing a train of light flashes (5 pulses, 20 Hz, Fig. 1.2B_1). The desensitization properties of ChR2 precluded using higher stimulus frequencies (Petreanu *et al*., 2009). Individual light-evoked inhibitory postsynaptic potentials (IPSPs, first flash -5.0±0.8 mV, last flash -4.9±0.6 mV) transiently suppressed AP firing while the decay of the IPSP led to rebound firing (78 ± 48% increase in APs relative to control trials, 15 ms time window). These effects are consistent with previous studies showing that brief membrane hyperpolarization generates rebound APs in mitral cells (Balu and Strowbridge, 2007; Desmaisons *et al*., 1999). We compared the firing rate with and without activation of cortical fibers over the time period coinciding with the onset of the train of flashes to 50 ms after the last flash. Although the firing rate of most cells (7/9) was reduced by activation of cortical fibers (Fig. 1.2B_2), other cells (2/9) showed no change or an increase in firing rate due to rebound spikes triggered by IPSPs.

We did not detect evidence for conventional fast excitatory synaptic responses elicited by photoactivation of cortical fibers in mitral cells, however, we observed small inward currents (average amplitude 15.1±3 pA, V_m=-80 mV, n=19) that preceded the onset of IPSCs (by 3.6±0.6 ms, n=6) and persisted in the presence of $GABA_A$ blockers (gabazine, 10 μM or picrotoxin, 100 μM). These evoked currents were blocked by

NBQX (12.9±4.5% of control, n=5) but had unusual properties including slow kinetics (10-90% rise time 6.7±0.9 ms, decay tau 36.3±1.1 ms, n=19), virtually no trial-to-trial amplitude variability (coefficient of variation 0.05 ± 0.01, n=19), and little sensitivity to membrane potential (7.5±2.7% reduction in amplitude from -80 mV to -40 mV, n=7) (Fig. S1.1). These responses were also observed in cells in which the primary apical dendrite was severed (n=3). Although we cannot rule out the possibility that these small responses reflect synaptic contacts that only occur onto electrotonically remote regions of lateral dendrites or axons, they could also reflect glutamate spillover from cortical fibers onto distal processes, intracellular detection of local field potentials, or gap junctional coupling with cells receiving direct synaptic input. Regardless of their exact origin, these small currents did not have an obvious effect on mitral cell excitability since they caused only weak membrane depolarization (0.3±0.1 mV at rest, n=9) and never elicited APs.

Cortical feedback drive direct excitation and feedforward inhibition of granule cells

Granule cells are thought to be the major target of direct excitation from cortical feedback projections (Strowbridge, 2009). Indeed, brief light flashes evoked EPSCs in GCs (Fig. 1.3A_1) with fast kinetics (10-90% rise time: 0.76±0.06 ms, decay tau: 1.49±0.08 ms, amplitude range:13 to 587 pA, n=20) and little jitter in their onset times (standard deviation (SD)=0.23 ±0.02 ms, n=20). Light-evoked EPSCs in GCs were abolished by tetrodotoxin (TTX, 1 μM, n=6) but were partially recovered following subsequent application of the K^+ channel blocker 4-aminopyridine (4-AP, 1 mM, n=5,

Fig. 1.3A_2). Consistent with previous studies (Petreanu *et al*., 2009), the synaptic response elicited in the presence of TTX and 4-AP indicates that we could trigger transmission via direct ChR2-mediated depolarization of boutons, however, the responses we observe under normal conditions reflect AP-mediated transmitter release from cortical fibers. Membrane depolarization (V_m=+40 mV) in the presence of picrotoxin (100 μM) revealed a slow NMDAR component to cortically-driven EPSCs that was abolished by APV (n=4), while the fast EPSCs were blocked by NBQX (n=7, Fig. 1.3A_3). The current-voltage relationship of the isolated AMPAR response was linear (n=5, Fig. 1.3A_4), indicating that AMPARs at cortical synapses on GCs are Ca^{2+}-impermeable (Hollmann and Heinemann, 1994).

We think it likely that GCs are a major source of cortically-evoked disynaptic inhibition onto mitral cells. Cell-attached recordings of GCs revealed that cortical input is sufficient to drive GCs to spike threshold (n=5, Fig. 1.3B_1). Furthermore, simultaneous whole-cell recordings indicated that the onset of evoked mitral cell IPSCs followed EPSCs in GCs with a disynaptic latency (3.2±0.4 ms, n=7, Fig. 1.3B_2). We also tested the relative contribution of glomerular layer interneurons to mitral cell inhibition. LED illumination was restricted to a spot (~150 μm diameter) and we compared the amplitude of IPSCs elicited when the photostimulus was over the GC layer versus when the illumination surrounded the glomerulus containing the dendritic tuft of the recorded mitral cell (filled with fluorescent indicator). Shifting the location of the photostimulus from the GC layer to the glomerular layer largely abolished light-evoked mitral cell IPSCs (Fig. 1.3C, 4.0±1.6% of GC layer response, n=6), indicating

that cortically-evoked mitral cell inhibition arises primarily from the GC layer. Taken together, these results are consistent with the idea that activation of cortical fibers is sufficient to elicit disynaptic inhibition onto mitral cells that results from AMPAR-mediated excitation of GCs.

Intriguingly, activation of cortical feedback projections also elicited feedforward IPSCs in GCs. $GABA_AR$-mediated IPSCs (recorded at the reversal potential for excitation) followed light-evoked EPSCs with a disynaptic delay (3.5±0.5 ms, n=14, Fig. 1.4A_{1-2}) and were completely abolished following application of glutamate antagonists (Fig. 1.4A_3). Short-latency feedforward inhibition plays an important role in regulating time windows for excitation (Pouille and Scanziani, 2001). Indeed, in current clamp recordings (V_m=-60 mV) of cells with a mixed EPSP-IPSP, blocking the disynaptic IPSP greatly prolonged the duration of cortically-evoked EPSPs (½width= 6.5±1.7 ms vs. 58.4±18.7 before and after gabazine, respectively) without effecting peak EPSP amplitude (110.4±7.7% of control, n=5, Fig. 1.4B). Although the amplitudes of light-evoked excitatory and inhibitory conductances were similar across the population of recorded GCs (average excitation (GE)=1.1±0.3 nS, inhibition (GI)=1.4±0.3 nS, n=42), the relative contribution of inhibition to the total conductance (GI/(GE + GI)) varied widely within individual cells (Fig. 1.4C). Anatomical reconstruction of dye-filled GCs did not reveal an obvious correlation between cell morphology and the excitation/inhibition ratio (n=7, data not shown). Heterogeneity in the relative amount of excitation vs. inhibition received by individual GCs suggests that cortical feedback inputs could have diverse effects: activation of the same cortical

fibers could cause a net increase in the excitability of some GCs while neighboring GCs are suppressed. We tested this idea by giving nearby (within 100 μm) GCs depolarizing current steps sufficient to elicit APs and interleaving trials with and without trains of light flashes. Indeed, we found that cortical fiber activation in the same region could either enhance or suppress AP firing in GCs (Fig. 1.4D_1). Although the majority of cells receiving light-evoked input responded with net excitation (7/12 cells, 3 slices), net inhibition was also observed (4/12 cells, Fig. 1.4D_2). Together, these results indicate that in addition to direct excitation, cortical projections drive feedforward inhibition of GCs and that the net effect of cortical input on individual GCs can vary between excitation and inhibition.

Cortical feedback projections preferentially target short axon cells

What circuit underlies cortically-evoked feedforward inhibition of GCs? Deep short axon cells (dSACs) in the GC layer are a heterogeneous class of GABAergic interneurons that mediate interneuron-selective inhibition: EM analysis indicates that dSAC terminals target GC dendrites but do not form synaptic contacts onto M/T cells (Eyre *et al*., 2008) and paired-recordings have shown that dSACs generate IPSCs onto GCs (Eyre *et al*., 2008; Eyre *et al*., 2009; Pressler and Strowbridge, 2006). However, the excitatory inputs governing the activation of dSACs are unclear. We targeted dSACs for recording based on the size of their cell bodies (>10 μm) and their multipolar morphology. Activation of cortical fibers elicited EPSCs with little onset jitter (SD=0.27±0.04 ms, n=10, Fig. 1.5A) indicating that, in addition to GCs, dSACs

are also a direct target of cortical feedback projections. We next made simultaneous recordings from dSACs synaptically connected to GCs (Fig. 1.5B_1, unitary conductance = 0.8 ± 0.4 nS, n=6) to probe the contribution of dSACs to cortically-evoked inhibition of GCs. Brief light flashes drove APs in dSACs that coincided with GC IPSCs. Interestingly, on interleaved trials in which the dSAC was hyperpolarized below spike threshold the amplitudes of light-evoked GC IPSCs were strongly attenuated (Fig. 1.5B_2). In all paired recordings, cortically-driven GC IPSCs were significantly smaller when the connected dSAC failed to fire APs (Fig. 1.5B_3, 71.7± 9.7% reduction, n=6, t-test, p=0.03). This suggests that relatively few dSACs contribute to cortically-evoked IPSCs in an individual GC. Furthermore, these results provide strong evidence that dSACs are a major source of the cortically-driven disynaptic inhibition of GCs.

We next considered whether cortical feedback projections preferentially target GCs or dSACs. To address this, we used simultaneous or sequential recordings from dSACs and GCs (within 300 μm) to compare the projections onto these two cell types. Surprisingly, dSACs consistently received stronger excitation than GCs (Fig. 1.5C, D). In all paired (12/12) or sequential (5/5) recordings, evoked EPSCs were larger in dSACs than GCs. Similar results were obtained in wild-type mice injected in PCx with an unconditional AAV-ChR2 construct, ruling out the possibility that these differences are unique to projections from Ntsr1-cre pyramidal cells (Fig. 1.5D). On average, the EPSC in dSACs (306±81 pA, n=17) was ~10 times larger than GCs (28±9 pA, n=17). This difference in EPSC amplitude could be due either to stronger unitary connections

between cortical fibers and dSACs or a higher convergence of cortical pyramidal cell axons onto dSACs.

To differentiate between these two possibilities, we determined the strength of single fiber connections onto both cell types using minimal optical stimulation. In these experiments, we reduced light intensity to the point at which clear failures of synaptic responses were observed on ≥50% of trials (Fig. 1.5E_1) and we measured the average amplitudes of successes in each cell. The average amplitude of the single-fiber EPSC was actually somewhat larger for inputs onto GCs compared to dSACs (29.8±4.6 pA and 17.0±3.8 pA for GCs (n=17) and dSACs (n=10), respectively; K-S test, $p = 0.04$, Fig. 1.5E_2). Together, these data suggest that dSACs receive stronger excitation than GCs due to a higher convergence of feedback inputs.

Glomerular layer targets of cortical feedback projections

In addition to their targets in the GC layer, the presence of cortical fibers in the glomerular layer suggests that additional classes of bulbar neurons receive cortical input. Therefore, we next explored how cortical feedback projections influence circuits in the glomerular layer by studying responses of three major classes of juxtaglomerular cells: principal external tufted (ET) cells, GABAergic superficial short axon cells (sSACs) and GABAergic periglomerular (PG) cells. ET cells lack lateral dendrites and receive excitation from olfactory sensory neurons as well as PG cell-mediated dendrodendritic inhibition on their apical dendritic tufts (Gire and Schoppa, 2009; Hayar *et al*., 2004). Similar to mitral cells, photoactivation of cortical fibers evoked

IPSCs onto ET cells with no evidence of direct excitation (n=6, Fig. 1.6A). Light evoked inhibition onto ET cells was disynaptic: IPSCs had high onset time jitter (SD=3.0±0.5 ms, n = 10) and were abolished by glutamate antagonists (APV, 50 μM + NBQX, 10 μM, n=3, 97±1% reduction). Light flashes elicited fast, monosynaptic EPSCs (onset time SD=0.31±0.05 ms, n=10) in PG cells (Fig. 1.6B) that were blocked by NBQX and APV (92±5% reduction, n=3), suggesting that PG cells are a likely source of disynaptic inhibition onto ET cells. sSACs are characterized by their exclusively periglomerular distribution of dendrites (Pinching and Powell, 1971a; Scott *et al*., 1987). Although the functional properties and sources of excitatory input to sSACs are not well understood, they are classically proposed to mediate inhibition of PG cells (Pinching and Powell, 1971b). We find that activation of cortical fibers elicits monosynaptic EPSCs (onset time SD=0.27±0.03 ms) in sSACs (Fig. 1.6C) mediated by glutamate receptors (97 ± 2% block by APV + NBQX, n=3). Recordings from neighboring (within 100 μm) sSACs (n=13) and PG cells (n=13) revealed that sSACs consistently receive stronger cortical input than PG cells (Fig. 1.6D). These findings suggest that cortical feedback could also modulate intra- and interglomerular signaling via inputs to multiple subtypes of glomerular interneurons.

Photoactivation of piriform cortex *in vivo*

The diversity of interneurons and local circuits under the control of cortical feedback projections (Fig. 1.6E) make it challenging to predict the role of cortical

activity on OB sensory processing. To address this issue, we studied how activation of PCx modulates odor responses in urethane-anesthetized mice.

We first established that we could effectively drive cortical activity *in vivo*. A craniotomy was performed to expose the ChR2-expressing anterior PCx and we used linear silicon probes to record local field potentials (LFPs) and unit activity. An LED fiber was positioned over the exposed cortical region and a long (4 s) ramping light stimulus was used to drive sustained activation of PCx. We chose this relatively unstructured stimulus because the ramp prevents the fast desensitizing transient of the ChR2 photocurrent and can initiate self-organized rather than externally-defined cortical activity patterns (Adesnik and Scanziani, 2010; Olsen *et al*., 2012). Consistent with previous findings in layer 2/3 of neocortex (Adesnik and Scanziani, 2010), this photostimulus generated rhythmic oscillation of the PCx LFP at gamma frequency (average 52.8 ± 4.3 Hz, n = 5 mice; Fig. 1.7B). LFP gamma oscillations were accompanied by an increase in the activity of simultaneously recorded single units, spiking coherently with the LFP at gamma frequency (Fig.1.7C). Furthermore, simultaneous recording of multiunit activity revealed that the light stimulus greatly enhanced AP firing in PCx ($p<0.005$, t-test, n=5 mice, Fig. 1.7D). Thus, under our conditions, photostimulation of pyramidal cells in layer 2/3 of PCx *in vivo* strongly increases population activity.

In a subset of experiments, we examined how photoactivation of layer 2/3 pyramidal cells influenced odor-evoked cortical activity. Odors (mixtures of three different monomolecular odorants, applied for 4 s at 30 s intervals) elicited LFP

oscillations in both the gamma (40-70 Hz) and beta (10-30 Hz) frequency ranges (Fig. 1.7E_1). However, when we coapplied odors with the photostimulus, the response resembled that of photostimulation alone: odor-evoked beta oscillations were abolished while photoinduced gamma oscillations dominated higher frequencies of the LFP (n=3 mice, Fig. 1.7E_2). Furthermore, co-application of odors and photostimulation consistently generated more AP firing compared to odors alone ($p<0.005$, t-test, n=15 odor-animal pairs, Fig. 1.7F,G). Thus, photoactivation uniformly increases PCx output both under basal conditions and in the presence of odors.

Driving cortical feedback *in vivo* amplifies inhibition in the OB

We next examined how photoactivation of PCx influences responses in the OB. A second craniotomy was made over the OB ipsilateral to the ChR2-expressing PCx and we recorded LFPs and unit activity in the mitral cell layer. We used a protocol in which cortical LED illumination either preceded or coincided with odor application on interleaved trials (Trial A, Trial B) to assess the effects of cortical activation on spontaneous and odor-evoked activity. Intriguingly, cortical photoactivation alone (A trials) caused a marked increase in OB LFP gamma oscillations ($p<0.005$, Holm test, n=10 odor-animal pairs, Fig. 1.8B_1, B_3). It has been proposed that synchronized reciprocal interactions between M/T and GCs underlie the generation of OB gamma oscillations (Rall & Shepherd, 1968). Our results indicate that gamma frequency cortical activity propagates to the OB and is sufficient to drive local gamma oscillations, presumably by synchronizing GC activity. As in cortex, odors elicited both

beta and gamma oscillations in the LFP under control conditions (A trials, $p<0.05$, Holm test, n=10, Fig. 1.8B_1, B_3). While odor-evoked gamma oscillations are thought to arise from reciprocal interactions between M/T cells and GCs, lesion studies suggest that beta oscillations additionally require a feedback loop involving cortical projections (Gray and Skinner, 1988; Martin *et al*., 2006; Neville and Haberly, 2003). Consistent with these studies, photostimulation that briefly disrupted odor-evoked beta oscillations in the cortex also acutely suppressed beta oscillations in the OB (B trials, $p<0.05$, Holm test, n=10, Fig. 1.8B_{2-3}).

Surprisingly, multi-unit recordings in the mitral cell layer revealed that cortical photostimulation had differential effects on spontaneous and odor-evoked M/T cell activity. Although spontaneous firing was not significantly affected by cortical activation ($p>0.05$), odor-evoked firing was consistently reduced ($p<0.001$, Wilcoxon signed-rank test, n=15 odor-recording site pairs, Fig. 1.8C_{1-2}). These results demonstrate that, under our conditions, cortical photoactivation preferentially reduces M/T cell population activity during the processing of sensory stimuli implying a synergistic effect between sensory input and cortical activity.

Because multi-unit activity is dominated by neurons with high firing frequencies, we determined the effect of cortical photostimulation on isolated single units whose average firing rates varied over a large range. At the single unit level, M/T cell odor-evoked responses varied from clear excitation (Fig. 1.8D_1) to pure decreases in firing due to lateral inhibition (Fig. 1.8D_2). Cortical photoactivation both reduced odor-evoked increases in firing (Fig. 1.8D_1) and augmented odor-evoked inhibitory

responses (Fig. 1.8D_2) in individual cells. The simplest interpretation of these effects is that cortical activation enhances recurrent and/or lateral inhibition. Across the population of M/T cell single units (n=40 odor-unit pairs, 7 mice), cortical photostimulation could both increase and decrease spontaneous firing rate (Fig. 1.8E_1, Fig. S1.2). In contrast, cortical activation consistently led to decreases in firing rates in the presence of odor stimuli ($p>0.05$ and $p<0.001$ for spontaneous and odor-evoked activity respectively, Wilcoxon signed-rank test, Fig. 1.8E_2). To confirm that cortical activity suppressed odor-responses independently of whether odors increased or decreased firing rate, we calculated an odor modulation index (OMI, $(R_{odor} - R_{baseline})/(R_{odor} + R_{baseline})$ where R_{odor}=firing rate during 4 s odor application, $R_{baseline}$=rate during first 2 s of each trial (Eliades and Wang, 2008)) for each odor-cell pair. Thus, OMI measures the relative change in firing rate during odor application compared to baseline conditions and ranges from -1 (complete suppression of activity) to +1 (strongly driven responses). Indeed, this analysis showed that photostimulation had a suppressive action on odor responses regardless of whether the firing rate of individual odor-cell pairs was increased ($p<0.001$, n=22) or decreased ($p<0.05$, n=18) by the odor alone (Wilcoxon signed-rank test, Fig. 1.8F).

We also asked whether there was any relationship between the effects of cortical activation on spontaneous and odor-evoked responses within individual cells. To address this, we calculated a light modulation index (LMI, $(R_{LED} - R_{Control})/(R_{LED} + R_{Control})$ where R_{LED}=average firing rate with photostimulation, $R_{Control}$=average rate without photostimulation) to compare the relative effects of cortical activation on both

spontaneous and odor-evoked firing for each odor-cell pair (LMI ranges from -1 for complete suppression of firing by photostimulation, to +1 indicating strong enhancement of the response). This analysis revealed little correlation ($r=0.5$, Spearman's correlation coefficient) between the effects of photostimulation on spontaneous activity and responses to odors within individual cells (Fig. 1.8G). However, across the population of M/T cells, the effect of cortical activation on odor-modulated activity was significantly greater than that on spontaneous activity ($p<0.05$, Wilcoxon signed-rank test). Thus, the effect of cortical feedback on M/T cell activity is context-dependent such that cortical activity preferentially suppresses M/T cell responses during sensory stimulation.

In additional recordings, we considered whether the cortical modulation of M/T cell activity was related to features of the sensory stimulus. We investigated whether the cortical suppression of M/T cell responses depended on odor identity by examining M/T single units tested with three different odors at matched concentrations (50 ppm, Fig. S1.2). Across this cell population (n=35 single units, 9 mice), cortical activation significantly suppressed odor-evoked M/T cell activity ($p<0.001$, Wilcoxon signed-rank test). However, the proportion of M/T cells in which odor responses were selectively modulated (suppression of responses to only one or two of the tested odors vs. suppression of responses to all three odors) was not significant (Fig. S1.2). Thus, under our conditions, the effects of cortical feedback on M/T cell responses were not highly specific to particular odors.

We next asked whether the actions of cortical feedback on odor-evoked M/T cell responses depended on odor intensity by examining responses of cells (n=30 single units, 12 mice) to the same odor at three different concentrations. Indeed, we found that cortical stimulation caused a significant suppression of M/T cell activity when odors were applied at concentrations of 10 and 50 ppm ($p<0.05$), but not when odors were present at a much lower concentration of 2 ppm (Fig. 1.8H). This result is consistent with the idea that the cortical suppression of M/T cell responses depends on sufficient levels of bulbar sensory input. Taken together, these data indicate that cortical feedback regulates sensory information processing in the OB primarily by acting as a gating mechanism that enhances odor-evoked M/T cell inhibition.

Discussion

Here we use an optogenetic approach to show that cortical feedback projections target diverse populations of interconnected OB interneurons. We show that activation of cortical fibers can drive disynaptic inhibition of mitral cells via fast, AMPAR-mediated excitation of GCs. However, activation of cortical fibers also elicits disynaptic feedforward inhibition of GCs and the effects of cortical activity on AP firing in GCs could vary from excitation to inhibition. Cortically-evoked inhibition of GCs results from dSACs that receive a higher convergence of inputs from cortical projections than GCs. Despite the potential for opposing actions on interneuron circuits, *in vivo* recordings reveal that the major effect of activating cortical feedback projections on M/T cells is to accentuate odor-evoked inhibition and reduce AP firing

during the processing of sensory input.

Functional properties of cortical feedback projections

We find that cortical feedback projections elicit mitral cell disynaptic inhibition that differs from classical dendrodendritic inhibition triggered by mitral cell activity. First, while mitral cell recurrent and lateral dendrodendritic inhibition is due to a long-lasting (many hundreds of ms) barrage of asynchronous IPSCs (Isaacson and Strowbridge, 1998; Schoppa *et al*., 1998; Urban and Sakmann, 2002) activation of cortical fibers evokes short-latency inhibition with a briefer time course (<100 ms). Second, recurrent and lateral dendrodendritic inhibition typically requires the activation of GC NMDARs (Chen *et al*., 2000; Isaacson and Strowbridge, 1998; Schoppa *et al*., 1998), while cortically-evoked IPSCs are insensitive to NMDAR antagonists and require AMPAR activation. Our results suggest that GCs are the likely source of cortically-evoked mitral cell inhibition. Cortical projections evoke short latency APs in GCs and fast (<2 ms) EPSCs mediated by Ca^{2+}-impermeable AMPARs. Although NMDARs are also present at GC cortical synapses, AMPAR-mediated transmission is sufficient to drive AP-dependent fast mitral cell inhibition.

We also show that when mitral cells are suprathreshold, fast cortically-driven IPSPs can both transiently suppress mitral cell APs and elicit rebound firing. Previous studies found that while small, brief IPSPs promote rebound spiking in mitral cells, larger hyperpolarizations due to summating IPSPs have a purely inhibitory action (Balu and Strowbridge, 2007; Desmaisons *et al*., 1999). Thus, cortically-driven IPSPs may

exert bidirectional control of mitral cell firing: small, phasic IPSPs could promote synchronization of APs in ensembles of mitral cells by triggering rebound spikes, while stronger IPSPs due to widespread activation of GCs by cortical input could inhibit large ensembles of mitral cells.

In addition to direct excitation, activation of cortical feedback projections evoked short-latency, disynaptic inhibition of GCs. Previous studies have found that dSACs are a heterogeneous class of interneurons that mediate axo-dendritic inhibition of GCs (Eyre *et al*., 2008; Eyre *et al*., 2009; Pressler and Strowbridge, 2006), however, the sources of excitatory input to dSACs have not been identified. We identified dSACs as the source of cortically-evoked disynaptic inhibition onto GCs and show that individual dSACs integrate excitatory input from a larger population of pyramidal cells than individual GCs. This preferential targeting suggests that dSACs could receive broadly-tuned cortical excitation, while GCs receive cortical excitation that is much more odor selective. One intriguing scenario is that individual GCs receive cortical input specifically from pyramidal cells whose odor tuning matches that of the reciprocally connected mitral cells.

Why do GCs receive feedforward inhibition from the cortex? In the simplest case, it ensures a brief time window for the integration of excitation. Indeed, while disynaptic inhibition strongly limits the duration of the cortically-evoked EPSP, its peak amplitude is unaffected due to the fast kinetics of the underlying EPSC. Thus, feedforward inhibition should enable GC excitation to be precisely time-locked to cortical input. Surprisingly, we found a marked heterogeneity across GCs in the relative

balance of excitation and inhibition evoked by cortical projections. Although most GCs receiving cortically-evoked responses were excited, a smaller fraction responded with net inhibition. This was observed in nearby GCs in which the same fiber population was activated, ruling out that the heterogeneity is simply due to differences in ChR2-expressing axons across experiments. The differences in excitation/inhibition ratio could reflect the fact that the GC population is continually being renewed by postnatal neurogenesis (Lledo *et al*., 2006). Activity-dependent processes that vary over the different lifetimes of individual cells may modulate the balance of excitatory and inhibitory connections.

In addition to targeting interneurons in the GC layer, we also show that cortical feedback projections influence circuits in the glomerular layer. While ET cells received disynaptic inhibition, cortical fibers produced direct excitation of both sSACs and PG cells. We found that cortical fibers drove stronger excitation of sSACs compared to PG cells, recapitulating the differential connectivity of cortical projections made onto dSACs and GCs. PG cells and ET cells are thought to regulate glomerular excitation via reciprocal dendrodendritic inhibition (Hayar *et al*., 2004; Murphy *et al*., 2005) and this intraglomerular circuit is proposed to gate "on/off" signaling from individual glomeruli (Gire and Schoppa, 2009). While the axonal targets and functional role of sSACs is a source of debate (Kosaka and Kosaka, 2011), they are generally thought to provide a mechanism for long-range interglomerular inhibition. Thus, in addition to modulating M/T cell inhibition via GCs, cortical feedback also has the capacity to shape intra- and interglomerular signaling that contributes to M/T cell

excitability. Our results are in general agreement with a study showing that feedback projections from another olfactory cortical region, the AON, target diverse types of OB neurons (Markopoulous *et al*., 2012). Differences in the functional effects of feedback projections in the two studies suggest that the AON and PCx may preferentially influence different OB circuits.

.

Optogenetic stimulation of piriform cortex *in vivo*

We studied how cortical feedback modifies OB activity *in vivo* using photoactivation of ChR2-expressing pyramidal cells in anterior PCx. We used a sustained light pulse that induced LFP oscillations and pyramidal cell firing in the gamma frequency range. Thus, rather than imposing a particular temporal structure to the cortical stimulus, we let the cortical network dictate its own inherent pattern of activity (gamma frequency output) to the OB. In contrast, trains of brief light pulses (like conventional extracellular stimulation) would drive highly synchronous cortical activity entrained to the frequency of the light stimulus. Trying to select optimal stimulation parameters based on their physiological relevance is challenging, however, given that odors drive gamma oscillations in the PCx, we think our choice of photostimulus is reasonable.

Impact of cortical feedback *in vivo*

We show that ChR2-mediated depolarization of pyramidal cells generates intrinsic gamma activity in the cortex that propagates to the OB and disrupts odor-

evoked beta oscillations in both brain regions. Odors evoke gamma and beta frequency LFP oscillations that are synchronous between the PCx and OB (Neville and Haberly, 2003) and the synchronization of neuronal activity during oscillations is suggested to contribute to odor coding (Laurent, 2002). When triggered by odors, gamma oscillations appear to originate in the OB and are relayed via the LOT to the cortex, while beta oscillations require reciprocal interactions between bulb and cortex (Gray and Skinner, 1988; Martin *et al*., 2006; Neville and Haberly, 2003). Our results suggest that gamma oscillations in the bulb can also arise from feedback projections that convey gamma activity intrinsically-generated from the olfactory cortex. It has been proposed that odor-evoked beta oscillations could result either from a M/T cell□pyramidal cell□GC loop or from intrinsic beta activity in cortex that is relayed back to the bulb (Neville and Haberly, 2003). Although we cannot exclude the possibility that the PCx could generate intrinsic beta oscillations under some conditions, our finding that ChR2-driven depolarization generates intrinsic gamma activity are most consistent with the idea that odor-evoked beta oscillations result from a feedback loop involving coordinated activity of M/T cells, pyramidal cells, and GCs.

Although activating PCx *in vivo* under our conditions had variable effects on spontaneous M/T cell activity, it consistently reduced M/T cell firing during odor stimulation. The effects of cortical activation on M/T cell responses were also sensitive to odor concentration, consistent with the notion of a synergistic effect between sensory input and cortical activity. The increases and decreases in spontaneous activity across different M/T cells suggests that cortically-evoked disynaptic inhibition is sufficient to

suppress spontaneous firing in some M/T cells, while others show a net increase in firing presumably due to IPSP-triggered rebound spikes or "disinhibition" mediated by dSACs. The major effect of cortical activation on M/T cell odor responses was a reduction in odor-evoked excitation and an enhancement of odor-evoked inhibition. The augmentation of purely inhibitory responses further implies that cortical activity amplifies lateral inhibition during sensory processing in the OB.

Although cortical fibers target multiple classes of interneurons in the OB, we suspect that cortically-driven GC excitation plays a dominant role during odor processing. In brain slices, tetanic stimulation of the GC layer (Chen *et al*., 2000; Halabisky and Strowbridge, 2003) or anterior PCx (Balu *et al*., 2007) has been shown to facilitate mitral cell-evoked recurrent and lateral inhibition. Thus, cortical excitatory input onto GC proximal dendrites could contribute to the relief of the Mg^{2+} block of NMDARs at distal dendrodendritic synapses and boost or "gate" inhibition onto mitral cells (Balu *et al*., 2007; Halabisky and Strowbridge, 2003; Strowbridge, 2009). Our *in vivo* findings that cortical input preferentially drives OB inhibition during sensory processing are in good agreement with this gating model. However, we do not rule out a contribution of glomerular layer interneurons to the enhancement of odor-evoked inhibition.

While GC-mediated inhibition contributes to odor discrimination (Abraham *et al*., 2010), the role of lateral inhibition in odor coding is controversial. Although it has been proposed to sharpen the odor tuning of M/T cells belonging to individual glomeruli in a center-surround fashion (Yokoi *et al*., 1995), this requires a chemotopic

map such that glomeruli that respond to similar odorant features are spatially clustered. However, studies have highlighted the lack of a fine scale glomerular chemotopic map and found that M/T cells are not preferentially influenced by nearby glomeruli (Fantana *et al*., 2008; Soucy *et al*., 2009). Rather than exerting local actions, lateral inhibition could underlie a more uniform reduction in the activity of M/T cells across all glomeruli and act as a gain control mechanism (Soucy *et al*., 2009). Furthermore, even "global" lateral inhibition that reduces activity in all M/T cells such that fewer in total are active could enhance odor discrimination by decorrelating activity patterns (Arevian *et al*., 2008; Cleland and Linster, 2012; Wiechert *et al*., 2010).

Our results imply that odor representations in the OB are dynamically regulated by brain state. Although we studied anesthetized mice, in awake and behaving animals higher overall levels of cortical activity should lead to enhanced odor-evoked recurrent and lateral inhibition and an increase in the sparseness of M/T cell odor representations. Thus, cortical feedback is poised to play an important role in shaping the initial stages of odor information processing in the brain.

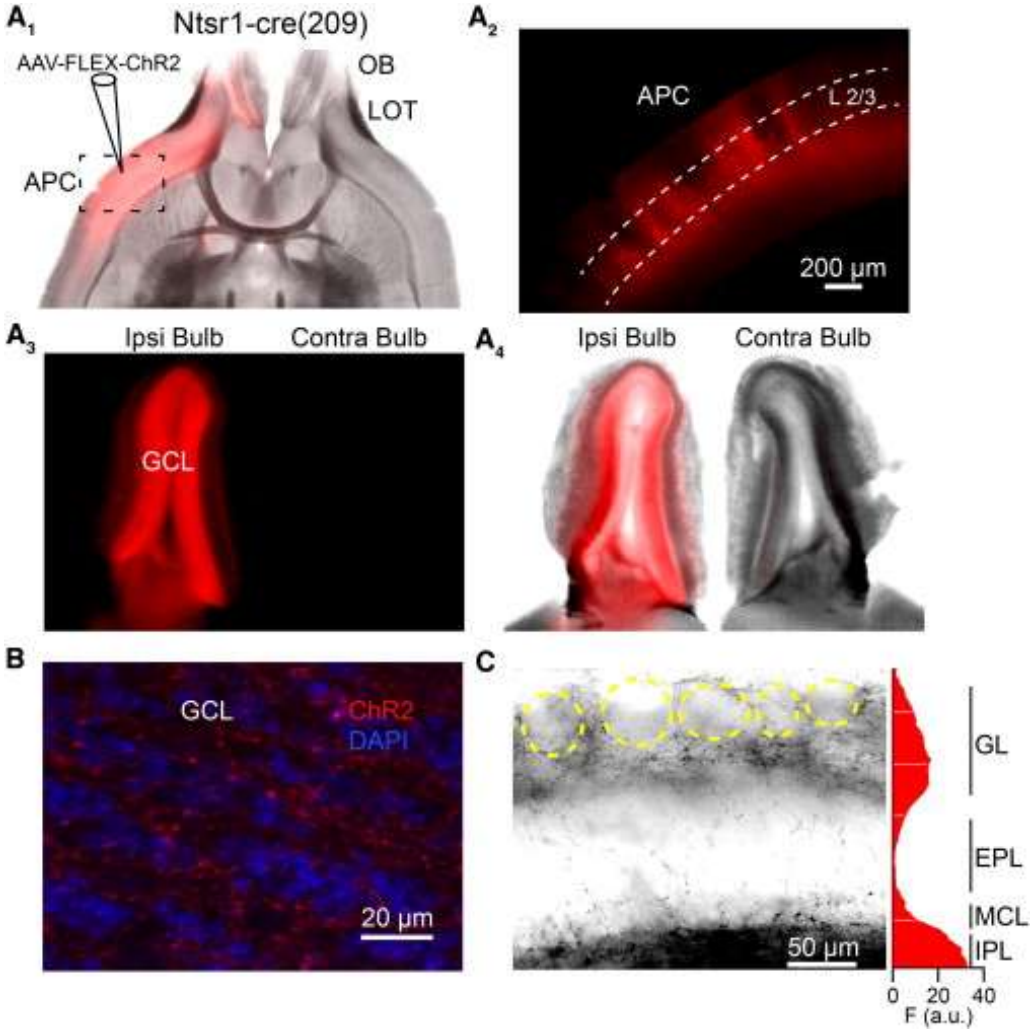

Figure 1.1 Conditional expression of channelrhodopsin-2 (ChR2) in piriform cortex pyramidal cells reveals cortical feedback projections to the olfactory bulb. A_1, Overlay of bright-field and fluorescence (red) image of a horizontal section (300 µm) of forebrain from an Ntsr1-cre mouse showing ChR2-mCherry expression in olfactory cortex. APC, anterior piriform cortex; OB, olfactory bulb; LOT, lateral olfactory tract. A_2, Blow-up of region in A_1 indicating expression of ChR2 in layer 2/3 pyramidal cells. A_3, ChR2 is expressed in the ipsilateral, but not contralateral OB from the same mouse. GCL, granule cell layer. A_4, Overlay of fluorescence and bright field images of the bulbs. B, 2-photon image (30 µm z-projection) of ChR2-mCherry in the GCL of a slice counterstained with DAPI. C, Left, Gray-scale fluorescence image of ChR2-mCherry (black) in a slice (300 µm) indicating few fibers in the mitral cell layer (MCL) and external plexiform layer (EPL), but numerous fibers and varicosities surrounding glomeruli (yellow circles). Right, average fluorescence intensity (F, arbitrary units) along the vertical axis of the image. IPL, internal plexiform layer; GL, glomerular layer.

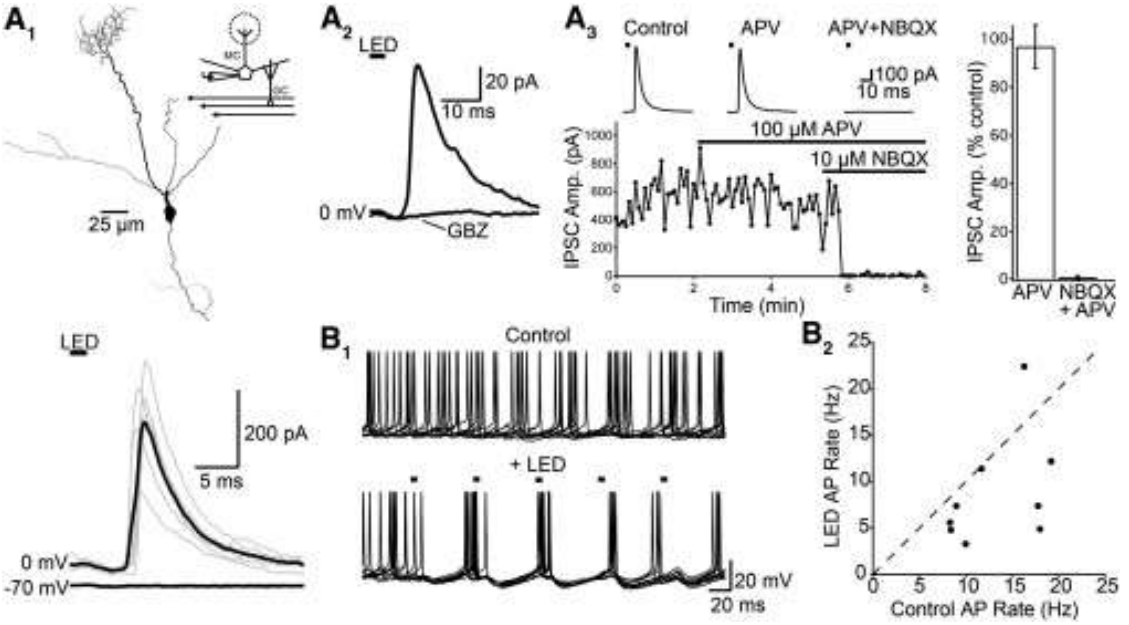

Figure 1.2 Cortical feedback drives disynaptic inhibition of M. A_1, Anatomical reconstruction (top) and voltage clamp recording (bottom) of a mitral cell. Brief LED flashes (4 ms, black bar) evoke IPSCs at 0 mV (gray: individual trials, black: average). *Inset:* Recording schematic. A_2, Light-evoked IPSCs are blocked by gabazine (GBZ, 10 µM). A_3, Light-evoked IPSCs are driven by AMPARs. Left, Time course of one experiment (bottom) and traces (top) showing that the IPSC is unaffected by APV (100 µM) but abolished following subsequent application of NBQX (10 µM). Right, Summary of the effects of APV alone (n=4) and coapplication of APV and NBQX (n=11) on IPSCs. B_1, Disynaptic IPSPs can reduce mitral cell firing. Current clamp recordings of a mitral cell depolarized to fire APs under control conditions (top) and on interleaved trials with a train of LED flashes (5 pulses, 20 Hz). Ten trials superimposed for each condition. B_2, Summary of the effects of light-evoked IPSPs (LED AP Rate) on firing (Control AP rate, n=9 cells). Each point represents one cell.

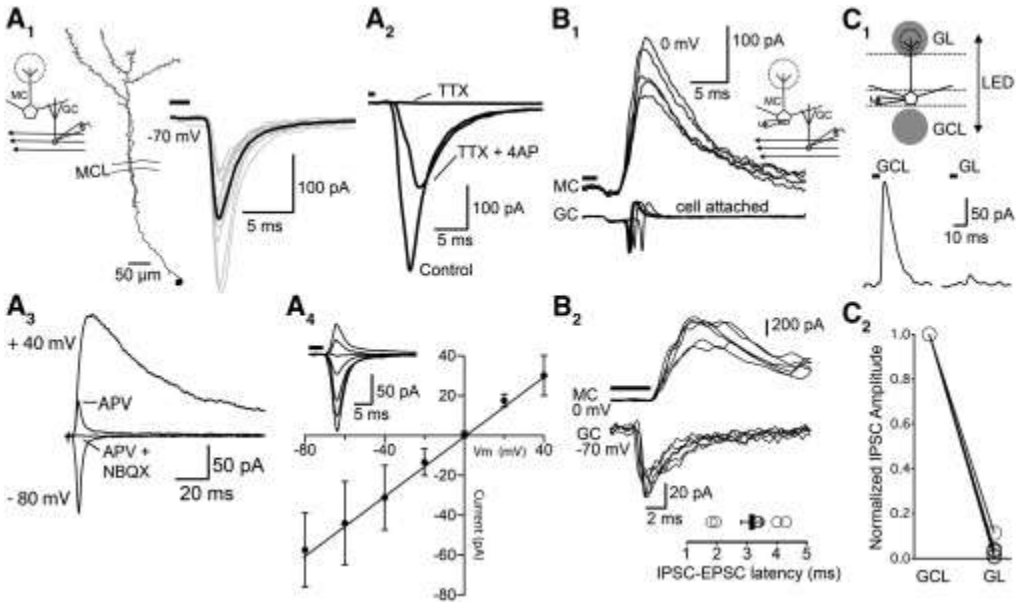

Figure 1.3 Cortical feedback directly excites granule cells (GCs). A_1, Anatomical reconstruction (left) and voltage clamp recording (V_m=-70 mV) (right) of a GC receiving light-evoked EPSCs. Bar, LED illumination. MCL, mitral cell layer. *Inset:* Recording schematic. A_2, Light-evoked GC EPSCs are blocked by TTX (1 µM) and partially recovered by application of 4-AP (1 mM). A_3, EPSCs have both AMPAR and NMDAR components. In the presence of picrotoxin (100 µM), depolarization to +40 mV reveals a slow current blocked by APV (100 µM). Subsequent addition of NBQX (20 µM) abolishes the fast EPSC. A_4, Current-voltage relationship of the AMPAR EPSC (in the presence of APV) is linear (n=5 cells). *Inset:* EPSCs from a representative cell. B_1, Simultaneous voltage clamp recording of a mitral cell (0 mV) and cell-attached recording of a GC show that light-evoked GC APs overlap with mitral cell inhibition B_2, Simultaneous voltage clamp recording of a mitral (0 mV) and granule (-70 mV) cell reveal that the onset of cortically-driven EPSCs precedes that of mitral cell IPSCs. *Bottom*, IPSC-EPSC latencies (n=7 cell pairs). C_1, Recording schematic (top) and light-evoked responses from a mitral cell (bottom, 0 mV) when illumination was directed to the GC layer (GCL) or the glomerular layer (GL). C_2, Summary data (n=6 cells) shows that shifting photostimulation to the glomerular layer reduces the amplitude of light-evoked IPSCs.

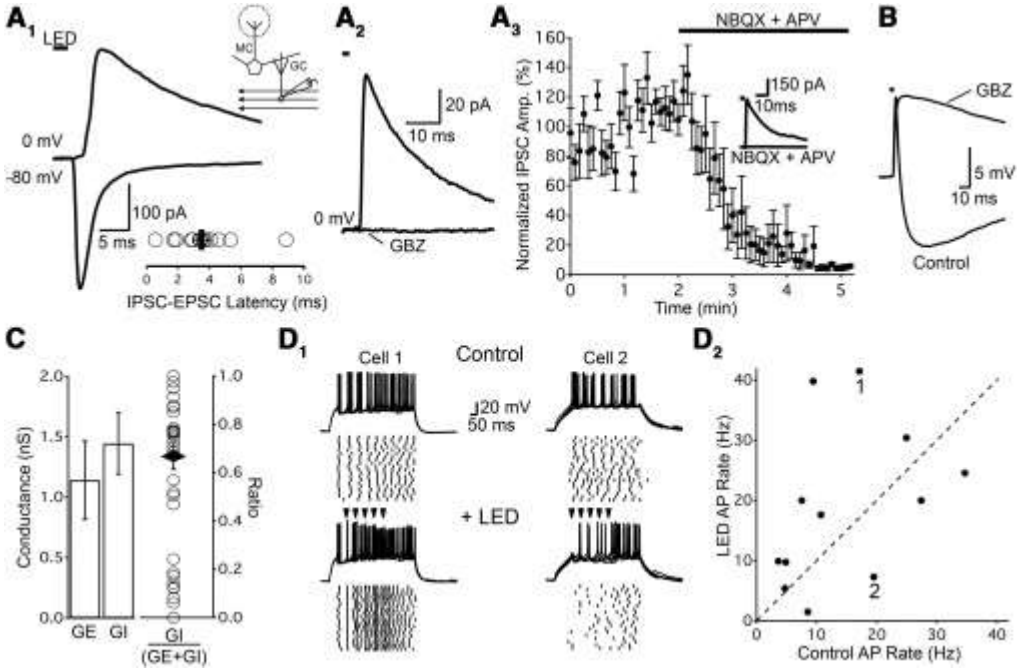

Figure 1.4 Cortical feedback drives disynaptic feedforward inhibition of granule cells (GCs). A_1, GC voltage clamp recording illustrating a light-evoked EPSC (-80 mV) and short-latency IPSC (0 mV). *Inset,* Latency between the IPSC and EPSC onset (circles, n=14 cells; bar, mean). A_2, Light-evoked IPSCs (V_m=0 mV) in GCs are abolished by gabazine (10 μM, GBZ). A_3, IPSCs are abolished by glutamate receptor antagonists (NBQX ,10 μM and APV, 100 μM, n = 8). *Inset:* responses from a representative cell (V_m= 0 mV). B, Current clamp recording of a GC (-60 mV) showing that disynaptic inhibition limits the time course, but not the amplitude of the cortically-evoked EPSP. C, *Left:* Average inhibitory (GI) and excitatory (GE) conductances in the same cells (n=42) evoked by photostimulation. *Right:* GI relative to total conductance was highly variable across individual cells (circles: individual cells; black diamond: mean ± SEM). Only cells with GI or GE >0.5 nS are included. D_1, Photoactivation of cortical fibers can lead to net increases or decreases in excitability in neighboring GCs. Traces show superimposed responses (5 consecutive trials) to depolarizing current injection (50 pA) on interleaved trials with (+LED) and without (Control) a train of 5 light pulses at 20 Hz (arrowheads). Rasters show APs for 20 trials. Cell 1 responded to activation of cortical fibers with an increase in firing during the LED train while Cell 2 showed a decrease in firing. D_2, AP rate of cells (n=12) measured during the train of LED stimuli show that cortical input increased firing in the majority of cells while some cells were inhibited. Cells shown in D_1 are indicated.

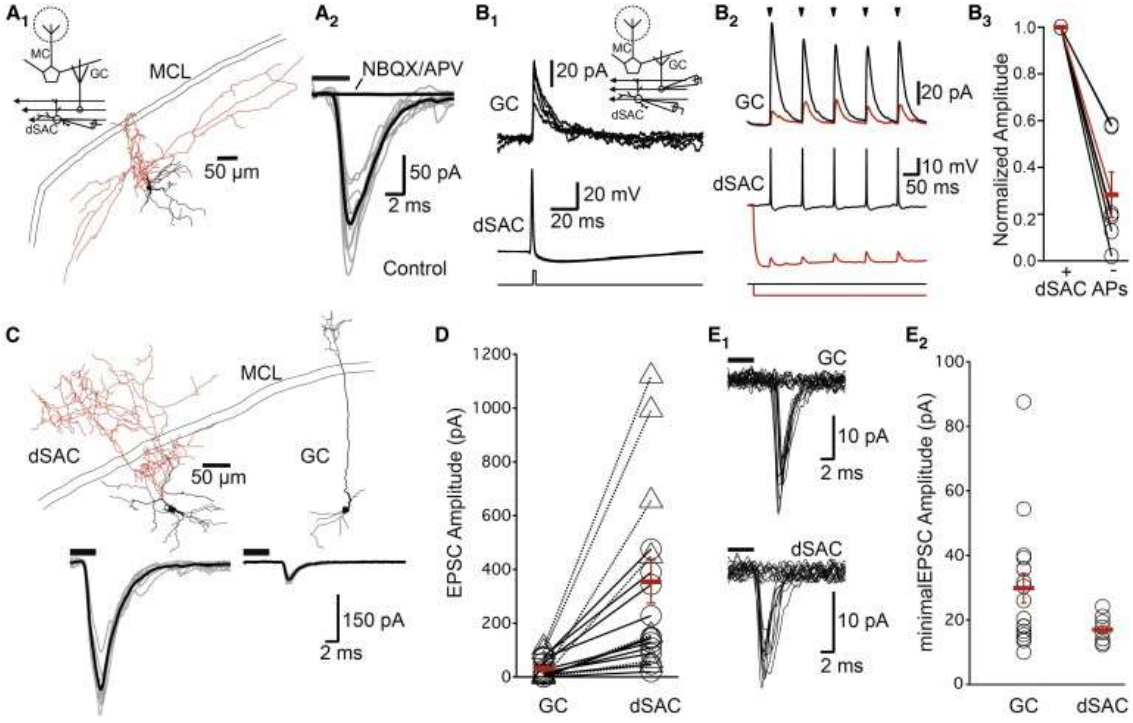

Figure 1.5 Deep short axon cells (dSACs) mediate disynaptic inhibition of granule cells (GCs) and receive a higher convergence of cortical feedback projections. A_1, Anatomical reconstruction of a dSAC (dendrites in black, axon in red, MCL, mitral cell layer). *Inset:* recording schematic. A_2, Light-evoked EPSCs (V_m=-70 mV) from the cell in A_1 before (Control) and after application of NBQX and APV. B_1, Simultaneous recording of a connected dSAC-GC pair. A current step triggers an AP in the dSAC (bottom), and a short-latency IPSC in the voltage-clamped GC (V_m=-50 mV). B_2, Recording from another connected dSAC–GC pair shows GC IPSCs (top, V_m=0 mV) and dSAC membrane potential (bottom) in response to a train of light flashes (arrowheads). Traces show responses under control conditions (black) and on interleaved trials when hyperpolarizing current was applied to prevent light-evoked APs in the dSAC (red). B_3, Light-evoked GC IPSCs are consistently smaller when the connected dSAC does not fire spikes (-dSAC APs, n=6 pairs). C, *Top*, Anatomical reconstruction of a simultaneously recorded dSAC and GC. *Bottom*, light-evoked EPSCs (V_m=-70 mV) are larger in the dSAC than the GC. D, Summary showing that light-evoked EPSCs are larger in dSACs than GCs from the same slices. Circles, pairs from Ntsr1-cre animals; triangles, pairs from wild-type animals expressing ChR2 unconditionally. Mean ± SEM shown in red. E_1, Minimal optical stimulation of a GC (top) and dSAC (bottom) reveal clear distinction between failures and single-fiber EPSCs (20 traces superimposed, V_m=-70 mV). E_2**,** The average single fiber EPSC amplitude (red bar) is similar between the cell types, suggesting dSACs receive a higher convergence of cortical inputs.

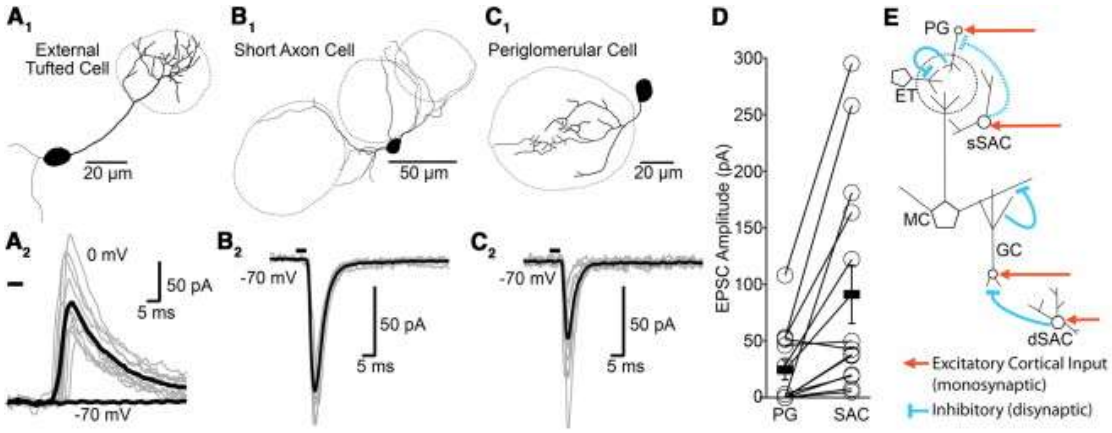

Figure 1.6 Cortical feedback projections activate circuits in the glomerular layer. A, Cortical feedback projections drive disynaptic inhibition of external tufted (ET) cells. A_1, Anatomical reconstruction of an ET cell. A_2, Voltage clamp recording from the cell in A_1 at -70 mV and 0 mV reveal that activation of cortical fibers elicits IPSCs. B, Cortical feedback projections provide direct excitatory input to superficial short axon cells (sSACs) B_1, Reconstruction of an sSAC. B_2, Light-evoked EPSCs (-70mV) from the same cell. C, Cortical feedback inputs provide direct excitation to periglomerular (PG) cells. C_1, Reconstruction of a PG cell. C_2, Light evoked EPSCs recorded in voltage clamp (-70 mV) from the same cell. D, Recordings from sSAC-PG cell pairs reveal that sSACs receive stronger excitation than PG cells. Bars, mean amplitudes of EPSCs. E, Circuit diagram illustrating OB neurons receiving direct excitation (red) and disynaptic inhibition (blue) elicited by cortical feedback projections. Dashed blue line is putative inhibitory connection. MC, mitral cell; GC, granule cell.

F**igure 1.7** Photoactivation of pyramidal neurons expressing ChR2 *in vivo* drives a sustained increase in gamma-synchronized firing in piriform cortex. A, Recording schematic and circuit diagram. A subset of layer 2/3 neurons express ChR2 (red). B, Photoactivation generates gamma oscillations. (Top) LFP trace during LED illumination. (Bottom) Average spectrogram (20 trials) from the same experiment. The trapezoid and white box indicate the period of LED illumination. White bar, period from which the trace was derived. C, Photoactivation drives gamma frequency firing of pyramidal cells. C_1, Raster plot of light-evoked firing of a single unit. C_2, Spike-LFP coherence for the same unit during baseline (grey) and LED (red) periods. Shaded regions, 95% confidence intervals. *Inset*, Spike-triggered average LFP. D, Summary results show that photostimulation causes a marked increase in AP firing. Pooled histogram of multi-unit activity (MUA), grey shading indicates +/- SEM. E, Photoinduced cortical gamma activity abolishes odor-evoked beta oscillations. Representative experiment showing the effects of odor and combined odor + LED stimulation on LFP activity. Example LFP traces (top) and average spectrograms (bottom). White boxes indicate the odor or odor+LED period and white bars the extent of the example LFP traces. Trapezoid and rectangle indicate LED and odor timing, respectively. E_1, Average spectrogram of LFP activity during odor application alone. E_2, Average spectrogram of LFP activity during interleaved trials with odor + LED. F, Summary results of the effect of photoactivation on firing activity in cortex during odor stimulation. Pooled MUA histogram averaged across odors (n=3 mice). Normalized activity in response to odors alone (grey) and odors+LED (red) plotted with shaded regions representing +/- SEM. G, MUA scatter plot of normalized firing rates for odors alone vs. odors+LED periods show that photoactivation increases AP output. Symbol shapes correspond to distinct odors (n=15 odor/animal pairs). Diagonal represents unity line.

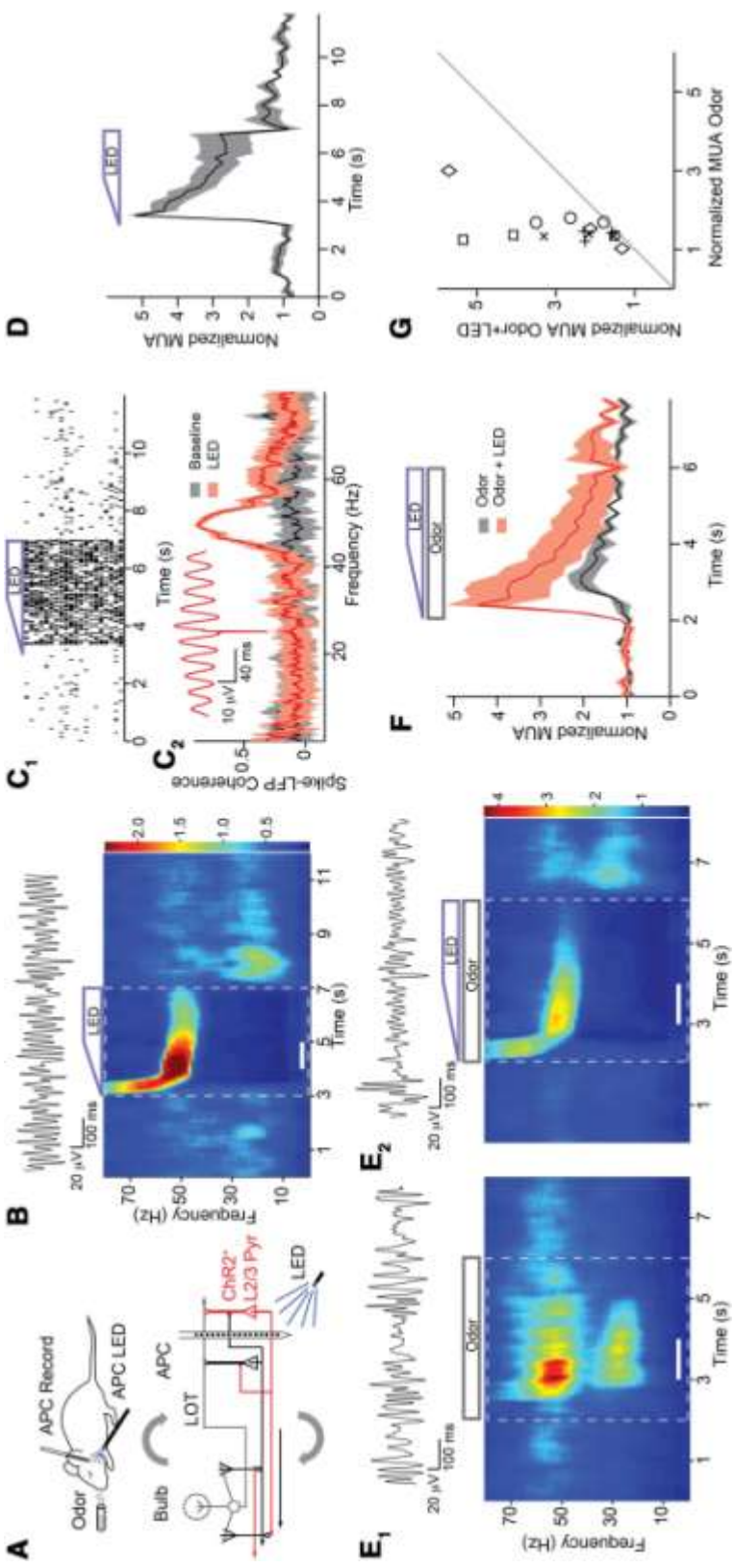
A
APC Record
APC LED
Odor
APC
LOT
Bulb
ChR2+
L2/3 Pyr
LED
B
LED
20 μV
100 ms
Frequency (Hz)
Time (s)
C1
LED
Time (s)
C2
Baseline
LED
10 μV
40 ms
Spike-LFP Coherence
Frequency (Hz)
D
LED
Normalized MUA
Time (s)
E1
Odor
20 μV
100 ms
Frequency (Hz)
Time (s)
E2
LED
Odor
20 μV
100 ms
Time (s)
F
LED
Odor
Odor
Odor + LED
Normalized MUA
Time (s)
G
Normalized MUA Odor+LED
Normalized MUA Odor

Figure 1.8 Activation of piriform cortex *in vivo* amplifies odor-evoked inhibition in the olfactory bulb. A, Recording schematic and circuit diagram. B, Photoinduced gamma activity in cortex propagates to the bulb and disrupts beta oscillations. On interleaved trials, cortical photostimulation preceded (B_1, Trial A,) or was coincident (B_2, Trial B) with odor application. B_1, (Top) LFP trace during odor application. (Bottom) Average spectrogram when cortical LED illumination (blue trapezoid) preceded odor application (grey box) for Trial A. B_2, (Top) LFP trace during coincident cortical photostimulation and odor application. (Bottom) Average spectrogram when LED illumination was coincident with odor application for Trial B. White bounding boxes represent periods over which spontaneous and odor-evoked LFP activity are calculated and white bars indicate periods used for LFP traces. B_3, Summary results showing that cortical photoinduced gamma activity reduces odor-evoked beta oscillations. Spectral power in the beta (10-30 Hz) and gamma (40-70 Hz) bands for the effects of photostimulation alone (Spont. + LED, Trial A), odor alone (Odor, Trial A), and Odor + LED (Trial B). LFP power is normalized to the 4 s period in Trial B when LED and odor stimulation was absent (* $p<0.05$ relative to control, # $p<0.05$ for pairwise comparisons). C, Cortical photostimulation reduces odor-evoked M/T cell firing but has minimal effects on spontaneous activity. C_1, Example of multi-unit activity from one experiment. Peristimulus time histograms (PSTHs) of firing rate under control conditions (black) and with LED illumination (red) reveal a selective suppression of odor-evoked but not spontaneous firing. C_2, Summary data of multi-unit activity showing that cortical photoactivation had variable effects on spontaneous firing but significantly suppressed odor-evoked activity (* $p<0.001$). D, Recordings from M/T cell single units reveal that cortical photostimulation reduces odor-evoked increases in firing and enhances odor-evoked inhibition. D_1, Odor-activated unit. (Top) Raster of AP firing on interleaved trials (Trial A, Trial B) are segmented to show spontaneous (left) and odor-evoked activity (right) under control conditions (black) and during photostimulation (red). Trapezoids and gray shading indicating timing of LED and odor stimulation, respectively. (Bottom) PSTHs under control conditions (black) and with LED illumination (red). D_2, Odor-inhibited unit. E, Raw AP rates of single units with (LED on) and without (LED off) photostimulation (n=40 units). E_1, LED activation of cortex has variable effects on spontaneous firing. E_2, Cortical activation consistently reduces firing during odor-evoked responses. F, Cortical activation suppresses firing rate independent of whether odor-evoked responses were excitatory or inhibitory. Scatter plot of odor modulation index (OMI) for single units. Odor-inhibited (blue, OMI<0) (n=18) and excited (green, OMI>0) (n=22) units are both affected by cortical stimulation. G, Little correlation between the effects of cortical activation on spontaneous and odor-evoked activity. Scatter plot of light modulation index (LMI), calculated for spontaneous and odor periods, quantifying the effect of the LED on firing rates for inhibited (blue) (n=18) and excited (green) (n=22) units. Horizontal and vertical grey lines and labels define quadrants categorically. H, Suppression of M/T cell responses by cortical activation is sensitive to odor concentration. Average LMI across single units (n = 30) when concentrations of 2, 10 and 50 ppm of a single odor were presented on interleaved trials. (* $p<0.05$ relative to control, # $p<0.05$ for pairwise comparisons, error bars represent +/- SEM).

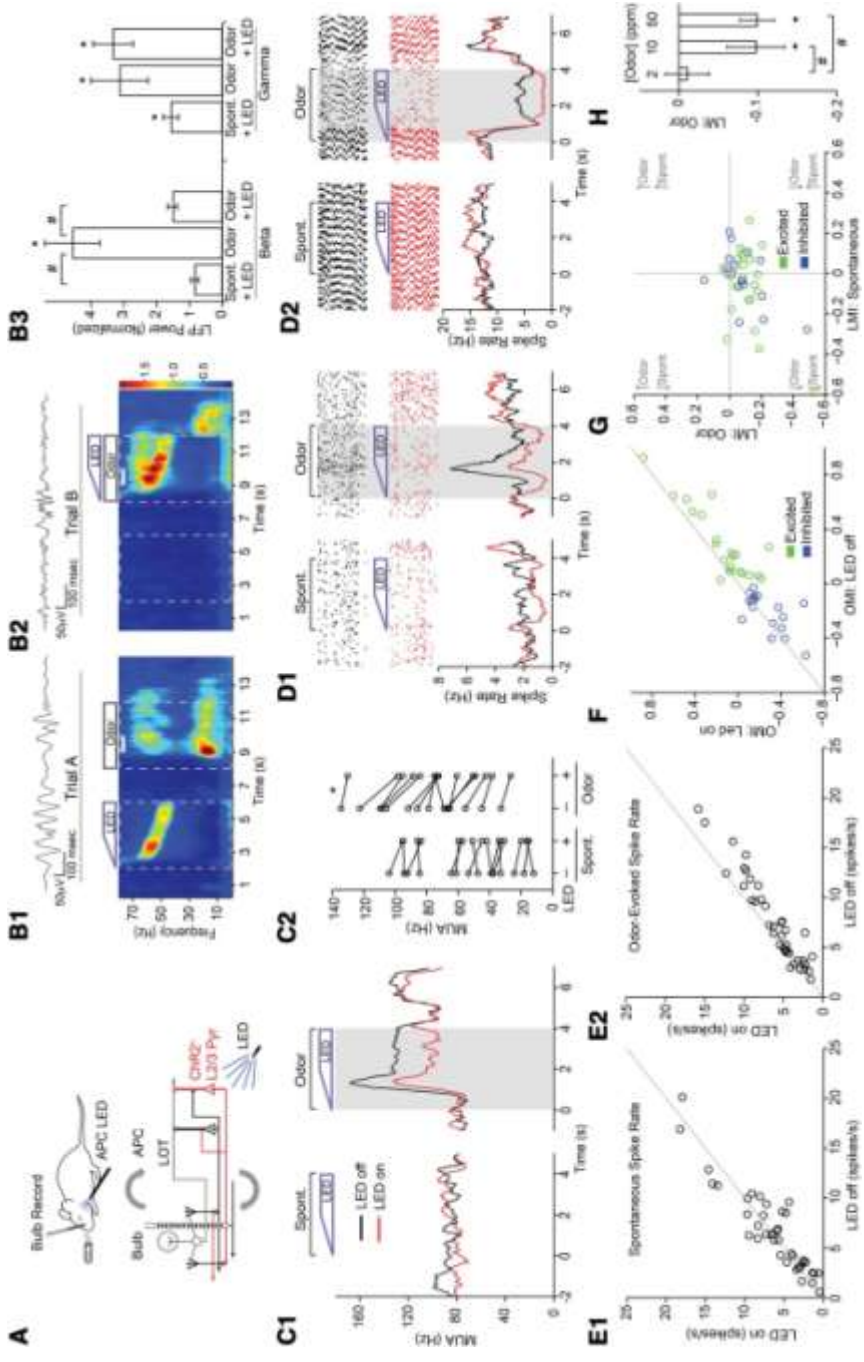
A
Bulb Record
APC LED
APC
Bulb
LOT
ChR2
L2/3 Pyr
LED
B1
Trial A
B2
Trial B
Frequency (Hz)
Time (s)
B3
LFP Power (Normalized)
Spont.
Odor
Odor + LED
Beta
Gamma
C1
MUA (Hz)
LED off
LED on
Spont.
Odor
LED
Time (s)
C2
MUA (Hz)
D1
Spike Rate (Hz)
D2
E1
Spontaneous Spike Rate
LED on (spikes/s)
LED off (spikes/s)
E2
Odor-Evoked Spike Rate
F
OMI LED on
OMI LED off
Excited
Inhibited
G
LMI Odor
LMI Spontaneous
H
[Odor] (ppm)

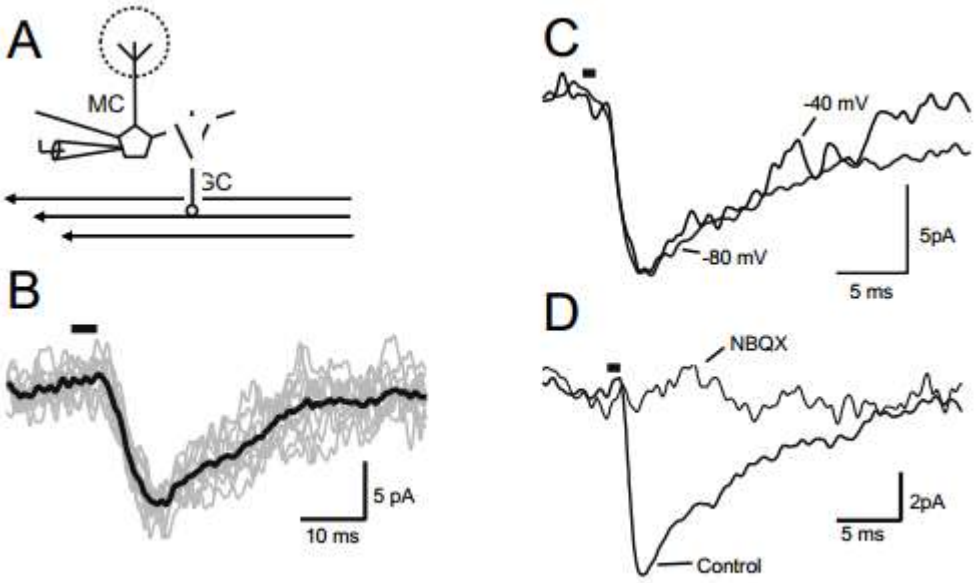

Figure S1.1 Activation of cortical fibers elicits small excitatory currents in mitral cells. A, recording schematic. B, Photostimulation (black bar) evokes small currents in the presence of picrotoxin (100 μM) with negligible trial-to-trial variability. Grey traces, 10 superimposed trials. Black trace, average response. C, Response in another cell showing that membrane depolarization only weakly affects the amplitude of the excitatory current. Traces are averages of 20 trials. D, The excitatory response is blocked by the AMPAR antagonist NBQX (10 μM). Traces are averages of 20 trials.

Figure S1.2 A, Cortical activation has variable effects on spontaneous firing rates of M/T single units. (Top) For each trial, we measured the difference in firing rate (ΔFR) between a 2 s "baseline" period (FRBaseline) and a subsequent 4 s period (FRSpont). The LED was activated during the 4 s time window on interleaved trials. (Bottom) ΔFR with LED on vs. ΔFR with LED off. The variance in ΔFR during "LED on" trials was significantly greater than that for "LED off" trials (σ ^2 LED off = 0.187, σ ^2 LED on = 3.09, $p < 0.01$, Ansari-Bradley test, n = 40). B, The effects of cortical activation are independent of odor identity. B1, M/T cell single unit showing uniform suppression of odor-evoked firing rate during LED trials for three different odors. B2, Single units were classified as modulated in an odor-specific fashion (specifically modulated) if the difference in firing rates between LED and control conditions for one or two but not all three odors was statistically significant (Wilcoxin sign-rank test). The difference in firing rates on a given trial between LED and control conditions was normalized by the average firing rate during all control trials for a given odor (ΔFRnorm = FRLED – FRCtl) / FRCtlAvg). Since the observed fraction of specifically modulated units could be affected by inaccuracies in classification due to variability in firing rates, we compared the frequency of occurrence of specifically modulated units to the frequencies from simulated data sets where odor identity was shuffled for each unit on a trial-by-trial basis. (Top) Table shows ΔFRnorm for a M/T unit over 4 trials, negative values indicate LED suppression of odor responses. Colored letters represent permutations of odor labels used to generate the shuffled data set. (Bottom) Table depicting shuffled data for this unit. For each trial, ΔFRnorm for a given "odor" is derived from the permutation found in the corresponding trial in the unshuffled data. Colored arrows trace the rearrangement of trial 1. B3, The number of units classified as specifically modulated (modulation to one or two, but not all three odors) was divided by the total number of units to derive the fraction of specifically modulated units (observed, blue vertical line). A histogram of the distribution of this fraction calculated over 10000 repetitions of the shuffle procedure is overlaid. The fraction of observed specifically modulated units was not significantly greater than the shuffled distribution, indicating that for the majority of cells cortical suppression is unlikely to be odor selective. B4, As an alternate means of detecting odor-specific modulation based on effect magnitude rather than binary classification, Kruskal-Wallis ANOVA was applied to test whether any difference in ΔFRnorm existed between odor conditions for each unit. Shown is a histogram of p values that are evenly distributed and only a few approach statistical significance ($p<0.05$).

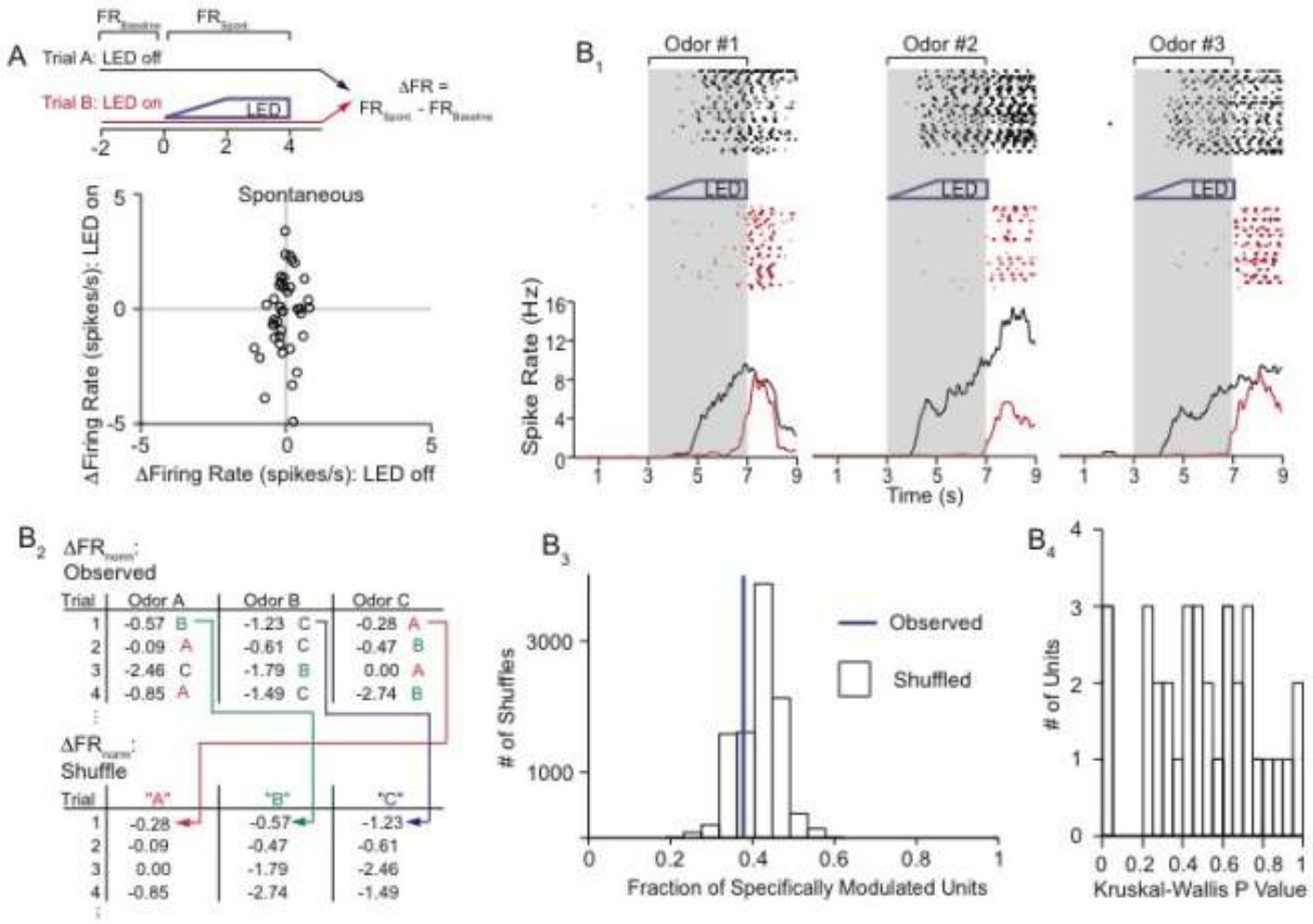
A
Trial A: LED off
Trial B: LED on
LED
ΔFR =
-2
0
2
4
Spontaneous
ΔFiring Rate (spikes/s): LED on
ΔFiring Rate (spikes/s): LED off
B1
Odor #1
Odor #2
Odor #3
Spike Rate (Hz)
Time (s)
B2
ΔFR: Observed
Trial
Odor A
Odor B
Odor C
1 -0.57 B -1.23 C -0.28 A
2 -0.09 A -0.61 C -0.47 B
3 -2.46 C -1.79 B 0.00 A
4 -0.85 A -1.49 C -2.74 B
ΔFR: Shuffle
"A"
"B"
"C"
1 -0.28 -0.57 -1.23
2 -0.09 -0.47 -0.61
3 0.00 -1.79 -2.46
4 -0.85 -2.74 -1.49
B3
# of Shuffles
Observed
Shuffled
Fraction of Specifically Modulated Units
B4
# of Units
Kruskal-Wallis P Value

Acknowledgments

This chapter is a reprint of the material as it appears in Boyd AM, Sturgill JF, Poo C, Isaacson JS. Cortical feedback control of olfactory bulb circuits. Neuron. 2012 Dec 20;76(6):1161-74. The dissertation author was co-first author of this material, responsible for the generation/analysis of all *in vitro* experiments (Fig1.1 – 1.6 and S1.1) in conjunction with co-first author James F. Sturgill who completed and analyzed all the *in vivo* experiments (Fig 1.7, 1.8, S1.2). This project also owes a significant debt to co-author Cindy Poo for methodological development and to last author Jeffry Isaacson for all resources and his continuous scientific, conceptual, and methodological input/training throughout.

Chapter 2. Broadcasting of cortical activity to the olfactory bulb

Summary

Odor representations are initially formed in the olfactory bulb, which contains a topographic glomerular map of odor molecular features. The bulb transmits sensory information directly to piriform cortex where it is encoded by distributed ensembles of pyramidal cells without spatial order. Intriguingly, piriform cortex pyramidal cells project back to the bulb, but the information contained in this feedback projection is unknown. Here we use imaging in awake mice to directly monitor activity in the presynaptic boutons of cortical feedback fibers. We show that the cortex provides the bulb with a rich array of information for any individual odor and that cortical feedback is dependent on brain state. In contrast to the stereotyped, spatial arrangement of olfactory bulb glomeruli, cortical inputs tuned to different odors commingle and indiscriminately target individual glomerular channels. Thus, the cortex modulates early odor representations by broadcasting sensory information diffusely onto spatially ordered bulbar circuits.

Introduction

Sensory regions of neocortex receive information from the thalamus and make corticothalamic feedback projections that serve to modify thalamic sensory processing (Briggs and Usrey, 2008). In the visual, auditory, and somatosensory systems the connectivity of feedback projections onto thalamic neurons is linked to the tuning preferences of the cortical cells involved and there is a high degree of reciprocity between topographically aligned areas of cortex and thalamus (He, 2003; Murphy *et al*., 1999; Temereanca and Simons, 2004). The olfactory system is unique in that sensory information bypasses the thalamus such that the primary olfactory (piriform) cortex receives sensory input directly from the olfactory bulb, the first brain region in which odor information is processed. Similar to corticothalamic pathways, olfactory cortex pyramidal cells send dense projections back to the olfactory bulb (Luskin and Price, 1983). However, the information sent back to the bulb from the piriform cortex (PCx) and the functional topography of feedback input has not been established.

The olfactory bulb contains a highly ordered spatial map of odorant molecular features. This reflects the fact that olfactory sensory neurons (OSNs) expressing only one out of ~1000 odorant receptors converge input onto two unique glomeruli (out of ~2000) in each olfactory bulb (Mombaerts *et al*., 1996). Within each glomerulus, OSNs contact a unique set of principal mitral cells that project sensory information to the PCx. Ultimately, different odors activate distinct glomerular channels generating a stereotyped topographic map of odor space in the olfactory bulb (Soucy *et al*., 2009). In contrast, studies of sensory representations in the PCx reveal that odors are encoded by

dispersed and overlapping populations of pyramidal cells without obvious spatial order (Stettler and Axel, 2009). Thus, the initial stereotyped and topographic representation of olfactory information in the bulb is discarded and replaced by a distributed ensemble coding strategy in the cortex.

Mitral cell odor responses are not solely determined by the excitatory input they receive from individual glomeruli. This reflects the fact that mitral cell activity is regulated by a variety of local GABAergic interneurons, the most prominent of which are periglomerular cells, which contact the apical dendritic tuft of mitral cells, and granule cells that inhibit mitral cell lateral dendrites (Shepherd *et al*., 2004). The axonal projections of PCx pyramidal cells are particularly dense in the granule cell layer and also surround but do not extend into glomeruli (Matsutani, 2010), suggesting that bulbar interneurons are the major targets of cortical feedback. Consistent with this idea, granule and periglomerular cells are strongly excited by cortical feedback projections (Boyd *et al*., 2012; Markopoulos *et al*., 2012) and activation of PCx amplifies odor-evoked mitral cell inhibition (Boyd *et al*., 2012). Thus, PCx can effectively gate odor-evoked olfactory bulb output and directly regulate the sensory input it receives.

Although cortical feedback has a strong impact on olfactory bulb circuits, the nature of the information contained in feedback projections is unclear. What is the olfactory cortex trying to "tell" the olfactory bulb? To address this question, we express the genetically-encoded Ca^{2+} indicator GCaMP6s (Chen *et al*., 2013) in PCx and use 2-photon imaging to study the activity of pyramidal cell axonal boutons in the olfactory bulb of awake mice. We determine the sensory information within long-range

cortical projections and show its modulation by brain state. In contrast to corticothalamic pathways, we show that the targeting of feedback input ignores local topographic order allowing the cortex to broadcast sensory information widely across olfactory bulb circuits.

Results

We co-injected two different viral vectors to express GCaMP6s (AAV 2/9-syn-GCaMP6s) and the activity-independent reporter TdTomato (AAV 2/9-syn-tdTomato) in PCx pyramidal cells (Fig. 2.1A_1, Fig. S2.1). To visualize cortical feedback inputs, we subsequently imaged the ipsilateral olfactory bulb of awake, head-fixed mice through a chronically implanted glass window ((Kato *et al*., 2012), Fig. 2.1A_1). The tdTomato signal was used for registration of image time series as well as estimation of residual movement-related artifacts that we used to establish the GCaMP response threshold (Experimental Procedures, Fig. S2.1). The labeling pattern in the olfactory bulb was consistent with previous reports of cortical projections (Boyd *et al*., 2012; Markopoulos *et al*., 2012): labeled axons and boutons were densest in the granule cell layer and prominent in the glomerular layer (Fig 2.1A_2). We never observed labeling in local bulbar neurons, indicating that signals arise exclusively from long-range cortical projections.

We resolved individual micrometer-sized varicosities *in vivo* (Fig. 2.1A_2) and assume that each represents a single presynaptic bouton (Petreanu *et al*., 2012). Co-injection of tdTomato and GCaMP led to co-expression of the two fluorescent proteins

in the same fibers and boutons as well as non-overlapping expression in separate populations of fibers. We first examined sensory-evoked activity in the awake state by testing the responses of individual boutons to a panel of seven structurally diverse, monomolecular odorants (each at 100 ppm). Individual boutons within a single field of view (85x85 or 128x128 μm) revealed diverse responses (Supplemental Movie 1). In both the granule cell and glomerular layer, odor application (4 s) elicited increases in the activity of single boutons (measured as dF/F). Individual boutons showed a range of odor tuning, from being odor selective to responding to all tested odors. Furthermore, immediately adjacent boutons could have divergent tuning properties (Fig. 2.1B). The time course of odor-evoked activity varied from phasic responses to long-lasting activity that persisted for many seconds after odor delivery. We observed odor-evoked decreases in fluorescence (negative dF/F responses) indicating that sensory stimulation could also suppress the basal activity of feedback projections. Pairwise correlation analysis of boutons indicated that, on average, a minimum of 20.5±2 distinct axons (n=23 fields) contributed to each imaging field (Fig. S2.1). There were no obvious differences between the properties of boutons in the two bulb layers (Fig. S2.2, total boutons=4948, n=9 granule cell layer fields, 18 glomerular layer fields, 16 mice) and results were pooled for further analysis.

Excitatory and suppressive responses had different temporal dynamics; while the onset time of excitation included both on- and off-responses, suppressive activity was more time locked to odor onset (Fig. 2.1C). Boutons with odor-evoked increases in activity (21.2% out of 5353 total boutons) were more prevalent than those showing

suppression (11.5%) and boutons with both excitatory and suppressive responses to different odors were rare (2.4%, Fig. 2.1D$_1$). The fraction of odor-activated boutons we observe (~24%) is consistent with a previous PCx imaging study using five odors that found ~35% of layer 2 neurons are odor responsive (Stettler and Axel, 2009). Since the optical detection of odor-evoked suppression relies on substantial basal activity, we are potentially underestimating decreases in feedback input. Nonetheless, the tuning properties of boutons in which odors elicited increases or decreases in activity were similar: ~50% of boutons responded with specificity (to two or fewer of the seven odors). Although most boutons (~65%) were unresponsive to the tested odors, virtually all boutons lacking odor-evoked responses (>90%) displayed spontaneous activity indicating they were functional. Thus, the majority of feedback inputs are likely to respond to odors more selectively. We considered the possibility that some odors may be more represented by cortical feedback than others. However, across the population of responsive boutons tested with the same panel of odors (n=554 boutons, 1674 responses), each odor was virtually identical in terms of its likelihood of eliciting excitatory responses (Fig. 2.1D$_2$). Similar results were observed using a larger panel of 14 odors (Fig. S2.2). Together, these results indicate that individual odors are represented equally by PCx feedback and that local regions of the bulb receive input from fibers with diverse response properties.

Olfactory bulb activity is dependent on brain state (Rinberg *et al*., 2006). Indeed, the transition from the awake to anesthetized condition strongly reduces bulbar interneuron activity and enhances odor-evoked mitral cell output (Cazakoff *et al*., 2014;

Kato *et al*., 2012; Wachowiak *et al*., 2013). How does cortical feedback input respond to this change in brain state? To address this, we imaged the same boutons in the awake and anesthetized state. Anesthesia caused a marked decrease in both spontaneous and odor-evoked cortical feedback (Fig. 2.2A,B). Relative to the awake condition, anesthesia reduced the number of boutons responding with odor-evoked excitation and suppression by 39.6% and 48.8%, respectively (n= 6 imaging fields from 4 mice). During anesthesia the strength of excitatory responses was reduced ($p<0.001$, Kolmogorov-Smirnov (KS) test, Fig. 2.2C_1) and excitation became more narrowly tuned (Fig. 2.2C_2). These effects on odor-evoked responses were indistinguishable with ketamine and urethane (Fig. S2.2), two chemically distinct anesthetics, suggesting that the differences in bouton activity reflect changes in brain state rather than pharmacological actions of the drugs. Furthermore, the duration of odor-evoked excitatory activity became markedly briefer in the anesthetized state (decay time awake = 4.2±0.2 s, anesthetized = 3.1±0.2 s, $p<0.001$, KS test, Fig. 2.2D_{1-2}) while the duration of suppressive responses was slightly enhanced (decay time awake = 2.3±0.1 s, anesthetized = 2.6±0.1 s, $p=0.001$, KS test, Fig. 2.2D_{3-4}). Overall, these results indicate that wakefulness enhances PCx feedback input to olfactory bulb circuits.

We next considered the functional organization of cortical projections within the olfactory bulb. Do feedback inputs adopt the topographic organization of the bulb such that the tuning of cortical inputs matches that of their target region? Or do they retain the diffuse and overlapping nature of odor representations found within the PCx itself? The observation that boutons with different tuning properties closely intermingle

(Fig. 2.1B) suggests that cortical inputs do not transmit sensory information in a strict, spatially segregated manner. We tested this by examining whether boutons with the same odor preference are spatially clustered within our imaging fields (85x85 or 128x128 μm), each of which are on the scale of a radially oriented glomerular column (~100 μm diameter, (Willhite *et al*., 2006)). We made maps of bouton odor preference (the odor eliciting the strongest excitatory response) within a field (Fig. 2.3A_1) and measured the pairwise distance between all boutons with the same (matched) or different (mismatched) odor preference. If boutons with the same odor preference cluster, the distance between boutons with matching preferences should be less than those that are mismatched. However, for granule cell and glomerular layer fields with at least 30 responsive boutons, the average distance between matched or mismatched boutons was nearly identical (Fig. 2.3A_2, 3B, matched= 55.0±1.5 μm, mismatched=56.9±1.7 μm, p=0.26, Wilcoxon signed-rank test, n=22 fields). Similarly, we found no difference when we compared the distance between boutons based on the number of odors eliciting responses (tuning broadness, matched= 55.5±1.9 μm, mismatched=56.6±1.4 μm, p=0.91, Wilcoxon signed-rank test). Furthermore, there was no relationship between distance and the tuning similarity (Soucy *et al*., 2009) of boutons (Fig. S2.3). Thus, for bulb domains on the scale of individual glomeruli, cortical feedback does not appear to provide input in a spatially segregated fashion.

Another simple test of spatial organization is to ask whether boutons responsive to a particular odor are overrepresented within our imaging fields. Therefore, for all excitation responsive odor-bouton pairs in each imaging field (n=22), we rank ordered

the seven odors by their probability of eliciting a response. On average, response probabilities within a field ranged from 20.0±0.5% (most preferred odor) to 7.6±0.6% (least preferred odor, Fig. 2.3C). If a field had an infinite number of odor-bouton response pairs, each odor should have a 14.3% (1/7) probability of contributing a response if odor responses are randomly distributed. However, the number of odor responses per field is limited and some odors may be more represented than others in each imaged field simply by chance. Indeed, given the number of odor-bouton response pairs we measured per field (range: 23 to 406 response pairs), our results are consistent with those expected due to random subsampling from a distribution of equal response probabilities (Fig. 2.3C). Thus, boutons activated by specific odors are not overrepresented on a glomerular spatial scale, suggesting that the targeting of feedback input lacks a segregated spatial order.

We took advantage of feedback projections in the glomerular layer to directly test if cortical boutons are co-tuned with the glomeruli they target. We first used intrinsic signal optical imaging to map glomerular activity (Rubin and Katz, 1999) in response to three odors (Fig. 2.4A,B_1) and then imaged bouton responses at the base of selected glomeruli. Immediately before 2-photon imaging, the red fluorophore Texas red dextran was injected i.v. (Fig. 2.4A). We visualized labeled blood vessels to align imaging fields to the surface vasculature and glomeruli observed during intrinsic signal imaging (Fig. 2.4B_1,B_2). If cortical projections are organized based on the odor map inherent to the olfactory bulb, boutons should show a preference for the odors activating their overlying glomeruli. However, beneath odor-specific glomeruli (n=9)

we found boutons activated by each of the three of the odors (Fig. 2.4B_{1-4}). Furthermore, the probability of bouton responses to a given odor was similar whether the 2-photon imaging field was beneath the glomerulus activated by that odor ("Field 1", Fig. 2.4B_3,B_4) or beneath glomeruli unresponsive to the odor ("Field 2", Fig. 2.4B_3,B_4). Overall, for each of the three odors tested, odor-evoked bouton activity was unrelated to the overlying glomerular odor map (n=9 fields beneath active glomeruli, 6 fields beneath non-active glomeruli, n=3 mice, Fig. 2.4C). Similar results were obtained using seven odors and more imaging fields tiling the dorsal olfactory bulb (Fig. S2.4). Taken together, our results indicate that cortical fibers transmit odor-evoked feedback input diffusely over the olfactory bulb without any obvious spatial segregation.

Discussion

In this study we use *in vivo* Ca^{2+} imaging to reveal the information contained within cortical feedback projections to the olfactory bulb. We show that PCx provides the bulb with diverse input: odors cause pyramidal cells to increase or decrease their feedback in a manner ranging from odor selective to apparently un-tuned. Compared to the anesthetized condition, wakefulness enhances both the magnitude and duration of excitatory cortical feedback, indicating that the cortical control of olfactory bulb circuits is dependent on brain state. Furthermore, although olfactory bulb circuits are spatially arranged to form a stereotyped odor map, PCx projections provide feedback input in a diffuse, intermingled fashion.

Cortical feedback inputs directly excite olfactory bulb interneurons and facilitate mitral cell inhibition (Boyd *et al*., 2012; Markopoulos *et al*., 2012). We found that odors elicit both increases and decreases in cortical feedback activity and that the PCx transmits a heterogeneous array of odor information to the bulb. For example, although the majority of feedback projections show odor-specific changes in activity, others appear to be "generalists" that simply signal the presence of any odor. Our results are similar to those found using electrophysiological recordings of layer 2/3 PCx cells in awake mice (Zhan and Luo, 2010). This suggests that cortical feedback does not arise from a distinct subpopulation of pyramidal cells and that it may provide the bulb with a readout of overall PCx activity. In addition, while PCx feedback can be time locked to odor onset, responses can also be quite delayed and even persist long after the odor is present. The wide variety in response features indicates that PCx feedback exerts complex and non-uniform effects on the olfactory bulb interneurons underlying mitral cell inhibition. Interestingly, local inhibition is proposed to enhance odor discrimination by decorrelating mitral cell activity patterns (Arevian *et al*., 2008; Wiechert *et al*., 2010). Heterogeneous odor-evoked patterns of feedback input could allow PCx to contribute to the decorrelation of mitral cell activity and thus enhance the discriminability of input it receives from the olfactory bulb.

Odor coding in the olfactory bulb differs between the awake and anesthetized brain state, namely, mitral cell odor representations are sparser and more temporally dynamic during wakefulness (Kato *et al*., 2012; Rinberg *et al*., 2006; Wachowiak *et al*., 2013). These changes lead to a marked improvement in the discriminability of mitral

cell odor representations (Kato *et al*., 2012). Intriguingly, despite the fact that sensory input to PCx is sparser, we find that wakefulness increases spontaneous activity as well as the strength and duration of odor-evoked excitatory cortical feedback. This suggests that cortical circuits are flexible and that PCx output can adapt to brain state-dependent changes in sensory input. What can explain the opposing changes in mitral cell activity and PCx feedback? Interestingly, wakefulness strongly increases the activity of olfactory bulb interneurons (Cazakoff *et al*., 2014; Kato *et al*., 2012; Wachowiak *et al*., 2013). For example, granule cells are predominantly inactive in the anesthetized state, but have high amounts of spontaneous activity and more broadly-tuned odor responses during wakefulness (Cazakoff *et al*., 2014; Kato *et al*., 2012). One explanation for the opposite changes in PCx and mitral cell activity is that brain state-dependent changes in interneuron activity are directly inherited from their PCx feedback input. Indeed, increased PCx feedback, acting to enhance the activity of local interneurons, could account for sparse mitral cell odor representations during wakefulness. Thus, modulation of PCx feedback may be a major factor regulating the state dependence of mitral and granule cell activity.

We show that PCx feedback inputs responding to different odors are dispersed throughout the granule cell and glomerular layer in a diffuse and overlapping fashion. Indeed, glomeruli tuned to specific odors are surrounded by feedback projections that transmit information regarding distinctly different odors. Thus, on the spatial scale of individual glomeruli, we find no evidence that feedback inputs and their olfactory bulb targets are co-tuned or that feedback is targeted with odor selectivity. We cannot

exclude the possibility that a diffuse spatial organization of feedback occurs on a much larger scale, for example between dorsal and ventral regions of the olfactory bulb. Our findings differ from a recent imaging study using GCaMP to examine the properties of feedback projections from the anterior olfactory nucleus (AON), an anterior subdivision of the olfactory cortex (Rothermel and Wachowiak, 2014). Imaging of the dorsal olfactory bulb suggested that individual odors could generate odor-specific patterns of activity. Unlike PCx, the AON receives olfactory bulb input that is topographically-organized (Ghosh *et al*., 2011; Miyamichi *et al*., 2011) raising the possibility that AON feedback is uniquely co-tuned with that of its target region.

Our results suggest that PCx feedback inputs broadcast odor information diffusely onto spatially ordered bulbar circuits. Thus, in contrast to the proposed "egocentric" enhancement of thalamic activity generated by visual, auditory, and somatosensory cortical feedback (Briggs and Usrey, 2008), PCx inputs are unlikely to selectively amplify the activity of mitral cells sharing the same tuning properties. Since PCx inputs target interneurons and drive mitral cell inhibition (Boyd *et al*., 2012), cortical feedback may regulate olfactory bulb output on a more global scale. Cortical feedback has been suggested to modulate the gain of thalamic output during brain states associated with attention (McAlonan *et al*., 2008) and the transition between sleep and wakefulness (Steriade, 2005). Feedback projections from the PCx may contribute a similar gain control function for the initial processing of odor representations in the olfactory bulb.

Figure 2.1 Cortical feedback inputs have diverse response properties. **A_1)** *Left*, viral vectors expressing GCaMP6s and tdTomato are injected in piriform cortex (PCx) to label olfactory bulb projections. *Right*, schematic of 2-photon imaging via a cranial window over the ipsilateral olfactory bulb (OB) in awake, head-fixed mice. **A_2)** *Left*, Td-Tomato expression in PCx axons from a coronal OB slice. Axonal projections are most prevalent in the granule cell and glomerular layer. *Right, In vivo* 2-photon image of tdTomato (red) and GCaMP6s (green) expressing boutons from the OB glomerular layer of an awake mouse. **B)** Odor-evoked GCaMP6s activity in individual boutons reveals a wide range of response properties. **B_1)** Responses from a glomerular layer imaging field show that boutons tuned to different odors are intermingled. *Left,* Image of GCaMP6s expression (white) shows ROIs (red outlines) drawn around individual boutons. *Right,* Responses of four boutons (rows) to four odors (columns). Grey lines are individual trails and black lines show the average response to each odor. Filled circles above each trace indicate a significant response (excitation: red, inhibition: blue) and the colored circles to the left of traces indicate ROIs marked in the GCaMP6s image. **B_2)** Responses in the granule cell layer from the same animal. **C)** Dynamics of odor-evoked feedback activity. Top: heat maps of the activity of all responsive bouton-odor pairs showing excitation (3855 bouton-odor pairs) or suppression (1907 bouton-odor pairs), sorted by their onset times (50% of peak). Bottom: histograms of the onset times of all responsive bouton-odor pairs show that excitatory responses are temporally more diverse in the awake state, while inhibitory responses are more time locked to odor onset. Vertical lines indicate the odor period. **D_1)** Odor tuning curve for boutons responding with excitation (red) or suppression (blue). *Inset*, proportion of all boutons with no response (NR), excitation only (E), suppression only (S), or both excitation and suppression (E&S). **D_2)** All odors have an equal probability of eliciting excitatory responses (n = 13 imaging fields). Dashed line indicates expected value (14.3%) if each odor randomly activates boutons with equal probability.

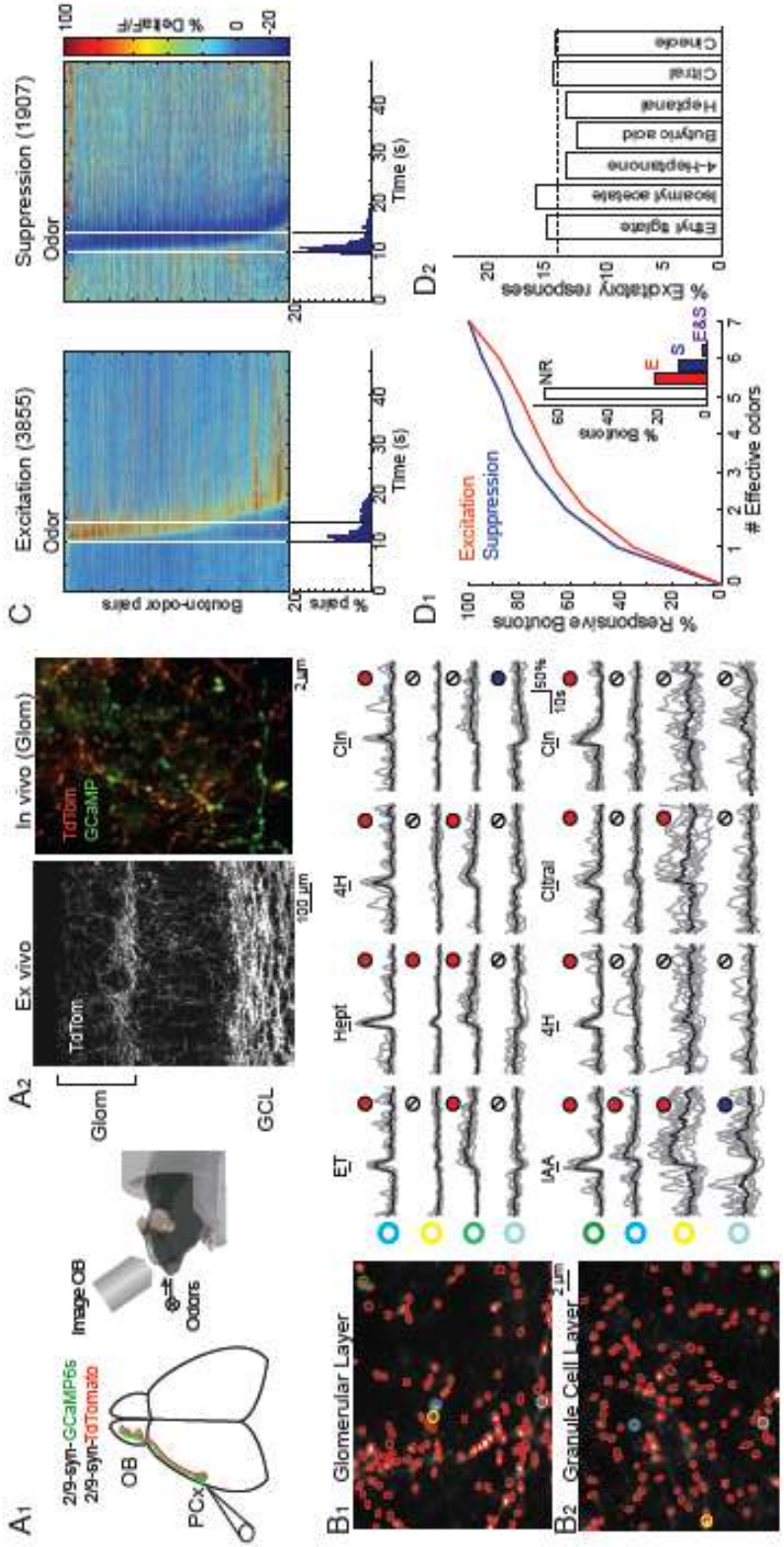
A1
2/9-syn-GCaMP6s
2/9-syn-TdTomato
OB
PCx
Image OB
Odors
A2
Ex vivo
TdTom
Glom
GCL
100 µm
In vivo (Glom)
TdTom
GCaMP
2 µm
B1 Glomerular Layer
B2 Granule Cell Layer
2 µm
ET
Hept
4H
Cin
IAA
4H
Citral
Cin
50%
10s
C
Excitation (3855)
Odor
Suppression (1907)
Odor
Bouton-odor pairs
% pairs
Time (s)
% DeltaF/F
100
0
-20
D1
% Responsive Boutons
# Effective odors
Excitation
Suppression
% Boutons
NR
E
S
E&S
D2
% Excitatory responses
Ethyl lactate
Isoamyl acetate
4-Heptanone
Butyric acid
Heptanal
Citral
Cineole

Figure 2.2 Cortical feedback activity is enhanced during wakefulness. **A)** Anesthesia reduces spontaneous activity. Heat map of dF/F values for 180 boutons from one imaging field in the awake state (left) and during ketamine anesthesia (right). **B)** Odor-evoked cortical feedback activity is reduced in the anesthetized state. Representative average responses of four boutons (rows) to four odors (black bars) from a single imaging field in the awake (black) and anesthetized state (red). BA; butyric acid, 2-4DM; 2-4 dimethylthiazole, Ani; anisole, ET; ethyl tiglate. **C)** Odor-evoked bouton excitation is stronger (**C_1**) and more broadly tuned (**C_2**) in the awake state. **D)** Odor-evoked excitation is more prolonged in the awake vs. anesthetized state. **D_1)** Heat maps of the activity of bouton-odor pairs showing excitation from the same animals in the awake (left) and anesthetized (right) state, aligned to their onset times and ordered by duration. Numbers of responsive bouton-odor pairs in each condition are in parentheses. **D_2)** Average time course of excitatory responses aligned by their rise times and peak normalized for the awake (black) and anesthetized (red) state. Shading, SEM. **D_3)** and **D_4)** Results for bouton-odor pairs showing odor-evoked suppression.

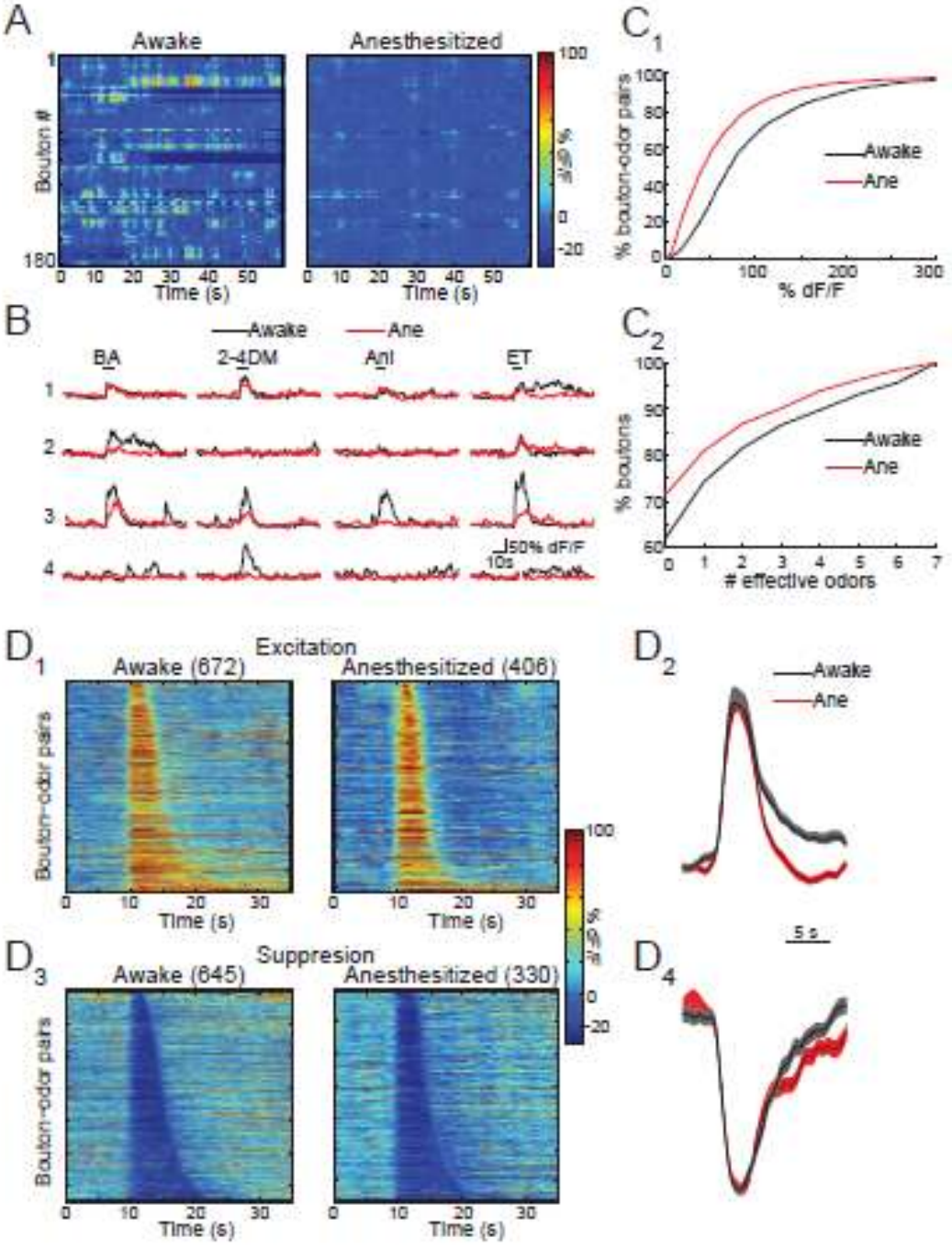
A
Awake
Anesthesitized
Bouton #
Time (s)
dF/F %
B
Awake
Ane
BA
2-4DM
AnI
ET
50% dF/F
10s
C1
% bouton-odor pairs
% dF/F
C2
% boutons
# effective odors
D1
Excitation
Awake (672)
Anesthesitized (406)
Bouton-odor pairs
D2
5 s
D3
Suppresion
Awake (645)
Anesthesitized (330)
D4

Figure 2.3 Cortical feedback inputs representing different odors are diffusely distributed at the spatial scale of individual glomeruli**. A)** Boutons responding to particular odors are not spatially segregated. **A_1)** Results from one granule cell layer imaging field showing all bouton ROIs (left) and map of the preferred odor for each responsive bouton (right). Color scale indicates each of the seven tested odors (Cin; cineole, Cit; citral, Hept; heptanal, BA; butyric acid, 4H; heptan-4-on, IA; isoamyl acetate, ET; ethyl tiglate. ROIs are shown enlarged for clarity. **A_2)** Cumulative frequency distribution of the pairwise distance between all boutons in A_1 with the same (Matched, n=296) or different (Mismatched, n=1702) odor preference. The two distributions are not significantly different (p=0.29, KS test). **B)** Summary data (grey, n=22 fields) reveals no significant difference in the mean distance between matched and mismatched responsive boutons (red, average±SEM). **C)** Rank-ordering orders by their probability of eliciting excitatory responses in individual imaging fields indicates that the fraction of responses elicited by any odor is consistent with random chance. Red circles, responses to rank ordered odors for both granule cell layer and glomerular imaging fields (mean ± SEM, n = 22 fields). The observed values fall within the curves expected from random chance for the largest (n=406) and smallest (n=23) number of responsive boutons per imaging field (dotted lines). Inset, response probability distribution for the most represented odor (Odor #1) derived from random subsampling using the sample sizes from 22 imaging fields. Experimentally measured probability (red line) falls within central 90% of the distribution (dotted lines).

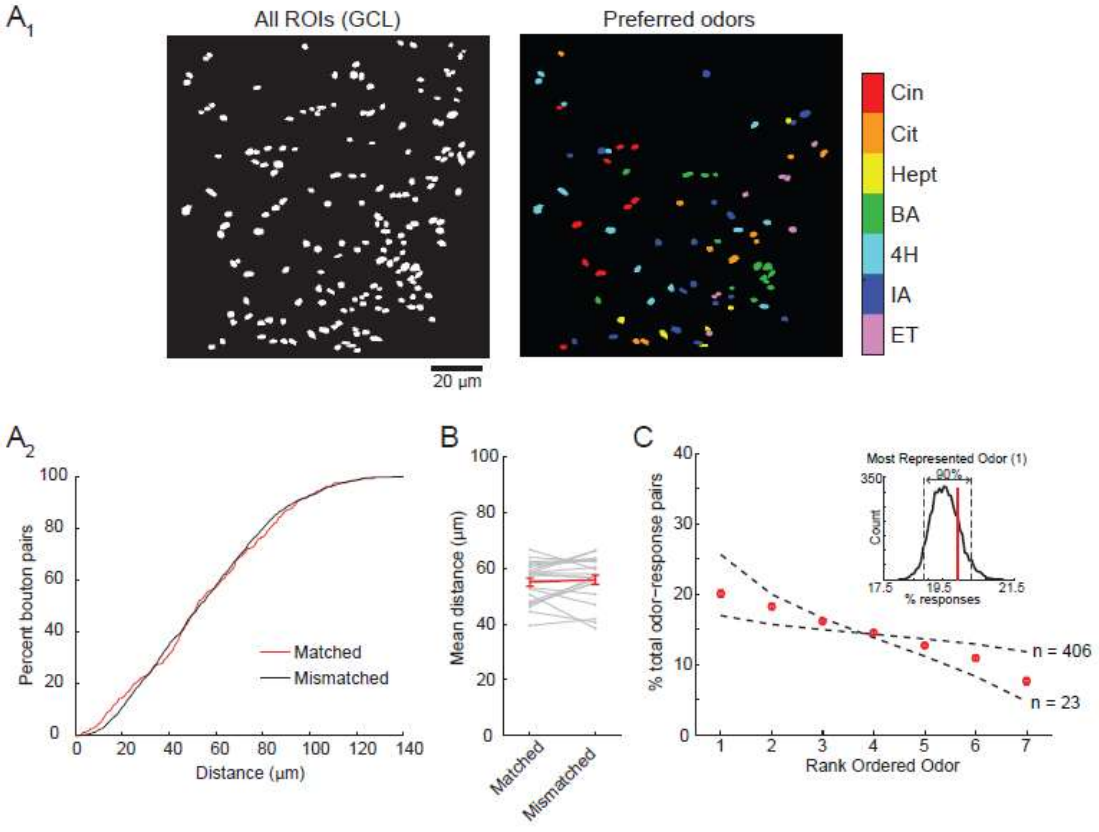
A1
All ROIs (GCL)
Preferred odors
Cin
Cit
Hept
BA
4H
IA
ET
20 µm
A2
Percent bouton pairs
Distance (µm)
Matched
Mismatched
B
Mean distance (µm)
Matched
Mismatched
C
% total odor−response pairs
Rank Ordered Odor
Most Represented Odor (1)
90%
Count
% responses
n = 406
n = 23

Figure 2. 4 Glomerular layer targeting of feedback inputs is unrelated to glomerular odor specificity. **A)** Schematic of experimental approach. **B_1)** Representative intrinsic signal optical imaging data from one mouse showing glomerular responses to three different odors (Ethyl tiglate (ET), Anisole (Ani), 2-Hexanone (Hex)) and the glomerular activity map superimposed on the olfactory bulb surface vasculature (bottom right). Colored circles highlight activated glomeruli; boxes represent fields selected for bouton imaging. Field 1 is centered over a glomerulus responding to ethyl tiglate and Field 2 indicates a region without a glomerular response to any of the odors. **B_2)** Targeted 2-photon imaging beneath an identified glomerulus. Top, blow up of region around Field 1 from B_1 showing overlay of intrinsic optical signal (red, ethyl tiglate) and surface vasculature. Bottom, 2-photon image stack of Texas red dextran-filled vessels aligned with the vasculature in the image above. **B_3)** Map of glomerular layer boutons responding with excitation within fields indicated in B_1. Colors indicate boutons responding selectively to individual odors (red, green, blue), boutons with overlapping responses to two odors (yellow, magenta, cyan), and boutons responsive to all three (white). ROIs are shown enlarged for clarity. **B_4)** Numbers of boutons responding with excitation to each odor for the fields in B_3. **C)** Summary of results (mean ± SEM) from all experiments using three odors indicates that individual odors were equally likely to activate boutons regardless of the responses of the overlying glomerulus. We calculated a variation index for each odor ((Observed fraction of responsive boutons / 0.33) – 1) for fields centered on an odor-responsive glomerulus (white circles) and fields within regions that did not show a glomerular response to any of the three odors (black circles). Variation index=0 if each odor (1 out of 3) has an equal probability of eliciting bouton responses in an imaging field. Odors were grouped between those that did (Glom+) or did not (Glom-) activate the odor-responsive glomerulus. In all cases, odors consistently had a variation index near zero.

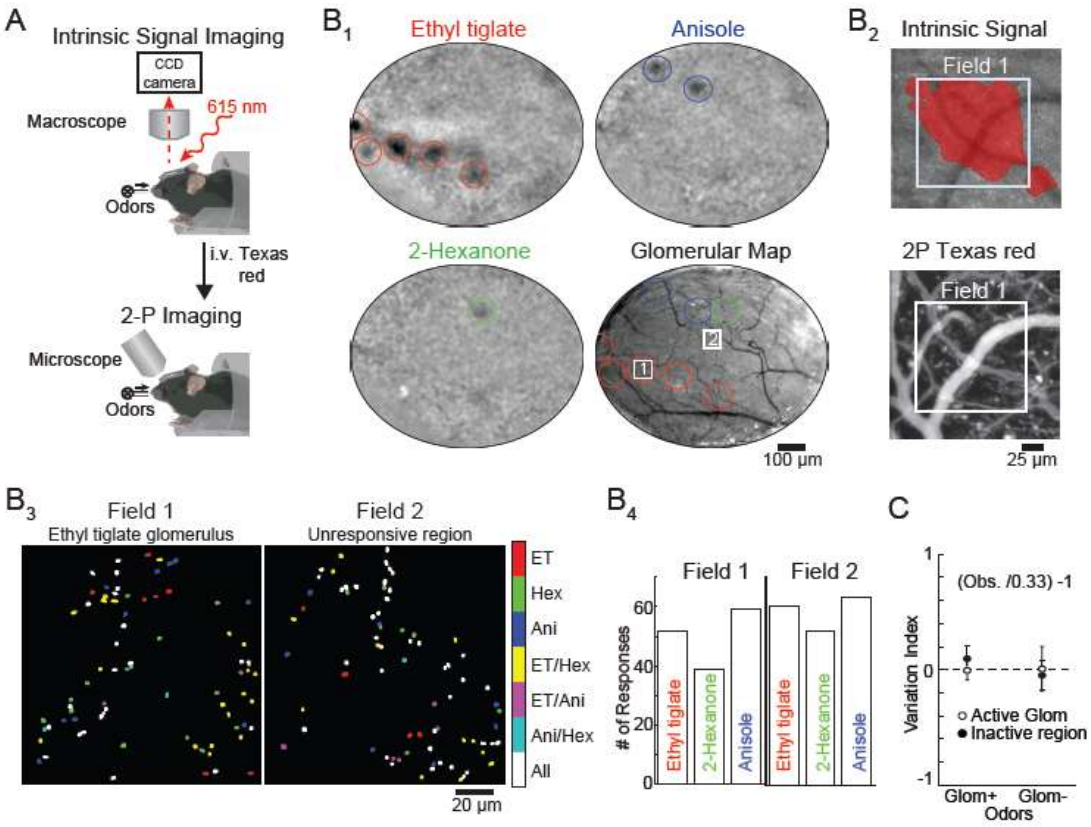
A
Intrinsic Signal Imaging
CCD camera
615 nm
Macroscope
Odors
i.v. Texas red
2-P Imaging
Microscope
Odors
B1
Ethyl tiglate
Anisole
2-Hexanone
Glomerular Map
1
2
100 µm
B2
Intrinsic Signal
Field 1
2P Texas red
Field 1
25 µm
B3
Field 1
Ethyl tiglate glomerulus
Field 2
Unresponsive region
ET
Hex
Ani
ET/Hex
ET/Ani
Ani/Hex
All
20 µm
B4
Field 1
Field 2
# of Responses
60
40
20
0
Ethyl tiglate
2-Hexanone
Anisole
Ethyl tiglate
2-Hexanone
Anisole
C
1
0
-1
(Obs. /0.33) -1
Variation Index
Active Glom
Inactive region
Glom+
Glom-
Odors

Figure S2.1 GCaMP expression in PCx, determining the impact of residual uncorrected movement on bouton GCaMP signals, and estimation of the numbers of axons in each imaging field. **A)** Ex vivo thin (50 μm) section through anterior piriform cortex of an Ntsr1-Cre mice injected with AAV-FLEX-GCaMP5G. LOT, lateral olfactory tract. **B)** Following image registration, ROIs were drawn around TdTomato-expressing boutons. In experiments testing bouton responses to seven odors (8 trials per odor), we used the same 10 sec response window for dF/F measurements of red TdTomato fluorescence (n=5 fields). To avoid potential contamination of TdTomato signals with evoked GCaMP responses in co-expressing boutons (due to possible bleed-thru of green fluorescence into the red detection channel), we measured the average maximum negative deflection per odor for determination of TdTomato dF/F. Bouton TdTomato responses (maximum dF/F) should therefore provide a good estimate the impact of residual, uncorrected movement on bouton fluorescence measurements. Shown in green are the average maximum GCaMP dF/F observed for each bouton-odor pair (n=23 fields). Points ≥85% dF/F are collapsed into the same bin. For response detection, a minimum response amplitude of 20% dF/F was chosen to ensure a false positive rate due to motion of ~1%. **C**) Left, sub region of an imaging field showing raw GCaMP fluorescence (grey scale). Image is an average of ~900 frames (60 s). Red and brown arrows indicate boutons emerging from the same axon. Blue arrow indicates a bouton that is not connected to the same axon. Right, spontaneous activity drives Ca2+ transients that are essentially identical in the boutons emerging from the same axon. In contrast, the bouton that is not from the same axon displays uncorrelated activity. **D**) Heat map of the correlation values (R) for 60 boutons from the field in A. Red arrowheads indicate the two boutons from the same axon (showing high correlations with other boutons from the same fiber) and the blue arrowhead indicates the bouton that is not from the same axon. Moreover, the lack of correlated activity between this bouton and all others suggests that it emerges from an axon contributing only this one bouton to the imaging field. **E**) To determine the effectiveness of using correlation values to assign boutons to the same axon, we took advantage of the fact that co-injecting viruses for GCaMP and TdTomato led to non-overlapping expression in some feedback fibers. Thus, we could directly compare the correlation values for boutons visually identified to belong to the same axon (green) with those that were clearly on independent fibers (red, GCaMP+ TdTomato- boutons vs GCaMP+ TdTomato+ boutons, n=4 imaging fields). For selection of boutons belonging tothe same fiber, we chose R=0.4 as the threshold to minimize false grouping. Most of the visibly connected boutons (green) with R≤0.4 were essentially completely inactive.

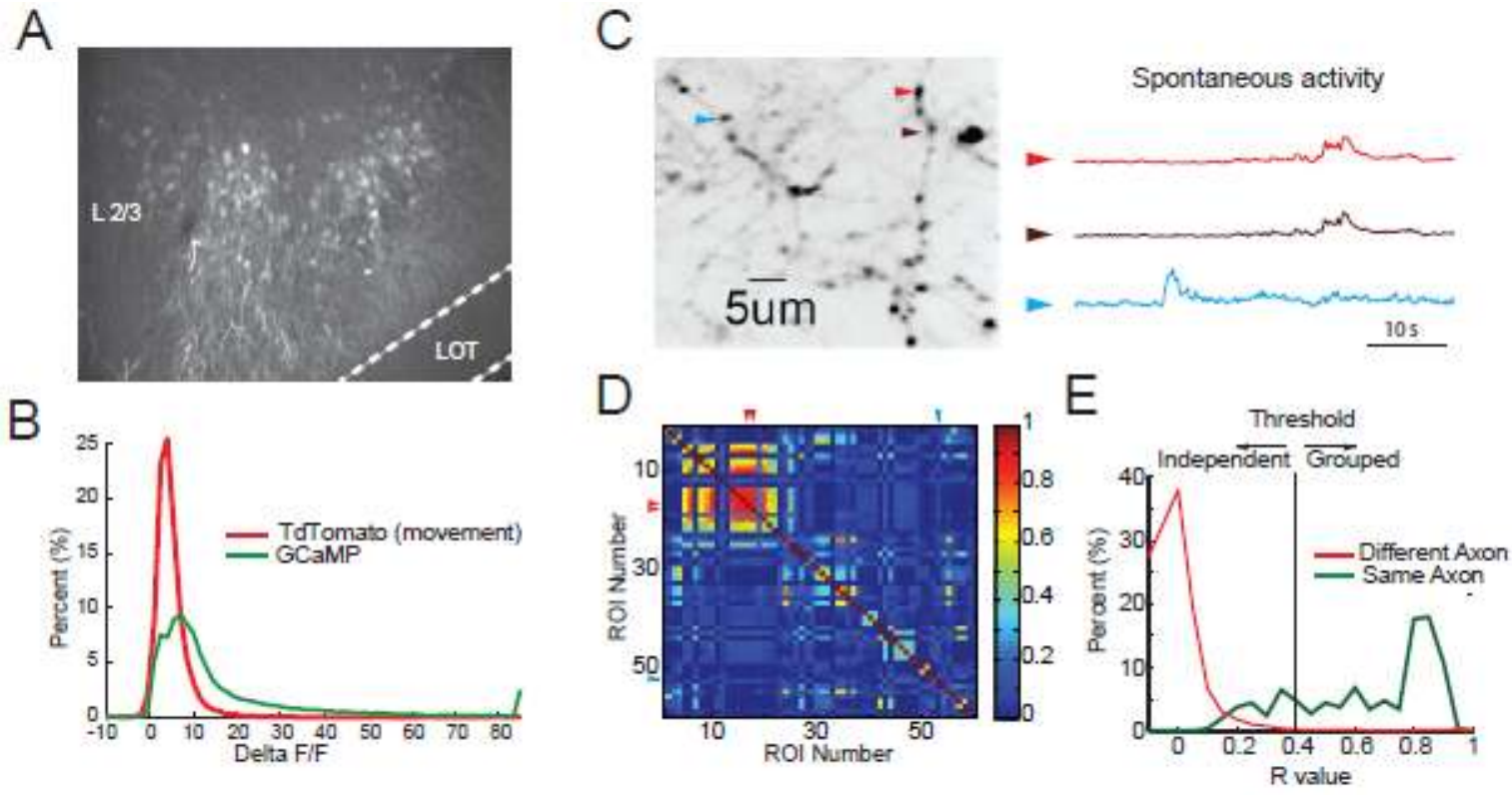
A
L 2/3
LOT
B
Percent (%)
Delta F/F
TdTomato (movement)
GCaMP
C
5um
Spontaneous activity
10 s
D
ROI Number
ROI Number
E
Threshold
Independent
Grouped
Different Axon
Same Axon
Percent (%)
R value

Figure S2.2 A larger panel of odors yields similar results and the effects of anesthesia produced by ketamine and urethane are equivalent, Related to Figure 2. **A)** When 14 odors are tested in each experiment, all odors have an equal probability of eliciting excitatory responses. Dashed line indicates expected value (7.14%) if each odor randomly activates boutons with equal probability (n=987 boutons, 2369 responses, 2 mice). AP, Acetophenone; 2-5 DMP, 2-5 dimyethylpyrazine; 2-4 DMT, 2-4 Dimethylthiazole; IAA, Isoamyl Acetate; Phen. Alc., Phenethyl alcohol. **B)** Tuning properties of boutons tested with 14 odors. Inset, relative fraction of nonresponding (NR) and excited boutons (E). **C,D)** Ketamine and urethane anesthesia cause similar changes in odor tuning (C1, D1) and response strength(C2, D2).

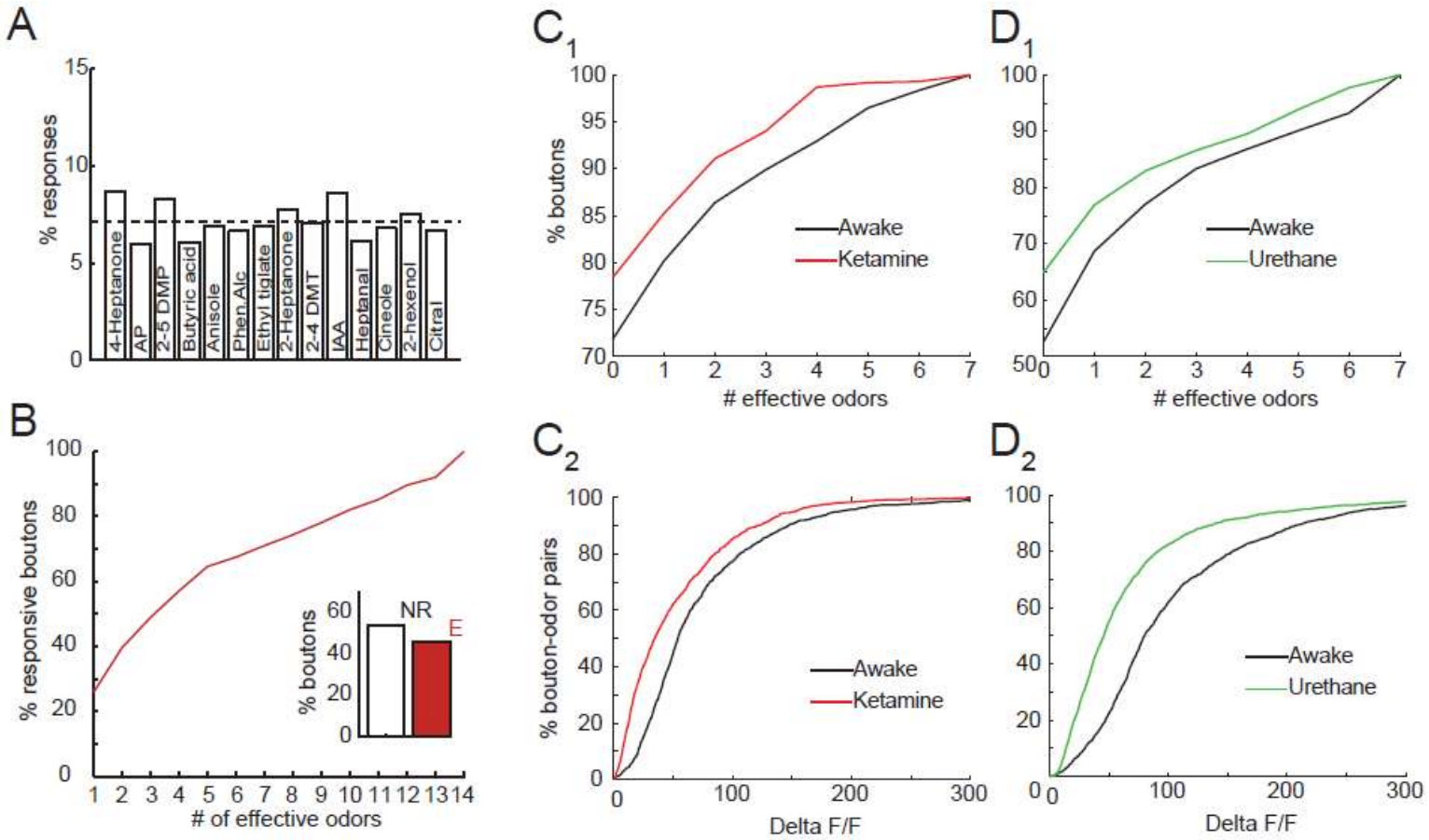
A
% responses
4-Heptanone
AP
2-5 DMP
Butyric acid
Anisole
Phen.Alc
Ethyl tiglate
2-Heptanone
2-4 DMT
IAA
Heptanal
Cineole
2-hexenol
Citral
B
% responsive boutons
# of effective odors
% boutons
NR
E
C1
% boutons
Awake
Ketamine
effective odors
D1
Awake
Urethane
effective odors
C2
% bouton-odor pairs
Awake
Ketamine
Delta F/F
D2
Awake
Urethane
Delta F/F

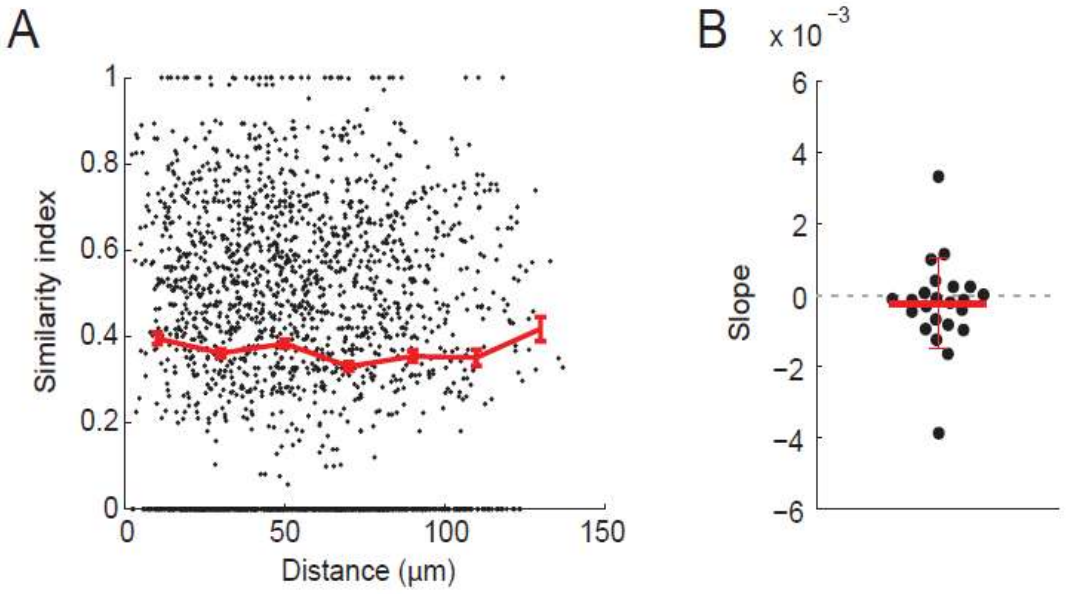

Figure S2.3 No relationship between tuning similarity and distance between boutons, Related to Figure 3. Similarity between the tuning of boutons (similarity index) was determined from the uncentered correlation coefficient (Soucy et. al, 2009):

S(A,B) = similarity of bouton A and B = $$\frac{\sum_{j=1}^{n} r_j^{(A)} r_j^{(B)}}{\sqrt{\sum_{j=1}^{n} r_j^{(A)} r_j^{(A)}} * \sqrt{\sum_{j=1}^{n} r_j^{(B)} r_j^{(B)}}}$$

where rj(A) = response of bouton A to odor j, and n = number of odors. Two boutons with the same odorant sensitivity have a similarity of 1, whereas boutons that respond to non-overlapping odor sets have a similarity of 0.

A). Data for boutons in Fig. 3A (n=4390 bouton pairs). Red line indicates binned similarity index. B). Regression line fit to the data from each experiment indicates no relationship between bouton distance and similarity index (Slope: -0.000251 ± 0.0013, p = 0.3511, n=22 fields).

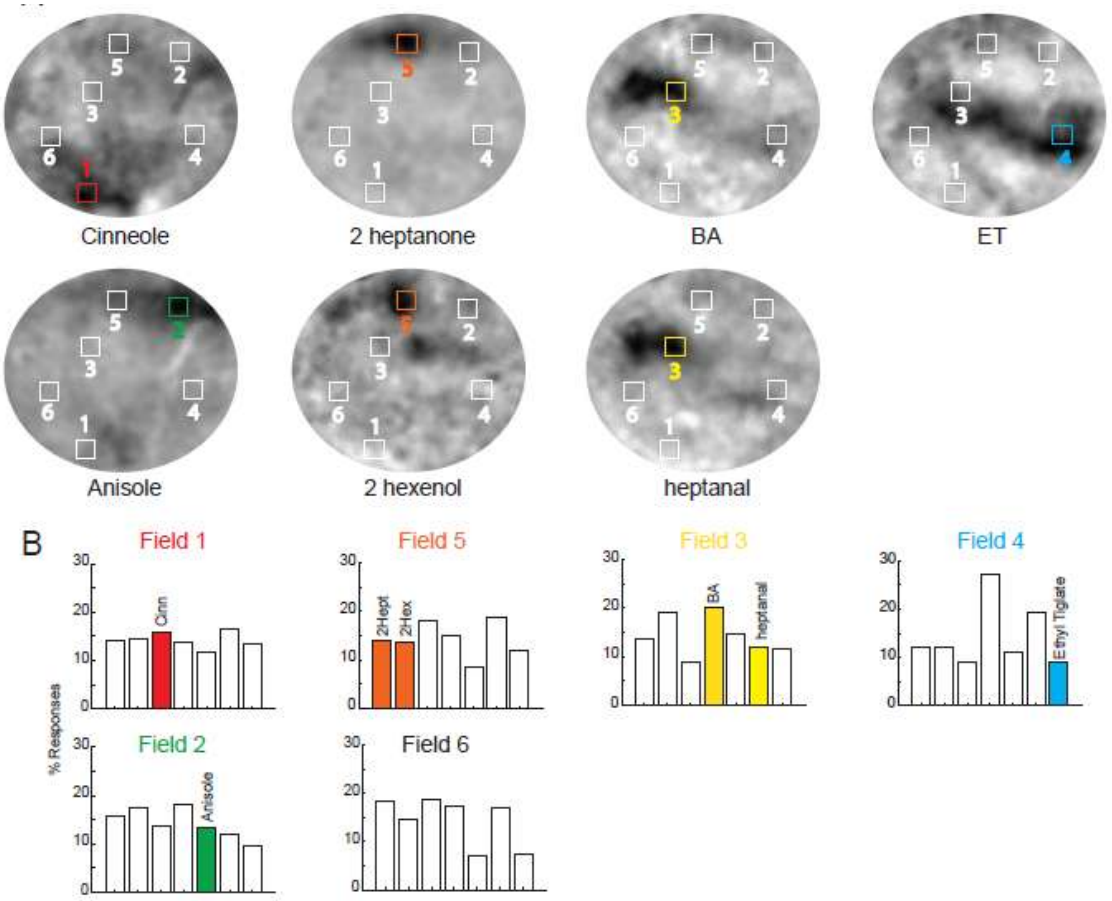

Figure S2.4 Tiling across six identified glomerular imaging fields with odors representing distinct functional groups does not reveal co-tuning of feedback projections or obvious spatial organization, Related to Figure 4.

A) Glomerular intrinsic optical imaging responses to 7 structurally distinct odors (represented functional groups include alcohol, aldehyde, ester, carboxylic acid, ketone) in one mouse. Boxes show locations of subsequent 2-photon imaging fields which span the glomerular sheet. **B)** % Responses for each of the 7 odors from cortical feedback boutons within each 2-photon imaged field. Colored squares in A indicate fields that overlay an activated glomerulus, the odors which activated that glomerulus are color matched in B. Field 1: 114 responsive boutons, field 2: 115 responsive boutons, field 3: 172 responsive boutons, field 4: 152 responsive boutons, field 5: 136 responsive boutons, field 6: 158 responsive boutons.

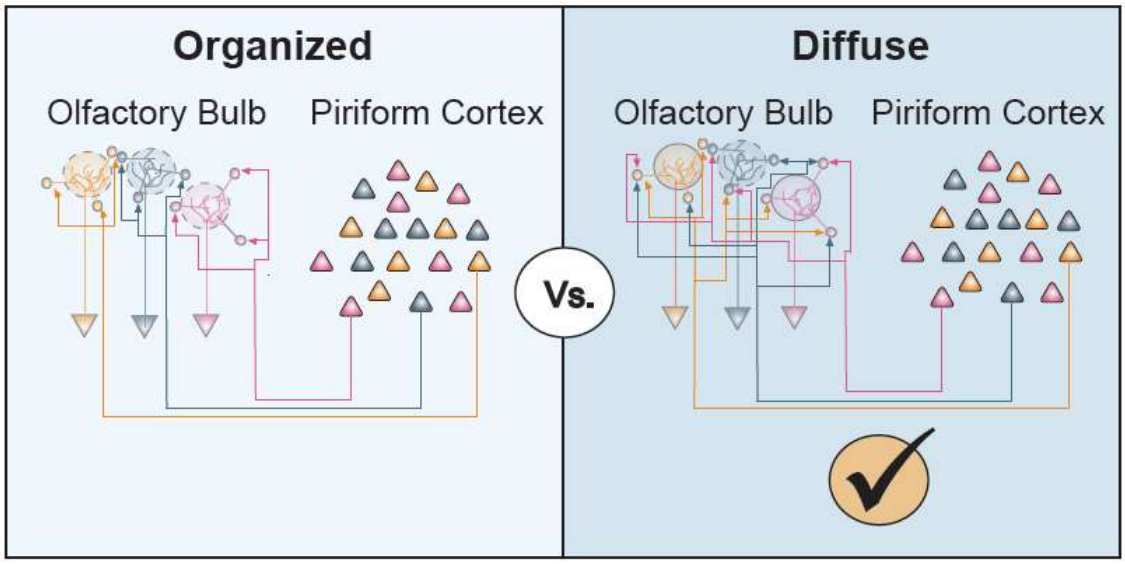

Figure S2.5 Graphical abstract depicting the diffuse organization of cortical feedback projections, which lack obvious matching spatial organization to glomerular OB targets.

Acknowledgments

This chapter is a reprint of the material as it appears in Boyd AM, Kato HK, Komiyama T, Isaacson JS. Broadcasting of cortical activity to the olfactory bulb. Cell Reports 2015 *In Press.* The dissertation author was the first author of this material, and conducted all experiments. Co-authors Hiroyuki Kato and Takaki Komiyama generously contributed analysis code, technical expertise, and assistance with initial setup and training. Last author Jeffry Isaacson provided extensive scientific input and resources throughout, as well as setup and training.

Conclusion

Mammalian brains integrate and use sensory information in a highly adaptive, flexible manner depending on environmental and behavioral context. While the sensory landscape is vast, animals routinely depend on the ability to isolate key features from a multitude of sensory inputs, and dynamically route limited processing power to accomplish behaviorally relevant tasks. This may mean reducing responsiveness to some stimuli which are irrelevant to the task at hand, while enhancing responsiveness to highly salient stimuli (Knudsen 2007; Baluch and Itti, 2011). In early stages of odor processing in the bulb, there is evidence that mitral and tufted cell activity can be modulated by behavioral context in an awake behaving animal (Kay and Laurent, 1999), suggesting higher cortical areas directly influence bulbar representations. `

While it can be convenient to consider a simplified model of odor processing as a linear path from the sensory periphery to the cortex, increasing evidence suggests that the cortex plays a pivotal role in modulating earlier stages of sensory processing (Restrepo *et al*, 2009; Noudoost *et al*, 2010). Descending cortical feedback projections are a universal feature across sensory systems, and allow the cortex to shape both the content and delivery of its own input. The goal of my thesis work was to establish the functional connectivity of this feedback pathway in the mammalian olfactory system, its impact on early odor processing, and to gain insight into the nature of the information PCx is sending back to OB.

Cortical feedback drives inhibition of M/T cells

M/T neurons represent the main relay between incoming OSN inputs and subsequent cortical processing. Their spiking is the sole output of the OB, and reflects not only the integration of a massive convergence of sensory inputs from OSNs, but also extensive shaping by local inhibitory inputs (Hamilton and Kauer, 1985; Hamilton and Kauer, 1989; Strowbridge, 2009). Our results suggest that M/T cells do not receive direct excitatory inputs from PCx feedback projections, although we do observe very small excitatory currents, which are insufficient to drive spiking under any conditions and may reflect spillover or extra-synaptic activation. This finding differs from results examining feedback from the anterior olfactory nucleus (AON), another higher order olfactory area, which was able to elicit weak excitatory responses in M/T cells sufficient to drive a slight increase in spike probability in the absence of odor *in vivo* (Markopoulous *et al*, 2012). However, like feedback from the AON, the predominant effect of PCx feedback on M/T cells is to drives substantial inhibition. We find that this inhibition is sufficient to reduce M/T cell spiking in vitro, and to reduce odor-evoked, but not spontaneous, M/T cell spiking *in vivo*.

Despite the absence of direct excitatory inputs from PCx to M/T cells, previous studies have established that small amplitude, short IPSCs frequently elicit rebound spiking in M/T cells while longer, larger hyperpolarizations routinely reduce spiking output (Balu and Strowbridge, 2007; Desmaisons *et al*, 1999). Our *in vitro* results demonstrate that in addition to reducing spiking, synchronous activation of cortical feedback projections can actually increase the firing rate of M/T cells by eliciting

rebound spiking. This raises the interesting possibility that depending on the synchronicity and timing of cortical input to OB interneurons, the cortex can bi-directionally modulate M/T cell output purely via disynaptic inhibition.

Cortical feedback generates excitation in granule cells

Our results confirm that cortical feedback directly excites granule cells. Extracellular stimulation of proximal, presumptive cortical synapses onto granule cells has previously been suggested to gate GC spiking, and thus recurrent and lateral dendrodendritic inhibition onto M/T cells, in conjunction with sensory-driven M/T input onto distal GC dendrites (Balu *et al*, 2007; Halabisky and Strowbridge, 2003). Given the fact that sensory stimulation has been found to sparsely and weakly activate granule cells (Cang and Isaacson, 2003; Kato *et al*, 2012), and cortical synapses onto GCs occur on proximal dendrites and are strongly facilitating, they may be uniquely poised to provide the coincident input needed to relieve Mg blockade of NMDA receptors at GC distal dendrites (Balu *et al* 2007).

Presumptive cortical feedback synapses onto proximal dendrites of GCs can undergo spike timing dependent plasticity (Gao and Stowbridge, 2009). LTP of cortical synapses onto proximal GC dendrites is particularly robust in young newborn granule cells (Nissant *et al*. 2009), and cortical inputs have been shown to be form some of the earliest connections with young granule cells (Arenkiel *et al*, 2011). This suggests that cortical feedback onto GCs may not only be important in regulating lateral inhibition onto M/T cells, but may play a crucial role in the integration of

newborn granule cells into existing bulbar circuits. We observe substantial variability in the amplitude of cortically evoked EPSCs in GCs *in vitro*, which may reflect age related differences in the relative input of cortical feedback projections to a given GC, although we cannot rule out the possibility that it is due to limited or variable ChR2+ expression in cortical feedback axons. An interesting possibility for future experiments is to examine whether the strength of cortical feedback projections onto GCs is correlated with either age or odor-specific learning.

Interestingly, we find that while in many GCs activation of cortical feedback projections evoked subthreshold excitatory inputs, in some cell-attached recordings, ChR2+ stimulation of cortical inputs was sufficient to evoke action potentials in GCs. This raises the possibility that the cortex may generate GC spiking *in vivo* even in GCs receiving little or no M/T cell driven excitation, serving to broadly enhance inhibition onto M/T cells and globally adjust the gain of OB output. Dual recordings of M/T and GCs show that GC spiking is coincident with M/T inhibition and that the onset of EPSCs in GCs always precedes IPSC onset in M/Ts. In conjunction with the extremely high density of projection axons in the granule cell layer, this suggests that GCs likely provide a substantial fraction of the observed inhibition in M/T cells.

In a 2010 study, Abraham *et al* show convincing evidence that manipulating AMPAR subtypes in GCs to allow for additional Ca2+ influx and subsequent GABA release both directly enhances GC mediated inhibition of M/T neurons, and enhances the speed and accuracy of odor discrimination (Abraham *et al*, 2010). Thus one role of

cortical enhancement of inhibition onto M/T neurons may be to sharpen odor tuning, and reduce the responsiveness of M/T neurons to non-preferred odors.

Cortical feedback drives inhibition of granule cells via excitation of dSACs

In examining the effects of cortical feedback projections on GCs, we found that many GCs receive cortically evoked inhibition as well as excitation, and that this inhibition substantially truncated the duration of cortically evoked excitation. Fast feed-forward inhibition has previously been shown to be an important regulator of spike timing, imposing limits on how long a postsynaptic cell has to integrate excitatory inputs and reach spike threshold (Pouille and Scanziani, 2001). Thus by driving both direct excitation and feed-forward inhibition onto GCs, cortical feedback projection may be able to generate precisely timed GC spike output. And while cortical excitation was sufficient to drive spiking in some GCs, the majority received subthreshold excitation. Thus GCs receiving coincident M/T and cortically mediated excitation may reach spike threshold, whereas if the timing of M/T and cortically mediated excitation is offset, cortically driven inhibition may prevent GC spiking in the majority of cells.

We establish that cortically driven inhibition of GCs is mediated by deep short axon cells, with relatively few dSACs contributing to cortically evoked IPSCs in a given GC. While a specific subtypes of dSAC, the Blanes cell, has previously been shown to provide inhibition to GCs, the source of dSAC's excitatory inputs had not previously been established (Eyre *et al* 2008, 2009; Pressler and Strowbridge 2006.). Interestingly, we find that compared to GCs, while the size of a unitary cortical input is

similar, dSACs receive a much higher convergence of cortical inputs and are thus preferentially driven by cortical activation. One prediction of this result is that given that dSACs are receiving input from many different pyramidal neurons, they are likely to show very broad odor tuning. Although seven distinct types of dSACs have been described (Eyre *et al*, 2008, 2009), a uniform molecular marker for this cell class has yet to be identified. However, given their large size relative to granule cells, in-vivo calcium imaging may still be a viable method to test this prediction. These results substantially expand our knowledge of the functional role of dSACs and establish a circuit by which cortical feedback can actually disinhibit M/T cells, via dSAC generated inhibition of GCs.

Glomerular layer targets of cortical feedback

Recordings in the glomerular layer during cortical feedback stimulation reveal that both periglomerular and superficial short axon cells receive monosynaptic excitatory inputs from PCx, while external tufted cells are inhibited disynaptically. While glomerular interneurons may contribute to the inhibition observed in M/T cells, we find GCs to be the main drivers. We observe cortically evoked inhibition in M/T cells missing their apical tuft, and thus lacking glomerular layer inhibitory contacts. In addition, focal ChR2+ stimulation of feedback axons in the glomerular layer surrounding of a given M/T cell's apical tuft evoked evoked minimal or no inhibition, while stimulation of the GC layer immediately below the soma of the M/T cell consistently evoked robust IPSCs, suggesting a larger contribution from GCs to

cortically evoked inhibition of M/T cells. However, given that ET cells provide substantial feedforward dendrodendritic excitation to M/T cells (Najac *et al* 2011; Gire *et al* 2012), cortically driven inhibition of ET cells via juxtaglomerular interneurons may reduce odor evoked excitation onto M/T cells as well.

In vivo activation experiments performed by postdoc James F. Sturgill confirm that although pathways for both inhibition and disinhibition of M/T cells by cortical feedback projections exist, the predominant effect of increasing activity in PCx is to suppress odor-evoked excitation, and enhance odor-evoked inhibition in single unit recordings of presumptive M/T cells. Interestingly, this suppressive effect was specific to odor evoked responses and increasing PCx activity had no consistent effect on spontaneous M/T cell spiking. In addition, we find that photoactivation of PCx neurons disrupts odor evoked beta oscillations both in PCx and in OB, indicating that the long range feedback loop plays a role in oscillatory dynamics, and odor evoked beta oscillations do not solely arise from the OB. This highlights the rich interconnectivity between the bulb and the cortex, and suggest a role for PCx in continuously modulating the temporal structure of OB output.

Our *in vivo* optogenetic results did not reveal any odor specificity of cortical feedback modulation. However, in these experiments while M/T cell excitation was driven by odor presentation, amplification of feedback activity (on top of the odor-evoked response) was accomplished via photoactivation of a random subset of PCx pyramidal neurons. If only the odor-activated population is amplified, odor specific modulation may become visible. Given recent advances which allow the use of

immediate early genes like c-fos to drive optogenetic construct expression in an inducible and activity dependent manner (Liu *et al*, 2012), odor specificity of cortical modulation of M/T cells can now be tested more directly.

Characterization of feedback projections in awake animals

Having established the postsynaptic targets of PCx feedback projections and the predominant effect of their activation in an anesthetized mouse, we subsequently sought to examine their endogenous activity in awake animals calcium imaging of feedback projection axons in the bulb. Using this technique we find that odor evoked increases in activity occurred in a higher percentage of cortical feedback boutons (21.2% of 5353 total boutons) than odor evoked suppression (11.5%), which may reflect the need for high levels of basal activity needed to detect suppression using GCaMP. The fraction of odor responsive boutons observed (24%) is similar to previous results from direct PCx imaging (Stettler and Axel, 2009), and we find that the majority of responsive boutons are narrowly tuned (~50% responding to 2 or fewer odors) while a smaller subset show broad responsiveness. Although the majority (~65%) of boutons did not respond to any of the tested odors, this likely reflects high odor selectivity, as nearly all cells (>90%) demonstrated spontaneous activity indicating their functionality. Responses had variable temporal dynamics, with some showing highly time-locked odor evoked responses while others responded to odor offsets or for prolonged periods lasting tens of seconds. Feedback projections in the glomerular layer and granule cell layer were similar in terms of their odor tuning,

spontaneous activity, and response frequency/amplitude, suggesting they may arise from the same pyramidal cell population. We did observe substantially more projections within GCL, consistent with prior results (Matsutani 2010, Boyd *et al* 2012, Markopoulous *et al*, 2012). In addition, we found that across a broad sample of boutons, different odors were equally likely to elicit responses. This held true for larger odor panels (14 odors), and odors which activate dorsal glomeruli were no more likely to elicit response than those whose glomerular activation is exclusively ventral, and thus distant from our imaging plane. Indeed, axons with distinct tuning properties and odor preferences were often found immediately adjacent to one another. Together, these results highlight the complexity and potential flexibility of the cortico-bulbar feedback loop. PCx sends a heterogeneous array of inputs to bulbar interneurons, which may serve a variety of functions that remain to be explored, such as altering the synchronicity of M/T cell firing or enhancing lateral inhibition onto M/T cells.

Previous studies have shown that OB activity is highly brain state dependent (Ringberg *et al*, 2006) and that anesthesia substantially reduces bulbar interneuron activity while increasing M/T odor-evoked activity relative to when the animal is awake (Cazakoff *et al*, 2014; Kato *et al*, 2012; Wachowiak *et al*, 2013). Most previous work in PCx has been done in anesthetized animals, in large part due to anatomical constraints which require jaw or eye removal to expose the PCx. In order to compare our results to prior findings in anesthetized animals and to determine whether cortical feedback projections would show decreased activity during wakefulness (due to relative decreases in M/T cell input to PCx) or increased activity during wakefulness (which

might contribute to the previously observed increased bulbar interneuron activity) we examined the effects of urethane and ketamine anesthesia. We find that anesthetics reduce the amplitude, duration, and frequency of odor-evoked responses, and also reduce spontaneous activity in cortical feedback boutons, suggesting that the enhancement of responsiveness in cortical feedback projections when animals are awake likely contributes to the increased bulbar interneuron activity in the awake state. Overall, our findings are consistent with prior characterizations of PCx activity (Stettler and Axel, 2009; Poo and Isaacson, 2009; Zhan and Luo, 2010), and we see no functional evidence to suggest that cortical feedback projections arise from a distinct or unique cell population within the cortex. However, this result will benefit from future imaging experiments in PCx, for example using retrobeads to label OB projecting pyramidal neurons and comparing their activity to unlabeled PCx neurons.

Cortical feedback projections show no functional topography.

Thalamocortical feedback projections in the visual, auditory, and somatosensory cortex have previously been shown to be topographically and functionally matched, so that cortical cells project to thalamic neurons with similar functional tuning properties. However, in each of these sensory systems both the relevant thalamic nuclei and primary sensory cortices are topographically organized. In the OB, the glomerular layer shows stereotyped spatial topography, while in PCx odor representations are encoded by diffuse ensembles of neurons lacking spatial discernable organization.

Our findings strongly suggest that PCx feedback projections are diffuse, overlapping, and do not demonstrate matching functional/spatial organization to their postsynaptic targets. Within random fields of view in both the glomerular and granule cell layer, we saw no evidence that a given odor was represented more than would be expected by chance. In addition, axons with the same odor preference were not clustered. Using a combination of intrinsic optical imaging to map glomerular layer odor preferences, and 2-photon imaging of the underlying feedback projections, we see no evidence that cortical feedback projections are co-tuned with their glomerular layer targets. Indeed, the percentage of bouton responses to a given odor had no relationship with whether or not that odor activated the overlying glomerulus, and glomeruli tuned to one specific odor were surrounded by feedback projections responding to all tested odors. Although we cannot rule out the possibility that co-tuning between cortical feedback projections and their post-synaptic targets may occur on a much broader scale, as has been reported for AON feedback to OB (Rothermel and Wachowiak, 2014), our results suggest that in contrast of 'egocentric' thalamocortical feedback, PCx feedback broadcasts odor information widely across spatially ordered bulbar circuits, and is unlikely to selectively target bulbar cells sharing the same tuning.

This thesis work provides methodological advances to the study of cortical feedback projections within the olfactory system and provides testable predictions for future work. Taken together, these results offer a substantial advancement of our understanding of the functional circuitry of feedback connections between the PCx and OB, as well as their role in modulating bulbar output.

References

Abraham NM, Egger V, Shimshek DR, Renden R, Fukunaga I, Sprengel R, Seeburg PH, Klugmann M, Margrie TW, Schaefer AT, Kuner T. Synaptic inhibition in the olfactory bulb accelerates odor discrimination in mice. Neuron. 2010 Feb 11;65(3):399-411.

Adesnik, H., and Scanziani, M. (2010). Lateral competition for cortical space by layer-specific horizontal circuits. Nature 464, 1155-1160.

Andolina IM, Jones HE, Wang W, Sillito AM. Corticothalamic feedback enhances stimulus response precision in the visual system. Proc Natl Acad Sci U S A. 2007 Jan 30;104(5):1685-90.

Apicella A, Yuan Q, Scanziani M, Isaacson JS. Pyramidal cells in piriform cortex receive convergent input from distinct olfactory bulb glomeruli. J Neurosci. 2010 Oct 20;30(42):14255-60.

Arenkiel BR, Hasegawa H, Yi JJ, Larsen RS, Wallace ML, Philpot BD, Wang F, Ehlers MD. Activity-induced remodeling of olfactory bulb microcircuits revealed by monosynaptic tracing. PLoS One. 2011;6(12):e29423.

Arevian, A.C., Kapoor, V., and Urban, N.N. (2008). Activity-dependent gating of lateral inhibition in the mouse olfactory bulb. Nat. Neurosci. 11, 80–87.

Atasoy, D., Aponte, Y., Su, H.H., and Sternson, S.M. (2008). A FLEX switch targets Channelrhodopsin-2 to multiple cell types for imaging and long-range circuit mapping. J Neurosci 28, 7025-7030.

Aungst JL, Heyward PM, Puche AC, Karnup SV, Hayar A, Szabo G, Shipley MT. Centre-surround inhibition among olfactory bulb glomeruli. Nature. 2003 Dec 11;426(6967):623-9.

Balu, R., and Strowbridge, B.W. (2007). Opposing inward and outward conductances regulate rebound discharges in olfactory mitral cells. Journal of neurophysiology 97, 1959-1968.

Balu, R., Pressler, R.T., and Strowbridge, B.W. (2007). Multiple modes of synaptic excitation of olfactory bulb granule cells. The Journal of neuroscience : the official journal of the Society for Neuroscience 27, 5621-5632.

Baluch F, Itti L. Mechanisms of top-down attention. Trends Neurosci. 2011 Apr;34(4):210-24.

Barnes DC, Hofacer RD, Zaman AR, Rennaker RL, Wilson DA. Olfactory perceptual stability and discrimination. Nat Neurosci. 2008 Dec;11(12):1378-80.

Bathellier, B., Buhl, D.L., Accolla, R., and Carleton, A. (2008). Dynamic ensemble odor coding in the mammalian olfactory bulb: sensory information at different timescales. Neuron 57, 586-598.

Bekkers JM, Suzuki N. Neurons and circuits for odor processing in the piriform cortex. Trends Neurosci. 2013 Jul;36(7):429-38.

Blauvelt, D.G., Sato, T.F., Wienisch, M., Knöpfel, T., and Murthy, V.N. (2013). Distinct spatiotemporal activity in principal neurons of the mouse olfactory bulb in anesthetized and awake states. Front. Neural Circuits 7, 46.

Boyd, A.M., Sturgill, J.F., Poo, C., and Isaacson, J.S. (2012). Cortical feedback control of olfactory bulb circuits. Neuron 76, 1161–1174.

Briggs, F., and Usrey, W.M. (2008). Emerging views of corticothalamic function. Curr. Opin. Neurobiol. 18, 403–407.

Buck L, Axel R. A novel multigene family may encode odorant receptors: a molecular basis for odor recognition. Cell. 1991 Apr 5;65(1):175-87.

Buck LB. Information coding in the mammalian olfactory system. Cold Spring Harb Symp Quant Biol. 1996;61:147-55.

Buonviso N, Chaput MA. Scott J.W.Mitral cell-to-glomerulus connectivity: an HRP study of the orientation of mitral cell apical dendrites J. Comp. Neurol., 307 (1991), pp. 57–64.

Buonviso N, Revial MF, Jourdan F. The Projections of Mitral Cells from Small Local Regions of the Olfactory Bulb: An Anterograde Tracing Study Using PHA-L (Phaseolus vulgaris Leucoagglutinin). Eur J Neurosci. 1991 Jun;3(6):493-500.

Cang, J., and Isaacson, J.S. (2003). In vivo whole-cell recording of odor-evoked synaptic transmission in the rat olfactory bulb. J Neurosci 23, 4108-4116.

Cauthron JL, Stripling JS. Long-term plasticity in the regulation of olfactory bulb activity by centrifugal fibers from piriform cortex. J Neurosci. 2014 Jul 16;34(29):9677-87.

Cazakoff, B.N., Lau, B.Y.B., Crump, K.L., Demmer, H.S., and Shea, S.D. (2014). Broadly tuned and respiration-independent inhibition in the olfactory bulb of awake mice. Nat. Neurosci. 17, 569–576.

Chen, T.-W., Wardill, T.J., Sun, Y., Pulver, S.R., Renninger, S.L., Baohan, A., Schreiter, E.R., Kerr, R.A., Orger, M.B., Jayaraman, V., et al. (2013). Ultrasensitive fluorescent proteins for imaging neuronal activity. Nature 499, 295–300.

Chen, W.R., Xiong, W., and Shepherd, G.M. (2000). Analysis of relations between NMDA receptors and GABA release at olfactory bulb reciprocal synapses. Neuron 25, 625-633.

Choi GB, Stettler DD, Kallman BR, Bhaskar ST, Fleischmann A, Axel R. Driving opposing behaviors with ensembles of piriform neurons. Cell. 2011 Sep 16;146(6):1004-15.

Christie, J.M., Schoppa, N.E., and Westbrook, G.L. (2001). Tufted cell dendrodendritic inhibition in the olfactory bulb is dependent on NMDA receptor activity. Journal of neurophysiology 85, 169-173.

Cleland, T.A., and Linster, C. (2012). On-Center/Inhibitory-Surround Decorrelation via Intraglomerular Inhibition in the Olfactory Bulb Glomerular Layer. Frontiers in integrative neuroscience 6, 5.

Contreras D, Destexhe A, Sejnowski TJ, Steriade M. Control of spatiotemporal coherence of a thalamic oscillation by corticothalamic feedback. Science. 1996 Nov 1;274(5288):771-4.

Cudeiro, J., and Sillito, A.M. (2006). Looking back: corticothalamic feedback and early visual processing. Trends in neurosciences 29, 298-306.

Davis, B.J., and Macrides, F. (1981). The organization of centrifugal projections from the anterior olfactory nucleus, ventral hippocampal rudiment, and piriform cortex to the main olfactory bulb in the hamster: an autoradiographic study. The Journal of comparative neurology 203, 475-493.

Davison, I.G., and Katz, L.C. (2007). Sparse and selective odor coding by mitral/tufted neurons in the main olfactory bulb. J Neurosci 27, 2091-2101.

De Olmos, J., Hardy, H., and Heimer, L. (1978). The afferent connections of the main and the accessory olfactory bulb formations in the rat: an experimental HRP-study. J. Comp. Neurol. 181, 213–244.

Desmaisons, D., Vincent, J.D., and Lledo, P.M. (1999). Control of action potential timing by intrinsic subthreshold oscillations in olfactory bulb output neurons. The Journal of neuroscience : the official journal of the Society for Neuroscience 19, 10727-10737.

Eyre, M.D., Antal, M., and Nusser, Z. (2008). Distinct deep short-axon cell subtypes of the main olfactory bulb provide novel intrabulbar and extrabulbar GABAergic connections. The Journal of neuroscience : the official journal of the Society for Neuroscience 28, 8217-8229.

Eyre, M.D., Kerti, K., and Nusser, Z. (2009). Molecular diversity of deep short-axon cells of the rat main olfactory bulb. The European journal of neuroscience 29, 1397-1407.

Franks KM, Russo MJ, Sosulski DL, Mulligan AA, Siegelbaum SA, Axel R. Recurrent circuitry dynamically shapes the activation of piriform cortex. Neuron. 2011 Oct 6;72(1):49-56.

Friedrich RW, Korsching SI. Combinatorial and chemotopic odorant coding in the zebrafish olfactory bulb visualized by optical imaging. Neuron. 1997 May;18(5):737-52.

Gao, Y., and Strowbridge, B.W. (2009). Long-term plasticity of excitatory inputs to granule cells in the rat olfactory bulb. Nat Neurosci 12, 731-733.

Ghosh S, Murray GM, Turman AB, Rowe MJ. Corticothalamic influences on transmission of tactile information in the ventroposterolateral thalamus of the cat: effect of reversible inactivation of somatosensory cortical areas I and II. Exp Brain Res. 1994;100(2):276-86.

Ghosh, S., Larson, S.D., Hefzi, H., Marnoy, Z., Cutforth, T., Dokka, K., and Baldwin, K.K. (2011). Sensory maps in the olfactory cortex defined by long-range viral tracing of single neurons. Nature 472, 217–220.

Giessel, A.J., and Datta, S.R. (2014). Olfactory maps, circuits and computations. Curr. Opin. Neurobiol. 24, 120–132.

Gire, D.H., and Schoppa, N.E. (2009). Control of on/off glomerular signaling by a local GABAergic microcircuit in the olfactory bulb. The Journal of neuroscience : the official journal of the Society for Neuroscience 29, 13454-13464.

Gire DH, Franks KM, Zak JD, Tanaka KF, Whitesell JD, Mulligan AA, Hen R, Schoppa NE. Mitral cells in the olfactory bulb are mainly excited through a multistep signaling path. J Neurosci. 2012 Feb 29;32(9):2964-75.

Glickfeld, L.L., Andermann, M.L., Bonin, V., and Reid, R.C. (2013). Cortico-cortical projections in mouse visual cortex are functionally target specific. Nat. Neurosci. 16, 219–226.

Gottfried JA. Central mechanisms of odour object perception. Nat Rev Neurosci. 2010 Sep;11(9):628-41.

Gray, C.M., and Skinner, J.E. (1988). Centrifugal regulation of neuronal activity in the olfactory bulb of the waking rabbit as revealed by reversible cryogenic blockade. Exp Brain Res 69, 378-386.

Haberly LB, Hansen DJ, Feig SL, Presto S. Distribution and ultrastructure of neurons in opossum piriform cortex displaying immunoreactivity to GABA and GAD and high-affinity tritiated GABA uptake. J Comp Neurol. 1987 Dec 8;266(2):269-90.

Haberly LB. Neuronal circuitry in olfactory cortex: anatomy and functional implications. Chem Senses. 1985 **10**:219–238.

Haberly, L.B. (2001). Parallel-distributed processing in olfactory cortex: new insights from morphological and physiological analysis of neuronal circuitry. Chem Senses 26, 551-576.

Haberly, L.B., and Price, J.L. (1978). Association and commissural fiber systems of the olfactory cortex of the rat. J. Comp. Neurol. 178, 711–740.

Halabisky, B., and Strowbridge, B.W. (2003). Gamma-frequency excitatory input to granule cells facilitates dendrodendritic inhibition in the rat olfactory Bulb. Journal of neurophysiology 90, 644-654.

Halabisky, B., Friedman, D., Radojicic, M., and Strowbridge, B.W. (2000). Calcium influx through NMDA receptors directly evokes GABA release in olfactory bulb granule cells. The Journal of neuroscience : the official journal of the Society for Neuroscience 20, 5124-5134.

Hamilton, K.A. & Kauer, J.S., Intracellular potentials of salamander mitral/tufted neurons in response to odor stimulation. *Brain Res* 338 (1), 181-185 (1985).

Hamilton, K.A. & Kauer, J.S., Patterns of intracellular potentials in salamander mitral/tufted cells in response to odor stimulation. J Neurophysiol 62 (3), 609-625 (1989).

Hayar, A., Karnup, S., Ennis, M., and Shipley, M.T. (2004). External tufted cells: a major excitatory element that coordinates glomerular activity. The Journal of neuroscience : the official journal of the Society for Neuroscience 24, 6676-6685.

Hazama M, Kimura A, Donishi T, Sakoda T, Tamai Y. Topography of corticothalamic projections from the auditory cortex of the rat. Neuroscience. 2004;124(3):655-67.

He J. Modulatory effects of regional cortical activation on the onset responses of the cat medial geniculate neurons. J Neurophysiol. 1997 Feb;77(2):896-908.

He, J. (2003). Corticofugal modulation of the auditory thalamus. Exp. Brain Res. 153, 579–590.

Hoogland, P. V, Welker, E., and Van der Loos, H. (1987). Organization of the projections from barrel cortex to thalamus in mice studied with Phaseolus vulgaris-leucoagglutinin and HRP. Exp. Brain Res. 68, 73–87.

Illig, K.R., and Haberly, L.B. (2003). Odor-evoked activity is spatially distributed in piriform cortex. J. Comp. Neurol. 457, 361–373.

Isaacson, J.S., and Strowbridge, B.W. (1998). Olfactory reciprocal synapses: dendritic signaling in the CNS. Neuron 20, 749-761.

Johnson DM, Illig KR, Behan M, Haberly LB. New features of connectivity in piriform cortex visualized by intracellular injection of pyramidal cells suggest that "primary" olfactory cortex functions like "association" cortex in other sensory systems. J Neurosci. 2000 Sep 15;20(18):6974-82.

Jones N, Rog D. Olfaction: a review. J Laryngol Otol. 1998 Jan;112(1):11-24.

Kadohisa M, Wilson DA. Separate encoding of identity and similarity of complex familiar odors in piriform cortex. Proc Natl Acad Sci U S A. 2006 Oct 10;103(41):15206-11.

Kato, H.K., Chu, M.W., Isaacson, J.S., and Komiyama, T. (2012). Dynamic sensory representations in the olfactory bulb: modulation by wakefulness and experience. Neuron 76, 962–975.

Kiyokage E, Pan YZ, Shao Z, Kobayashi K, Szabo G, Yanagawa Y, Obata K, Okano H, Toida K, Puche AC, Shipley MT. Molecular identity of periglomerular and short axon cells. J Neurosci. 2010 Jan 20;30(3):1185-96.

Knudsen EI. Fundamental components of attention. Annu Rev Neurosci. 2007;30:57-78.

Lagier, S., Panzanelli, P., Russo, R.E., Nissant, A., Bathellier, B., Sassoe-Pognetto, M., Fritschy, J.M., and Lledo, P.M. (2007). GABAergic inhibition at dendrodendritic synapses tunes gamma oscillations in the olfactory bulb. Proceedings of the National Academy of Sciences of the United States of America 104, 7259-7264.

Laurent, G. (2002). Olfactory network dynamics and the coding of multidimensional signals. Nat Rev Neurosci 3, 884-895.

Li L, Ebner FF. Cortical modulation of spatial and angular tuning maps in the rat thalamus. J Neurosci. 2007 Jan 3;27(1):167-79.

Linster C, Cleland TA. Decorrelation of Odor Representations via Spike Timing-Dependent Plasticity. Front Comput Neurosci. 2010 Dec 28;4:157.

Liu X, Ramirez S, Pang PT, Puryear CB, Govindarajan A, Deisseroth K, Tonegawa S. Optogenetic stimulation of a hippocampal engram activates fear memory recall. Nature. 2012 Mar 22;484(7394):381-5.

Lledo, P.M., Alonso, M., and Grubb, M.S. (2006). Adult neurogenesis and functional plasticity in neuronal circuits. Nat Rev Neurosci 7, 179-193.

Luna, V.M., and Schoppa, N.E. (2008). GABAergic circuits control input-spike coupling in the piriform cortex. J Neurosci 28, 8851-8859.

Luo M, Katz LC. Response correlation maps of neurons in the mammalian olfactory bulb. Neuron. 2001 Dec 20;32(6):1165-79.

Luskin, M.B., and Price, J.L. (1983). The topographic organization of associational fibers of the olfactory system in the rat, including centrifugal fibers to the olfactory bulb. The Journal of comparative neurology 216, 264-291.

Madisen, L., Mao, T., Koch, H., Zhuo, J.M., Berenyi, A., Fujisawa, S., Hsu, Y.W., Garcia, A.J., 3rd, Gu, X., Zanella, S., et al. (2012). A toolbox of Cre-dependent optogenetic transgenic mice for light-induced activation and silencing. Nature neuroscience.

Markopoulos, F., Rokni, D., Gire, D.H., and Murthy, V.N. (2012). Functional properties of cortical feedback projections to the olfactory bulb. Neuron 76, 1175–1188.

Martin, C., Gervais, R., Messaoudi, B., and Ravel, N. (2006). Learning-induced oscillatory activities correlated to odour recognition: a network activity. The European journal of neuroscience 23, 1801-1810.

Matsutani, S. (2010). Trajectory and terminal distribution of single centrifugal axons from olfactory cortical areas in the rat olfactory bulb. Neuroscience 169, 436-448.

McAlonan, K., Cavanaugh, J., and Wurtz, R.H. (2008). Guarding the gateway to cortex with attention in visual thalamus. Nature 456, 391–394.

Meister M, Bonhoeffer T. Tuning and topography in an odor map on the rat olfactory bulb. J Neurosci. 2001 Feb 15;21(4):1351-60.

Migliore M, Shepherd GM. Dendritic action potentials connect distributed dendrodendritic microcircuits. J Comput Neurosci. 2008 Apr;24(2):207-21.

Miyamichi K, Shlomai-Fuchs Y, Shu M, Weissbourd BC, Luo L, Mizrahi A. Dissecting local circuits: parvalbumin interneurons underlie broad feedback control of olfactory bulb output. Neuron. 2013 Dec 4;80(5):1232-45.

Miyamichi, K., Amat, F., Moussavi, F., Wang, C., Wickersham, I., Wall, N.R., Taniguchi, H., Tasic, B., Huang, Z.J., He, Z., et al. (2011). Cortical representations of olfactory input by trans-synaptic tracing. Nature 472, 191–196.

Mombaerts, P., Wang, F., Dulac, C., Chao, S.K., Nemes, A., Mendelsohn, M., Edmondson, J., and Axel, R. (1996). Visualizing an olfactory sensory map. Cell 87, 675–686.

Murphy PC, Duckett SG, Sillito AM. Feedback connections to the lateral geniculate nucleus and cortical response properties. Science. 1999 Nov 19;286(5444):1552-4.

Murphy PC, Sillito AM. Corticofugal feedback influences the generation of length tuning in the visual pathway. Nature. 1987 Oct 22-28;329(6141):727-9.

Murphy PC, Sillito AM. Functional morphology of the feedback pathway from area 17 of the cat visual cortex to the lateral geniculate nucleus. J Neurosci. 1996 Feb 1;16(3):1180-92.

Murphy PC, Sillito AM. The binocular input to cells in the feline dorsal lateral geniculate nucleus (dLGN). J Physiol. 1989 Aug;415:393-408.

Murphy, G.J., Darcy, D.P., and Isaacson, J.S. (2005). Intraglomerular inhibition: signaling mechanisms of an olfactory microcircuit. Nat Neurosci 8, 354-364.

Murphy, P.C., Duckett, S.G., and Sillito, A.M. (1999). Feedback connections to the lateral geniculate nucleus and cortical response properties. Science 286, 1552–1554.

Murthy, V.N. (2011). Olfactory maps in the brain. Annu. Rev. Neurosci. 34, 233–258.

Nakashima, M., Mori, K., and Takagi, S.F. (1978). Centrifugal influence on olfactory bulb activity in the rabbit. Brain research 154, 301-306.

Neville KR, Haberly LB, Shepherd GM (Ed.) Olfactory Cortex, Oxford University Press, New York (2004)

Neville KR, Haberly LB. Beta and gamma oscillations in the olfactory system of the urethane-anesthetized rat. J Neurophysiol. 2003 Dec;90(6):3921-30.

Neville, K.R., and Haberly, L.B. (2003). Beta and gamma oscillations in the olfactory system of the urethane-anesthetized rat. J Neurophysiol 90, 3921-3930.

Nissant, A., Bardy, C., Katagiri, H., Murray, K., and Lledo, P.M. (2009). Adult neurogenesis promotes synaptic plasticity in the olfactory bulb. Nat Neurosci 12, 728-730.

Noudoost B, Chang MH, Steinmetz NA, Moore T. Top-down control of visual attention. Curr Opin Neurobiol. 2010 Apr;20(2):183-90.

Ojima H, Mori K, Kishi K. The trajectory of mitral cell axons in the rabbit olfactory cortex revealed by intracellular HRP injection. J Comp Neurol. 1984 Nov 20;230(1):77-87.

Olsen SR, Bortone DS, Adesnik H, Scanziani M. Gain control by layer six in cortical circuits of vision. Nature. 2012 Feb 22;483(7387):47-52.

Peters, A.J., Chen, S.X., and Komiyama, T. (2014). Emergence of reproducible spatiotemporal activity during motor learning. Nature 510, 263–267.

Petreanu, L., Gutnisky, D.A., Huber, D., Xu, N., O'Connor, D.H., Tian, L., Looger, L., and Svoboda, K. (2012). Activity in motor-sensory projections reveals distributed coding in somatosensation. Nature 489, 299–303.

Petreanu, L., Mao, T., Sternson, S.M., and Svoboda, K. (2009). The subcellular organization of neocortical excitatory connections. Nature 457, 1142-1145.

Pinching, A.J., and Powell, T.P. (1971a). The neuron types of the glomerular layer of the olfactory bulb. Journal of cell science 9, 305-345.

Pinching, A.J., and Powell, T.P. (1971b). The neuropil of the periglomerular region of the olfactory bulb. Journal of cell science 9, 379-409.

Poo C, Isaacson JS. A major role for intracortical circuits in the strength and tuning of odor-evoked excitation in olfactory cortex. Neuron. 2011 Oct 6;72(1):41-8.

Poo, C., and Isaacson, J.S. (2009). Odor representations in olfactory cortex: “sparse” coding, global inhibition, and oscillations. Neuron 62, 850–861.

Pouille, F., and Scanziani, M. (2001). Enforcement of temporal fidelity in pyramidal cells by somatic feed-forward inhibition. Science 293, 1159-1163.

Pressler, R.T., and Strowbridge, B.W. (2006). Blanes cells mediate persistent feedforward inhibition onto granule cells in the olfactory bulb. Neuron 49, 889-904.

Rall, W., and Shepherd, G.M. (1968). Theoretical reconstruction of field potentials and dendrodendritic synaptic interactions in olfactory bulb. Journal of neurophysiology 31, 884-915.

Rennaker RL, Chen CF, Ruyle AM, Sloan AM, Wilson DA. Spatial and temporal distribution of odorant-evoked activity in the piriform cortex. J Neurosci. 2007 Feb 14;27(7):1534-42.

Ressler KJ, Sullivan SL, Buck LB. Information coding in the olfactory system: evidence for a stereotyped and highly organized epitope map in the olfactory bulb. Cell. 1994 Dec 30;79(7):1245-55.

Restrepo D, Doucette W, Whitesell JD, McTavish TS, Salcedo E. From the top down: flexible reading of a fragmented odor map. Trends Neurosci. 2009 Oct;32(10):525-31.

Rinberg, D., Koulakov, A., and Gelperin, A. (2006). Sparse odor coding in awake behaving mice. J. Neurosci. 26, 8857–8865.

Rothermel, M., and Wachowiak, M. (2014). Functional imaging of cortical feedback projections to the olfactory bulb. Front. Neural Circuits 8, 73.

Rubin, B.D., and Katz, L.C. (1999). Optical imaging of odorant representations in the mammalian olfactory bulb. Neuron 23, 499-511.

Schaefer ML, Finger TE, Restrepo D. Variability of position of the P2 glomerulus within a map of the mouse olfactory bulb. J Comp Neurol. 2001 Jul 30;436(3):351-62.

Schoppa NE, Urban NN. Dendritic processing within olfactory bulb circuits. Trends Neurosci. 2003 Sep;26(9):501-6.

Schoppa, N.E. (2006). Synchronization of olfactory bulb mitral cells by precisely timed inhibitory inputs. Neuron 49, 271-283.

Schoppa, N.E. (2009). Inhibition acts globally to shape olfactory cortical tuning. Neuron 62, 750-752.

Schoppa, N.E., and Urban, N.N. (2003). Dendritic processing within olfactory bulb circuits. Trends in neurosciences 26, 501-506.

Schoppa, N.E., and Westbrook, G.L. (1999). Regulation of synaptic timing in the olfactory bulb by an A-type potassium current. Nature neuroscience 2, 1106-1113.

Schoppa, N.E., Kinzie, J.M., Sahara, Y., Segerson, T.P., and Westbrook, G.L. (1998). Dendrodendritic inhibition in the olfactory bulb is driven by NMDA receptors. The Journal of neuroscience : the official journal of the Society for Neuroscience 18, 6790-6802.

Scott, J.W., McDonald, J.K., and Pemberton, J.L. (1987). Short axon cells of the rat olfactory bulb display NADPH-diaphorase activity, neuropeptide Y-like immunoreactivity, and somatostatin-like immunoreactivity. The Journal of comparative neurology 260, 378-391.

Shepherd, G.M., Chen, W.R., and Greer, C.A. (2004). The Olfactory Bulb. In Shepherd, G.M., Chen, W.R., and Greer, C.A. (2004). The Synaptic Organization of the Brain. G.M. Shepherd, Ed. (New York: Oxford University Press, USA), P. 719., G.M. Shepherd, ed. (New York: Oxford University Press, USA), p. 719.

Shipley, M.T., and Adamek, G.D. (1984). The connections of the mouse olfactory bulb: a study using orthograde and retrograde transport of wheat germ agglutinin conjugated to horseradish peroxidase. Brain Res. Bull. 12, 669–688.

Sillito AM, Cudeiro J, Jones HE. Always returning: feedback and sensory processing in visual cortex and thalamus. Trends Neurosci. 2006 Jun;29(6):307-16.

Sillito AM, Jones HE, Gerstein GL, West DC. Feature-linked synchronization of thalamic relay cell firing induced by feedback from the visual cortex. Nature. 1994 Jun 9;369(6480):479-82.

Sillito AM, Jones HE. Corticothalamic interactions in the transfer of visual information. Philos Trans R Soc Lond B Biol Sci. 2002 Dec 29;357(1428):1739-52.

Soucy, E.R., Albeanu, D.F., Fantana, A.L., Murthy, V.N., and Meister, M. (2009). Precision and diversity in an odor map on the olfactory bulb. Nat Neurosci 12, 210-220.

Staubli U, Schottler F, Nejat-Bina D. Role of dorsomedial thalamic nucleus and piriform cortex in processing olfactory information. Behav Brain Res. 1987 Aug;25(2):117-29.

Steriade, M. (2005). Sleep, epilepsy and thalamic reticular inhibitory neurons. Trends Neurosci. 28, 317–324.

Stettler, D.D., and Axel, R. (2009). Representations of odor in the piriform cortex. Neuron 63, 854–864.

Stokes, C.C., and Isaacson, J.S. (2010). From dendrite to soma: dynamic routing of inhibition by complementary interneuron microcircuits in olfactory cortex. Neuron 67, 452-465.

Strowbridge, B.W. (2009). Role of cortical feedback in regulating inhibitory microcircuits. Ann N Y Acad Sci 1170, 270-274.

Suzuki N, Bekkers JM. Distinctive classes of GABAergic interneurons provide layer-specific phasic inhibition in the anterior piriform cortex. Cereb Cortex. 2010 Dec;20(12):2971-84.

Suzuki, N., and Bekkers, J.M. (2012). Microcircuits mediating feedforward and feedback synaptic inhibition in the piriform cortex. The Journal of neuroscience : the official journal of the Society for Neuroscience 32, 919-931.

Tan J, Savigner A, Ma M, Luo M. Odor information processing by the olfactory bulb analyzed in gene-targeted mice. Neuron. 2010 Mar 25;65(6):912-26.

Temereanca, S., and Simons, D.J. (2004). Functional topography of corticothalamic feedback enhances thalamic spatial response tuning in the somatosensory whisker/barrel system. Neuron 41, 639–651.

Thévenaz, P., Ruttimann, U.E., and Unser, M. (1998). A pyramid approach to subpixel registration based on intensity. IEEE Trans. Image Process. 7, 27–41.

Tsumoto, T., Creutzfeldt, O.D., and Legéndy, C.R. (1978). Functional organization of the corticofugal system from visual cortex to lateral geniculate nucleus in the cat (with an appendix on geniculo-cortical mono-synaptic connections). Exp. Brain Res. 32, 345–364.

Uchida, N., Takahashi, Y.K., Tanifuji, M., and Mori, K. (2000). Odor maps in the mammalian olfactory bulb: domain organization and odorant structural features. Nat Neurosci 3, 1035-1043.

Urban, N.N., and Sakmann, B. (2002). Reciprocal intraglomerular excitation and intra- and interglomerular lateral inhibition between mouse olfactory bulb mitral cells. The Journal of physiology 542, 355-367.

Van Essen, D.C. (2005). Corticocortical and thalamocortical information flow in the primate visual system. Progress in brain research 149, 173-185.

Vassar R, Chao SK, Sitcheran R, Nuñez JM, Vosshall LB, Axel R. Topographic organization of sensory projections to the olfactory bulb. Cell. 1994 Dec 16;79(6):981-91.

Wachowiak M, Shipley MT. Coding and synaptic processing of sensory information in the glomerular layer of the olfactory bulb. Semin Cell Dev Biol. 2006 Aug;17(4):411-23.

Wachowiak, M., and Cohen, L.B. (2001). Representation of odorants by receptor neuron input to the mouse olfactory bulb. Neuron 32, 723-735.

Wachowiak, M., Economo, M.N., Díaz-Quesada, M., Brunert, D., Wesson, D.W., White, J.A., and Rothermel, M. (2013). Optical dissection of odor information processing in vivo using GCaMPs expressed in specified cell types of the olfactory bulb. J. Neurosci. 33, 5285–5300.

Wiechert, M.T., Judkewitz, B., Riecke, H., and Friedrich, R.W. (2010). Mechanisms of pattern decorrelation by recurrent neuronal circuits. Nature neuroscience 13, 1003-1010.

Willhite, D.C., Nguyen, K.T., Masurkar, A. V, Greer, C.A., Shepherd, G.M., and Chen, W.R. (2006). Viral tracing identifies distributed columnar organization in the olfactory bulb. Proc. Natl. Acad. Sci. U. S. A. 103, 12592–12597.

Wilson DA, Stevenson RJ. Olfactory perceptual learning: the critical role of memory in odor discrimination. Neurosci Biobehav Rev. 2003 Sep;27(4):307-28.

Wilson DA, Sullivan RM. Cortical processing of odor objects. Neuron. 2011 Nov 17;72(4):506-19.

Wilson, R.I., and Mainen, Z.F. (2006). Early events in olfactory processing. Annu Rev Neurosci 29, 163-201.

Yan J, Suga N. Corticofugal modulation of time-domain processing of biosonar information in bats. Science. 1996 Aug 23;273(5278):1100-3.

Yokoi, M., Mori, K., and Nakanishi, S. (1995). Refinement of odor molecule tuning by dendrodendritic synaptic inhibition in the olfactory bulb. Proceedings of the National Academy of Sciences of the United States of America 92, 3371-3375.

Young A, Sun QQ. GABAergic inhibitory interneurons in the posterior piriform cortex of the GAD67-GFP mouse. Cereb Cortex. 2009 Dec;19(12):3011-29.

Zhan, C., and Luo, M. (2010). Diverse patterns of odor representation by neurons in the anterior piriform cortex of awake mice. J. Neurosci. 30, 16662–16672.

Zhang Y, Burk JA, Glode BM, Mair RG. Effects of thalamic and olfactory cortical lesions on continuous olfactory delayed nonmatching-to-sample and olfactory discrimination in rats (Rattus norvegicus). Behav Neurosci. 1998 Feb;112(1):39-53.

Zhang Y, Suga N, Yan J. Corticofugal modulation of frequency processing in bat auditory system. Nature. 1997 Jun 26;387(6636):900-3.

Zhang, F., Wang, L.P., Boyden, E.S., and Deisseroth, K. (2006). Channelrhodopsin-2 and optical control of excitable cells. Nat Methods 3, 785-792.